ABSTRACT

CHEN, GUANG. A Computational Mechanics Model for the Delamination and Buckling of Paper during the Creping Process. (Under the direction of Dr. M. K. Ramasubramanian).

The manufacture of low density paper such as tissue and towel utilizes the creping process that consists of adhesively bonding the paper in wet state onto the surface of a smooth drying cylinder and scraping it off with a blade once dried. This intricate failure and fracture process however is still not thoroughly understood and stands on the way of enhancing the production efficiency and reducing the development and testing costs before commercial production. The research on creping process by this dissertation has comprehensively reviewed the most relevant literature and ideas for this problem and has developed a capable method in understanding the relationship between control parameters and the creped paper's quality.

In this dissertation, a mechanics of materials description of the creping process is presented. Based upon previous experimental observations, the mechanism of this creping process is proposed as a periodic debonding with certain fracture and failure criteria applied and a repeating delamination buckling sequence of elastic thin film. The study has concluded the delamination and buckling as the basic fracture and failure aspects in creping process and uses them to create analytical creping model.

The stress analysis as the pre-investigation and foundation of fracture energy calculations later is described first. Data from experiments about creping length versus creping angle can be reproduced with the same behavior qualitatively by applying a reasonable set of values as input parameters to the stress criterion based calculation. Parametric study shows the adhesive shear strength and the sheet stiffness most prominently

affect the creping length and the force required to crepe or the creping force. The stress analysis provides some guidance in understanding the creping process primitively. Its limitations include the lack of a satisfactory way to measure the adhesive shear strength and inability to address the buckling and post-buckling behaviors in a continuous creping process.

By selectively using the solution of stresses in adhesive, a computational one-dimensional fracture mechanics model is developed for one creping length cycle. This fracture energy model, with fracture energy criteria applied, calculates strain energies and energy release rates of mixed-mode in different delamination buckling stages, and approaches to a desired creping length in an iteration manner. Buckling strain criterion is also employed to determine the buckling state of paper. Numerical calculations of the fracture model generate the delamination history in one creping length, showing the continuity and discontinuity phenomena in delamination procedure. Mode I and mode II effects are demonstrated: creping length decreases as the critical energy release rates increases; creping length decreases asymptotically with increase in critical energy release rates. The non-linear relation between the fracture criteria values and creping length indicates that creping length not only reduces its value to smaller one but also reduces its sensitivity to critical fracture energies, as the critical fracture energies increase; the creping length would become very large if critical fracture energy in any mode decreases to a very small value. In the parametric study, results show that the effects of creping blade angle, adhesive elastic modulus cause a decrease in creping length for increasing values of these parameters whereas the effects of paper thickness and paper elastic modulus show an increase with increase in the parameters.

The assumptions and results of fracture energy model are consistent with the previous research and approved by high speed camera video observations and prior experimental data.

This fracture energy method developed in this dissertation has significantly extended the calculation's ability for creping problem and can satisfactorily and efficiently predict the paper's creping results which in turn could optimize the crepe paper production in complex practical conditions.

A Computational Mechanics Model for the Delamination and Buckling of Paper during the Creping Process

by
Guang Chen

A dissertation submitted to the Graduate Faculty of
North Carolina State University
in partial fulfillment of the
requirements for the degree of
Doctor of Philosophy

Mechanical Engineering

Raleigh, North Carolina

2011

APPROVED BY:

_____	_____
Dr. M. K. Ramasubramanian Committee Chair	Dr. Fuh-Gwo Yuan
_____	_____
Dr. Kara Peters	Dr. Larry Silverberg

DEDICATION

To my parents

BIOGRAPHY

Guang Chen was born in the city of Luoyang, which is one of the most famous ancient capital cities in China. He had a very happy life during his childhood and entered the key middle school and key high school in local area because of excellent study. In the college entrance exam, he was admitted by Beihang University (Beijing University of Aeronautics and Astronautics) in Beijing and studied there for four years as an undergraduate. The university continued to admit him further as a master student in the accelerated BS/MS program for his outstanding remarks and achievements during undergraduate. In 2006, he applied for the PhD program in the Department of Mechanical and Aerospace Engineering in North Carolina State University, USA, and was admitted in the early of 2007. He came to Raleigh in August 2007 and began his doctoral study in NC State as an international student. His research area mainly focuses on the structure and solid mechanics, failure and fracture analysis, and electro-mechanical experiment system.

ACKNOWLEDGMENTS

First of all, I would like to give many thanks to Dr. M. K. Ramasubramanian, my advisor and the committee chairman, from the deep of my heart. Under his careful and patient guide, I therefore could penetrate into the professional area, solve the difficulties one and another, come up with creative ideas continuously, and have the confidence to finish my study and achieve a new level of knowledge.

Meanwhile, I would appreciate Dr. Fuh-Gwo Yuan for his insight suggestion to the work of my dissertation, and his rigorous scholarship impressed me a lot. I would appreciate Dr. Kara Peters who is very patient and helpful during my doctoral study, and I feel honor to have been in her class. I would appreciate Dr. Larry Silverberg for his significant questions in my preliminary written test and his kindness and responsibility. I would also appreciate Dr. Steffen Heber for his assistance to be the Graduate School Representative in both my preliminary oral test and final defense.

I would show my grateful words to the Proctor & Gamble Co. who is the sponsor of this creping project. With this help, we can continue on our creping research prosperously in the past few years in both computational and experimental studies, and thus can achieve considerable results in this field.

I should give my thanks to my labmates Swapnil Gupta, Kalyan Katuri and Sameer Tendulkar. Swapnil Gupta works on the same creping project with me and has given me plenty of meaningful enlightenment through our discussion of method and result. Kalyan Katuri is always responsive to my questions and any other problem I have encountered, and

he encouraged me a lot during my study. Sameer Tendulkar helps very much in the arrangement of every group meeting, in borrowing lab tools and in computer workstation assistance.

I here also thank James Schaefer who has contributed so much to the upgrading and reinstalling of the micro creping simulator and to the convenience in software control for the measurement of creping experiment.

In the end, I sincerely pass my gratitude to my parents and grandmother who have brought me up and wish to support me at any time. I thank all of my friends who have brought comfort, encouragement, and happiness to me during these years.

TABLE OF CONTENTS

LIST OF TABLES

LIST OF FIGURES

CHAPTER 1

INTRODUCTION

1.1 Background

1.1.1 Preface

Delamination accompanied with buckling is a phenomenon that may occur in many ordinary life or industrial situations such as films, coatings or other combined materials under compression. As the increasing need of modern society, more and more combined or composite materials are designed and developed to maximize specific attributes of the parts or structures and deployed in demanding working conditions subjecting them to the possibility of failure by buckling induced delamination. Therefore, a wide body of knowledge has been developed describing the failure of composite materials under compression. The goal of all failure analysis can be either to provide input to design in order to mitigate the loss from failure or to control the fracture and failure in specific ways to manufacture products.

Failure or fracture can be useful in manufacturing where it is required to break down material into numerous particles in a controlled manner, cutting and machining of metals, or softening hard materials into more compliant and absorptive states such as tissue and towel types of absorbent grades of papers. The study of these failure processes in manufacturing and the ability to control them improve the quality and efficiency of the production.

The creping process in towel and tissue's manufacture, which is the main focus of this dissertation, is about the delamination and buckling of a thin paper attached onto another rigid material, the dryer drum surface, with adhesives through adhesive bonding, and during the process of being scraped off with a blade analogous to the machining of a metal with a cutting tool in a lathe.

1.1.2 The Crepe Paper Industry and Creping Devices

The word of crepe, which is originally from French, refers to a kind of thin pancake meaning curled. When used in the industry, especially in paper industry, crepe paper usually indicates a kind of paper fully patterned with many tiny wrinkles and corrugations. This character can greatly enhance the softness, absorbency, and ductility of crepe paper. Creping process is critical to producing a variety of paper products including tissue and towel papers, papers for party decorations, and packaging materials.

In people's daily life, there is a huge need of tissue and towel paper around the world market, like hygienic tissue paper, facial tissues, paper towels, wrapping tissue, toilet tissue, napkins, etc. Correspondingly, the crepe paper production has been very prosperous and taken about 20-30% of all paper industry in global market every year. Take tissue for example, it is known that world's estimated production of tissue is 21 million tons (European Tissue Symposium, 2010). Only the global tissue market is worth approximately 62 billion USD annually, and it accounts for 10% of the total paper and board market (European Tissue Symposium, 2009).

Therefore, the competition in this industry is very intense. The fact makes every company in this area try to improve crepe paper's quality and the massive production efficiency as much as possible from every single method. However, most of those companies, even including the large ones that have more advanced technologies, are still limited to the traditional methods based on testing experience. For example, several combinations of control parameters are input to different creping tests respectively, and the crepe paper samples with different qualities are produced. The parameter combination that yields better crepe paper quality is recorded. These methods usually cost great amount of resource like electric power, water, paper, adhesive, and testing equipment, because the tests need to be conducted repeatedly in order to obtain a stable and reproducible crepe paper's quality. Unfortunately, the progress of improving crepe paper's production is much more difficult than expected, since there are too many combinations of parameters. Even for the same combination, the same testing experience does not always work on different creping machines.

A theoretical analysis for the creping process is appealed to reduce the testing cost and figure out the control method of creping result. Firstly, the reason about the softness and high stretchiness qualities of crepe paper should be explained. The softness and high stretchiness come from the weak fiber-to-fiber bonding and wrinkled pattern (i.e., the morphology of crepe paper discussed later). According to experimental observations (Beacham, 1998; Ramasubramanian and Shmagin, 2000), when a tissue sample is strained in the tensile test,

the fiber-to-fiber bonds begin to fail from the very early stages of the stress-strain curve and completely slip away before the fibers are significantly strained (Sun, 2000). The weak fiber-to-fiber bonds and wrinkled pattern are realized by the creping process of crepe paper manufacturing.

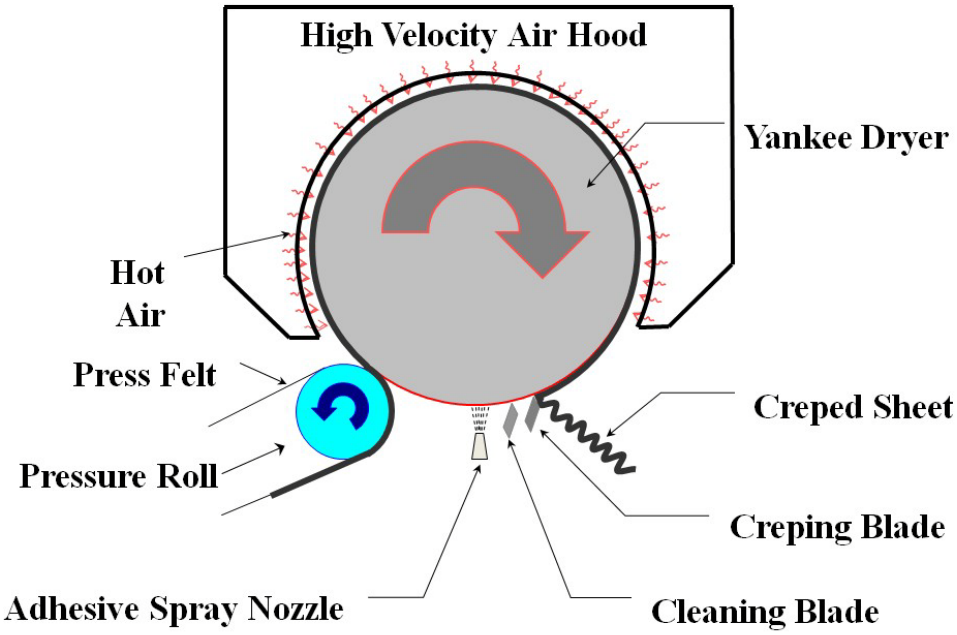

Figure 1.1 Sketch of the industrial creping machine

The creping process begins with adhesive chemicals sprayed onto the pre-heated rotating drum. Then a light weight (small mass per unit area) sheet is transferred to a Yankee dryer made of cast iron. The Yankee dryer's surface is polished smoothly and steam-heated in order to evaporate the moisture content of the sheet. Once the attached sheet is dried, it is

scraped off by the creping bladed and then wound into a roll. After the creping process, the paper usually becomes very soft, and absorptive.

Figure 1.1 shows the sketch of a general industrial creping device (Ramasubramanian and Shmagin, 2000). An adhesive spray nozzle is located in the position between where the flat paper is applied on drum's surface and where the cleaning blade works. As in commercial scale, the Yankee dryer is usually 2.4-7.0 meters (8-23 feet) in diameter, and up to 5.5 meters (18 feet) wide (Ramasubramanian and Shmagin, 2000). The surface of the drum is polished smooth. The rotation speed of Yankee dryer cylinder could be from 1000 m/min (3280.84 ft/min) up to 2500 m/min (8202.10 ft/min) in commercial machine (Ramasubramanian and Shmagin, 2000).

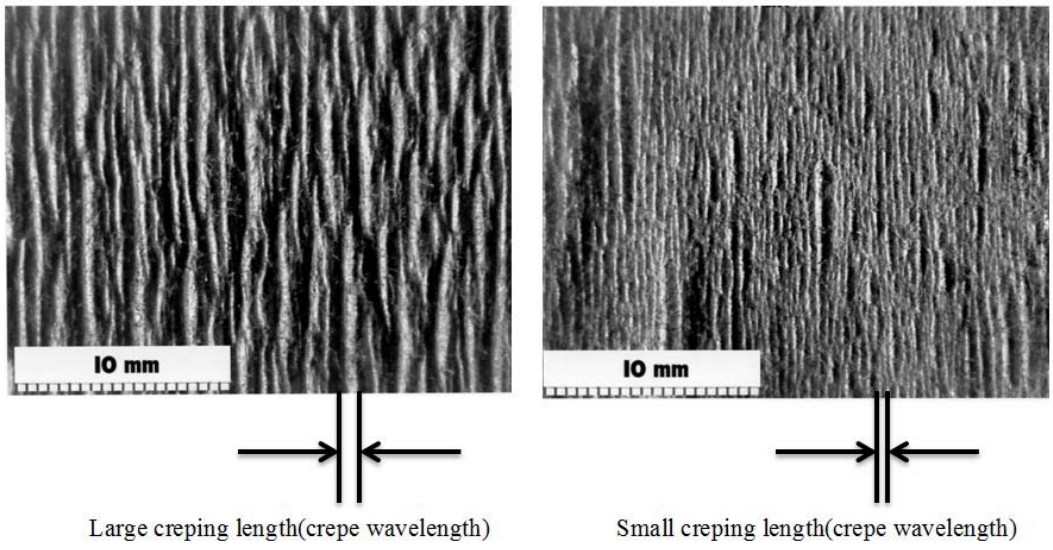

Figure 1.2 Structure patterns of sheet after creping with different creping lengths (crepe wavelengths)

An important measurement of creping results is the creping length (or crepe wavelength). In the paper industry and in laboratory experiments, the creping length is usually defined as the average distance between the small neighboring parallel long blisters in the crepe paper. Creping length predominantly determines the quality of crepe paper such as towels and tissue grades. Finer and softer crepe paper is usually with a smaller creping length. Figure 1.2 displays two samples of crepe sheet with different creping lengths.

Apparently, creping process and its result are controlled by many control factors. The most important ones are density and thickness of paper before creping, strength of adhesive bonding to the drum, rotational speed of drum, and creping blade geometry (i.e., tip shape, installation angle), etc.

There is no direct approach to represent the entire creping process in one simple formula. But it is possible that the creping process consists of a series of basic physical phenomena that can simplify this complex problem into many fundamental problems. Several works in the past have developed and contributed to those problems related to creping process, such as the failure modeling in laminated thin films (Chai *et al.*, 1981; Evans and Hutchinson, 1984; Hutchinson and Suo, 1992), crack propagation in dissimilar materials (Geubelle and Knauss, 1994; Lambros and Rosakis, 1995; Huang *et al.*, 1998). They have extended both scope and depth in understanding the intricate creping mechanism. Related topics and works that could be meaningful are reviewed and discussed in the next section.

1.2 A Review of Research Associated with Creping Process

According to great quantities of industrial data and experimental observations (Beacham, 1998; Ramasubramanian and Shmagin, 2000), delamination and buckling of paper would occur during most part of creping process. Delamination and buckling are two essential kinds of failure and fracture, although they may behave in different manners or generate different results in morphology under various physical conditions featured by material properties, mechanical loading types, and structure geometries. Those failure and fracture phenomena are the basis for summarizing the prior work and literature related to paper creping problem.

Strictly speaking, the researches of delamination and buckling have a long history that could be traced back to centuries ago. This section mainly concentrates on the work in the past few decades since the middle of 20^{th} century when the failure analysis was substantively developed in both theory and calculation. The review of research is divided into the following several topics, trying to give an impression of the studies that may be contributive to creping analysis in form of delamination and buckling.

1.2.1 Delamination and Buckling of Surface Thin Layers

Paper is a thin layer bonded through adhesive coating on the Yankee dryer in creping process. The Yankee dryer is a drum with smooth surface and large radius relative infinite to paper layer's thickness so that it can be assumed as a flat and thick substrate. The delamination and buckling behaviors in such a structure usually have complicated features,

and are difficult to solve and apply leaving many practical failure and fracture problems still not fully understood. Therefore a lot of work has been devoted to investigate on the elastic thin layer delamination and buckling behaviors. The intricate nature of this issue lies in the instabilities of propagation in failure structure, mathematically known as the bifurcation in solutions.

(a) Characteristics in general delamination and buckling of thin layers

Many studies tried to explain the thin layer fracture process in the terms of delamination growth rate. The growth rate of stability and instability both exist in the thin layer delamination and buckling. A study referred frequently is a one-dimensional model of failure in laminated plates proposed by Chai, *et al.* (1981). The fracture energy based method was developed to calculate the delamination of a laminated thin film near the surface of an infinitely thick medium. It shows that the growth of delamination in an initially delaminated structure may be stable, unstable, or change from unstable to stable upon loading. Another research on the delamination and spalling in compressed film was established by Evans and Hutchinson (1984) using a combination of fracture mechanics and post-buckling theory. The method is also based on fracture energy by calculating the energy release rate (ERR). Mode I and mode II fractures are both involved in terms of stress intensity factors as the conditions at interface crack. Analysis of the pre-compressed films reveals that such films are only susceptible to delamination once the film buckles.

The stable and unstable delamination regions of a thin film layer as a clamped isotropic circular plate were also specified by Hu *et al.* (1999). The plate is assumed under

axisymmetric compression. Buckling and post-buckling solutions are calculated as well by von Kármán's geometrically nonlinear thin plate theory in the manner of Taylor's series expansion. The stability of delamination growth shows dependence on the fracture toughness of composite materials and the elastic constant of bridging fiber. If both the fracture toughness and elastic constant are large enough the delamination growth is stable, otherwise it would fall to unstable region.

Since most fractures in ductile materials can only be reached after experiencing an elastic-plastic period, the nonlinear delamination of thin films with plastic dissipation accounted (Wei and Hutchinson, 1997) could be somehow a considerable reason in physics for the unstable delamination and buckling in pure elastic assumption. The research proposes two models either with elastic film and elastic-plastic substrate or with elastic-plastic film and elastic substrate. In the latter model which is closer to creping problem, plastic dissipation makes a significant contribution to the delamination, so the dimensionless critical energy release rate increases sharply as the interface parameters like interface toughness increase.

The work on delamination buckling of coatings shows critical conditions and the similar co-existed stability and instability in buckling growth. Driven by the work of Evans and Hutchinson (1984) and the others (Anderson, 1985; Hutchison, *et al.*, 1992; Evans and Hutchinson, 1995; Chan, 1997), a process of buckling and buckle propagation in compressed oxide layers detaching from superalloy substrate was investigated by Wang and Evans (1998). Below the buckling critical load, the film of oxide layer is stable and adherent; when

the critical load exceeds buckling load, and interfacial toughness (equivalent to the adhesive index) is not exceeded, buckling occurs but does not propagate; and when the loading exceeds buckling load and the adhesion index exceeds the critical value, the buckling of oxide layer is formed and propagated. Some instability characters of propagation are revealed in this study. The buckle extends abruptly when it enters the region with relative low toughness on the interface. Discontinuities of buckle size also appear due to the interface heterogeneities or the stress variation.

The instability of thin layer delamination and buckling over a flat substrate does not remain in the scope of growth rate mentioned above, but also in propagation morphology. This is more obvious if investigated over 2-D domain.

Crosby and Bradley (1999) studied the failure of compressively strained thin films on solid substrates, particularly for a winkle of the delamination propagation along a sinusoidal path only driven by mode I effect. Following the work on the morphological transitions (Yuse and Sano, 1993) in crack propagating instabilities known as Hopf bifurcations, and the theory of sinusoidal wrinkles (Gioia and Ortiz, 1997), they demonstrated the occurrence of sinusoidal wrinkles and their bifurcating branches formed by higher intrinsic strains. They also observed the wrinkles developed as the form of sharply folded ridges in experiment. With the suggested relation between sinusoidal corrugations and intrinsic strain in the film prior to delamination (Gioia and Ortiz, 1998), they explained the sinusoidal wrinkle propagation as the result of the lateral oscillation and the bending energy cost. The research

of Crosby and Bradley (1999) illustrated a kind of unstable crack propagation of thin layer and tried to discover its initiation mechanism.

Another kind of propagation morphology called “varicose” pattern was obtained by Jagla (2007) in 2-D numerical model later. In the calculation over fixed stripe geometry, the author related the buckling patterns to the strain mismatch and the Poisson’s ratio of the thin film and verified the previous results (Audoly, 1999) on the instability mode of the uniform Euler column. If the Poisson’s ratio is no less than 0.25 there would be an undulated wrinkle of buckling pattern; if the Poisson’s ratio is no greater that 0.25 a symmetric “varicose” buckling pattern should appear. The interplay of the delamination and buckling was further studied in showing that highly nonlinear transition of propagation status (i.e., completely developed or unable to develop) is attributed to the factors in the non-delaminated part. For the delamination in complete status, a “brain-like” delamination pattern was obtained.

(b) Buckling-driven delamination of thin layers

Similar wavy pattern propagations in laterally compressed thin films are also known as buckling-driven delamination, whose origin and the driven force are usually attributed to the thin film blisters buckled away from a flat surface. Actually the patterns of buckling-driven delamination are various, including straight-sided patterns and circular patterns with or without wavy edges. A notable one called “telephone-cord-like” pattern was described by Priest *et al.* (1962) in 1960’s. It was further studied by Yu *et al.* (1991), Boucif *et al.* (1991), and Gioia and Ortiz (1997).

Hutchinson and Suo (1992) studied the buckling-driven delamination in straight-sided and circular patterns and concluded a mixed-mode fracture behavior of interface, but most of relevant work was confined in the steady-state problem. Thouless *et al.* (1992) investigated the problem in plane strain condition. The experimental part is a thin mica sheet bonded to mild steel substrate through a brittle thermoplastic resin, quite close to the creping conditions. Besides, an important delamination character close to that in creping process was observed as well. The crack stops to propagate in some places while it continues in other places, even though an initial crack of interface is made to extend through the entire width of specimen. This propagation-arrest delamination character was noted as fracture resistance related to loadings. The systematic and reproducible result, as the author believed, is not associated with geometry but rather with thickness of mica film and adhesive layer. The research provided a directive significance to understand the formation of the morphology shown in Figure 1.2 previously as many straight parallel ridges, but almost each of those ridges appears discontinuously along its direction meanwhile interlaced between one and another on crepe paper.

More analytical and numerical studies regarding the behavior of thin layers in buckling-driven delamination were carried out (Jensen and Sheinman, 2001; Jensen and Sheinman, 2002; Gruttmann and Pham, 2007). Finite element method was commonly used to calculate the fracture energy in delamination, buckling and post-buckling. The observations by Thouless *et al.* (1992) were verified by Jensen and Sheinman (2001) that parts of the crack front would close due to bifurcation buckling while others extend much faster with higher

energy release rate and more significant mode I stress intensity factor. It was also well established by Tvergaard and Hutchinson (2008) that interfaces are significantly tougher in the presence of a mode II stress intensity factor.

The tendency of buckle-driven delamination to grow at its curved front while the sides of it remain stationary for a straight-sided blister on flat substrates, has been shown by Hutchinson (2001) due to mixed-mode associated with the side and front. Jensen and Sheinman (2002) demonstrated that delamination tends to grow along the curved front leaving behind arrested cracks along the sides. The results have shown that straight line growth is most likely to be observed at low stress levels while curved line growth is more likely at higher stresses.

Yu and Hutchinson (2002) studied the influence of substrate compliance on buckling-driven delamination of thin films. When the substrate modulus is comparable to that of the film, or higher, the usual assumption is justified to the effect that the film is clamped along its edges. When the substrate is very compliant the energy release rate at the curved front exceeds that along the straight sides.

If the compressed thin film is over a substrate whose surface is not flat, especially with a sharp corner, then the crack underneath the film tends to grow in a steady-state, rather than in the unstable direction. Sørensen *et al.* (2008) demonstrated this phenomenon by combining the results from interface fracture mechanics and theory of thin shells. Compared with previous results with a flat substrate, the analysis shows the delamination is no longer a bifurcation problem. The energy release rate along the propagating crack front was obtained.

It shows that steady state crack propagation along the front would happen in the region with highest energy release rate, compared to crack propagation at the sides. Expectedly, the strong relationship between the delamination and the angle of the corner was presented. Some other results are shown in the study: the existence of steady state delamination could be explained by mode dependent interface fracture toughness; the crack closure would take place if the stress level sufficiently high; the range of stress values in which the crack is open is strongly limited.

It can be concluded from the above that delamination and buckling behavior in surface thin layers could be applied to modeling the creping process. Ramasubramanian *et al.* (2011) developed a creping model by assuming a thin elastic sheet layer bonded to a rigid substrate with infinite thickness. It could be traced back to an earlier similar model of the paper-metal structure with adhesive joint (Ramasubramanian and Crews, 1998) and also the model of thin short-fiber composite bonded to rigid surface (Sun, 2000).

By calculating the stresses in adhesive and by using a stress failure criterion, Ramasubramanian *et al.* (2011) presented the study of the critical delamination solution under buckling forces and the parametric effects from material properties to show some consistence with previous results of computational analysis (Ramasubramanian and Sun, 1999; Ramasubramanian and Sun, 2000; Sun, 2000) and experimental observations (Ramasubramanian and Shmagin, 2000).

Nevertheless, the stress failure criterion is limiting in such a model for delamination and buckling analysis. It is less capable of accounting for the instability factors of the

delamination mentioned earlier in this section. More specifically, for example, it could not recognize the change in stress directions which may easily happen in the dynamic and unstable creping process. The disadvantage of stress criterion automatically becomes a motivation for this dissertation to calculate the failure problem of sheet-adhesive structure over a rigid and thick substrate by other approaches, like fracture energy method.

1.2.2 Delamination in Composites and Adhesive Joints

The basic knowledge of the fracture at the joints of different parts usually obtained from DCB (Double-Cantilever Beam) experiment. The opening mode effect is firstly reviewed in the method of testing for composites and adhesive joints developed by Chai (1986a). It was motivated by the inter-laminar fracture of laminated composites. Three types of mode I fracture specimens were used in the experiment: DCB with adhesive joint, DCB of composites and SDCB (i.e., a stiffened DCB) of composites. According to another work by Chai (1986b), the fracture energy per unit area of adhesive joint specimen is calculated as

$$G_{Ic} = \frac{np\delta}{2ba} \tag{1.1}$$

where a, b, p and δ are the crack length, beam width, critical load and critical deflection, respectively, and constant n was determined from the compliance plot by Chai (1986a). In similar, the fracture energy of DCB and SDCB composite specimens is evaluated by compliance method

$$G_{Ic} = \frac{p^2}{2b}\frac{\partial C}{\partial a} \tag{1.2}$$

where $C = \delta / p$.

The fracture work G_{Ic} is found to be a material property independent of ply orientation and test specimen geometry with only planer and smooth surfaces included. However, because of the increased damage zone in crack tip by crack extension, the delamination of composites shows a resistant behavior. That is, the significance of calculated G_{Ic} is greatly reduced by the damage zone whose character heavily depended on the specimen geometry.

Compared from the test results, adhesive fracture work depends heavily on adhesive ductility and adherend rigidity. The stresses in adhesive are found to be far exceeded by uniaxial yield stress at separation revealing the nonlinearity in adhesive joint specimen. The effect of the matrix on the inter-laminar strength of laminated composites was also assessed. A large part of fracture surface has been shown to be associated with debonding of the matrix from fibers.

The result of shear fracture on DCB test samples was shown later by Chai (1988). Mode II and mode III fracture in adhesive joints bonding the DCB were explained in material aspects. The shear energy release rate exhibits a phase of plateau and then declines as the adhesive thickness decreases. In the fracture tests, different adhesive types and DCBs were investigated in mode I, II and III loading experiments. It is argued that all critical energy release rates G_{Ic}, G_{IIc} and G_{IIIc} in each mode respectively would converge to a common value G_c as the adhesive thickness goes to zero. To apply the result to a mixed mode fracture, the fracture criterion for bonded joints is also presented as

$$\left(\frac{G_I}{G_{Ic}}\right)^m + \left(\frac{G_{II}}{G_{IIc}}\right)^n + \left(\frac{G_{III}}{G_{IIIc}}\right)^k = 1 \tag{1.3}$$

where the indices m, n and k are real numbers. As pointed out in this study, the fracture work G_{IIc} and G_{IIIc} are coincided and heavily depend on the adhesive thickness in the whole thickness range. Then a shear fracture work G_{sc} and asymptotic fracture work G_c are used in the following relation

$$G_{sc} = G_c + \alpha t, \ t < t_L \tag{1.4}$$

It is effective when adhesive thickness t is less than a specific value t_L. The constant values of α and t_L are given for each adhesive type in experiment. By denoting the total energy release rate $G_T = G_I + G_{II} + G_{III}$, the fracture criterion reduces to

$$\left(\frac{G_I}{G_{Ic}}\right)^m + \left(\frac{G_T - G_I}{G_{sc}}\right)^n = 1 \tag{1.5}$$

For t small enough, an approximation of $G_{Ic} \sim G_c$ is made for the case relevant to inter-laminar fracture of composites, and the above form is given by

$$\left(\frac{G_I}{G_c}\right)^m + \left(\frac{G_T - G_I}{G_c + \alpha t}\right)^n = 1 \tag{1.6}$$

The criterion is further reduced to

$$G_T - G_c + \frac{\alpha t}{G_c}(G_I - G_c) = 0 \tag{1.7}$$

by choosing both indices of m and n to be 1 (Johnson and Mangalgiri, 1985). So the criterion $G_T - G_c = 0$ is reached if the slope of $G_c / \alpha t$ far greater than 1.

The effect of the bonding joint's thickness concluded from this research is important to the creping problem because the thickness of adhesive layer is also very small about in the same scale compared to H3502 with t_L around 4 μm and BP-907 with t_L around 40 μm in the DCB experiment (Chai, 1988). Those results have revealed a possibility that the fracture effect in shear mode may yield the similar effect in opening mode when the thickness of adhesive bonding joint falls below some certain value like t_L. That is to say, it is possible for the mode I fracture work to have the effects on creping result not far different from those of mode II fracture work. In micro scale, if take a look at the microstructure of the adhesive crack, the micro-cracks (Chai, 1988) occupies the entire thin adhesive layer along the main crack. Most of their orientation agrees with that of maximum tensile stress, indicating a result of strong mode I effect in each local area with micro-crack.

The problem of crack propagation on one of the interfaces between a thin adhesive layer and its two elastic substrates was considered by Tvergaard and Hutchinson (1996). The adhesive layer is assumed elastic-plastic. The fracture process is governed by a traction separation law through an elastic-plastic continuum as a boundary condition along the line extending ahead of the crack. In the case of an interface joining dissimilar materials, the separation law necessarily involves both the normal and shear tractions and the two associated relative displacements of the surfaces across the interface. In the case of the

adhesive joint comprised of a thin ductile (elastic-plastic) adhesive layer joining two elastic substrates on its both sides, Tvergaard and Hutchinson (1996) observed that the normalized steady-state toughness increases strongly with the yield strength of the adhesive layer, with all other parameters held fixed. For very thin layers, the enhancement of toughness due to plastic deformation is negligibly small. The ratio of the substrate elastic modulus to that of the adhesive layer has a fairly significant effect such that the kind of joints with relatively stiff elastic substrates have higher toughness, all other parameters remaining the same.

On the mixed-mode stand, one conclusion from a meso-mechanical mixed-mode model of thin adhesive layers by Salomonsson (2008) revealed that the fracture energy is low and essentially governed by the cohesive properties of the adhesive without major plastic dissipation. This is especially the case for an adhesive layer with peel dominated loadings. In shear dominated loading cases plastic dissipation gives a substantial contribution to the fracture energy. When the adhesive layer thickness is considered, the layer is treated as a deformable elastic or elastic-plastic material. In the creping process, the role of adhesive layer is very important. If the adhesion is extremely strong, the crack propagation goes through the sheet there by leaving a layer of fibers on the dryer drum. If adhesion is weak, the sheet comes off clean from the drum, creping length is large, and the product is unacceptable.

The repeated application of adhesive on the same spot creates a steady state layer of adhesive and hemicelluloses components from the fiber, depending on the fibers used, and the sheet adheres to a more repeatable sticky surface thus may form (Oliver, 1980).

Therefore, it is reasonable to consider the creping process as a thin paper bonded to a rigid substrate (i.e., Yankee dryer or drum) with a thin layer of deformable adhesive, subjected to compression at the free end by the creping blade.

Fracture analysis of adhesive joints with mixed-mode loading was further investigated in the attempt of giving adhesive deformation expressions. A b/a model was given by Alfredsson *et al.* (2007) assuming two beam-like adherends and adhesive as a thin layer in between. The model tried to calculate fracture energy from the deformations in adhesive layer. First of all, the peel and shear stresses in adhesive layer are claimed respectively

$$\sigma = \frac{\overline{E}}{t} w, \quad \tau = \frac{G}{t} v \tag{1.8}$$

where $\overline{E}$ and G are effective adhesive Young's Modulus and shear modulus respectively, w and v are deformations of peel and shear respectively. In order to differentiate the notation from the shear modulus, the author denoted energy release rate by J , and got:

$$J_1(\hat{w}) = \int_0^{\hat{w}} \sigma \, dw = \frac{1}{2} \frac{\overline{E}}{t} \hat{w}^2, \quad J_2(\hat{v}) = \int_0^{\hat{v}} \tau \, dv = \frac{1}{2} \frac{G}{t} \hat{v}^2 \tag{1.9}$$

where $\hat{w}$ and $\hat{v}$ are crack tip deformations in peel and shear. J_1 and J_2 are claimed as energy release rates corresponding to mode I and mode II. Then one can use fracture criterion

$$\frac{J_1}{J_{1C}} + \frac{J_2}{J_{2C}} = 1 \tag{1.10}$$

as common method to determine the fracture work of generating new delamination. Thus, the question falls to how to determine the deformations in terms of $\hat{w}$ and $\hat{v}$. In Alfredsson's

study, $\hat{w}(x)$ and $\hat{v}(x)$ are functions of x along the position in longitudinal direction of adherends. They are solved for both unbalanced (i.e., different stiffness in adherends) and balanced (i.e., the same stiffness in adherends) cases. Further, by using an End-loaded semi-infinite system, the force and moment balance are created on both ends of the b/a model.

If applied to paper creping problem, the thickness (t_2) of the lower beam should be set as infinity. That indicates the control parameter $\eta = t_1 / t_2$ in this article should be zero, because the Yankee dryer's radius is huge compared to the thickness of paper. In this case, some coefficients in $\hat{w}(x)$ and $\hat{v}(x)$ functions would turn to infinity and blow up the deformation functions of adhesive layer. This b/a model seems to be limited to adherends that are not far different from each other, although it meaningfully tried to solve the fracture problem of adhesive joints in terms of adhesive deformations.

The incompatibility of the structure assumptions between this b/a model and creping model intrigues the effort to calculate the stresses or deformations without including adherends on both sides of adhesive.

1.2.3 Interfacial Crack Problem in Bi-materials

The importance of studying crack on the interface of bi-materials or dissimilar materials for creping analysis may be attributed primarily to the need of revealing the intrinsic mechanism of delamination during creping process. The propagation of interfacial crack is one of the failure modes in fiber-reinforced composites, adhesive joints and thin films. The fact that cracks often happen along the interface of adhesive and sheet helps apply the bi-

material model to the interfacial delamination analysis of sheet-adhesive structure in creping model.

The bi-material model originated from separating an isotropic homogeneous plate supposedly along the crack into two regions with different properties. Some basic bi-material delamination features had already been demonstrated in the work traced back to the middle of last century. Williams (1959) in his foundational work split the stress field solution of an integrate plate with crack into dissimilar media, and then deduced an oscillating character related to stress:

$$\sigma \sim r^{-1/2} \begin{pmatrix} \sin \\ \cos \end{pmatrix} \lambda_j \log(r) \tag{1.11}$$

where σ is the stress, r is the distance from the point of crack, and λ_j is the stress eigen value controlled by a shear modulus ratio of the dissimilar materials.

This is known as the primary character of the bi-material problem. Closely, Erdogan (1963) studied the relevant problem of stress distribution in two semi-infinite elastic plane with different properties bonded together along the real axis. Later Erdogan (1965) developed this issue further in the bonded dissimilar material with cracks. This time, Erdogan extended the work of Williams (1959) by incorporating the tractions on the crack surfaces, in-plane moments, residual stresses from temperature changes, concentrated load couple at an arbitrary place, and one-sided wedge loading at the crack. Meanwhile, Rice and Sih (1965) extended the Williams' theory in another way by applying the complex-variables (Muskhelishvili, 1953) integrated with eigenfunction-expansion.

However, England (1965) argued that if the stress solutions by Williams (1959) and Erdogan (1963) are applied to such a bi-material model under equal and opposite normal opening load over the single crack, they would generate wrinkle and overlap at the crack tip which is physically inadmissible. Since then, it seems that the study on interface crack of bi-material is gradually divided into two directions: one is focusing on solving the of stress field near the crack tip, the other pays more attention to the oscillating character and its result in crack propagation.

(a) In the direction of crack tip field:

The incompleteness of stress field solution near crack tip motivated Rice (1988) to give a complete expansion of Williams result based on the extension to the analytic functions (Rice, 1968). Following the work of Cherepanov (1962, 1979), England (1965) and Erdogan (1965), Rice (1988) associated the elastic interface crack problem with the complex stress intensity factor K as

$$K = (\sigma_{yy}^{\infty} + i\sigma_{xy}^{\infty})(1+2i\varepsilon)L^{-ie}\sqrt{\pi L/2} \tag{1.12}$$

where L is the interface crack length, σ_{yy}^{∞} and σ_{xy}^{∞} are the remote uniform stresses, ε is the imaginary part of stress eigen value given by Williams (1959). This method shows its capability in studying small scale nonlinear material behavior and/or small scale contact zones at the crack tip.

Corresponding with the result above, a numerical analysis of evaluating the stress intensity factors in mode I, II and III was soon presented by Matos *et al.* (1989). The authors

set their effort on calculating the *J*-integral of a virtual crack extension, and then obtained the stress intensity factors by perturbation. Finite element method was employed in the numerical analysis and good agreement was achieved with Crack Surface Displacement (CSD) method and energy method.

Lu and Chiang (1993) extended the stress intensity factor research scope by applying photoelasticity to the interfacial crack of bi-material problem. Two photoelasticity approaches were used to determine the complex intensity factor (Rice, 1988) in equation (1.12). Although the authors admitted that the accuracy of this application might be influenced by neglecting higher order terms in asymptotic solution, the study was intended to offer a basis for such applications later on.

(b) In the direction of crack propagation:

A kinking phenomenon of crack extension out of interface was investigated by Hu and Hutchinson (1989) and Mukai *et al.* (1990). Based on these works, Geubelle and Knauss (1994) setup the criteria to determine the crack propagation orientation, which was noted as the kink direction or kink angle, from the effect of stress field rotation at the crack tip. The maximum stress criterion (Erdogan and Sih, 1963) and maximum energy release rate criterion (Palaniswamy and Knauss, 1978; Wu, 1978) were introduced and pointed out that the crack propagation direction is not unique in homogeneous situation. Results by maximum energy release rate criterion were believed to be in better accordance with experiment results, noticed by the author.

More results in crack propagation of bi-material were demonstrated, such as the transonic delamination of bi-material interface, shock waves emanated from the crack contact zone. Parallel computational and experimental researches in this area were carried out. Those dynamic features were previously believed not feasible in physics, but was challenged by Liu *et al.* (1993) and Lambros and Rosakis (1994) in their experiments. Encouraged by the results above, Yu and Yang (1995) investigated the dynamic debonding by in-plane deformation including stress and strain. Nearly at the same time, Lambros and Rosakis (1995) also conducted and analyzed these transonic crack growths in their further experiment and showed impressive phenomena. Huang *et al.* (1998) generalized the intersonic propagation of interfacial crack tip from without crack face contact to with crack face contact, validating the experimental results. And in experiment Rosakis (1998) observed the two traveling shock waves from the intersonically moving crack tip and crack contact end predicted theoretically.

The insightful knowledge of interfacial crack propagation, especially the dynamic delamination results from analysis and experiment, provides important theoretical assumptions for creping model in this dissertation. For example, buckling plate or column should be the rational assumption at the very beginning of creping process, even all the sheet is bonded at the original state. The crack may extend at a sonic speed level that is roughly ten times of the Yankee dryer's full rotation speed. So the initial crack that is much longer than sheet shortening distance would possibly appear at the beginning. This is discussed in the next chapter in details.

1.2.4 Post-buckling, Dynamic Buckling, and Other Aspects

In the dimensions of crepe paper consisting of many small ridges/blisters, three scales of lengths are pointed out. The smallest one is the sheet-thickness-scale (i.e., around a hundred of micrometers), the middle one is the creping-length-scale (i.e., usually below a few millimeters or a tenth of inch) and the largest one is sheet-length-scale (i.e., order of several meters or feet). The ridges are actually formed by folding the debonded and buckled sheet along a creping-length-scale distance in the creping direction. Apparently, the buckling deflections are in fact very large relative to the sheet-thickness-scale. A large buckling deflection often associates with post-buckling and dynamic characteristics, especially under impact factors when creping blade hits on the edge of debonded sheet. Therefore, the review of those buckling behaviors becomes necessary in this section.

On the primary consideration in this dissertation, the study of post-buckling behavior needs to deal with the delamination for creping analysis, as the crack propagation manner is always the determinant of creping length and hence control the crepe paper pattern and quality. Because the post-buckling also involves with instability factors, energy based method would possibly be a good choice to solve such a problem. Whitcomb and Shivakumar (1988) calculated strain-energy release rate in the delamination of a post-buckled laminates. The results show large variation of strain-energy release rate along the delamination front. In order to further understand the intrinsic nature of post-buckling, Adan *et al.* (1994) delivered the research on post-buckling behaviors of beams under one lateral rigid constraint. The author developed the nonlinear kinematic approach based on the total

potential energy equations. The sudden dynamic change in post-buckling shape called snapping effect was also incorporated in analytical equations. The results here show agreement with the two distinct types of experimental phenomena, symmetric and asymmetric post-buckling responses.

The symmetric post-buckling response was further derived theoretically by Chai (1998) in a similar linear column post-buckling problem but with bi-lateral rigid constraints on both sides. In this analytical work, Chai presented the deflection equations in different post-buckling regions for small and large deformation analysis. For the symmetric post-buckling response, two conclusions were pointed out. In the small deformation, there is buckling mode (i.e., number of buckles or waves) transition to the next higher buckling mode as post-buckling contact with bi-lateral constraints becomes large enough. In the large deformation, the mode transition is prohibited beyond mode 2. If any rigid lateral constraint changes to an elastic surface, also referred much earlier as Winkler foundation by Siede (1958), nonlinearity should appear in the solution to post-buckling shape (Kounadis *et al.*, 2006).

Extended to 2-D area, problems like post-buckling in plates and shells appear to be solved more conveniently and straightforward by numerical approaches. No matter which method is applied like Reference Surface Element model (Zhu, 2003) or the Finite Element Methods (Kim and Hong, 1997; Chen and Virgin, 2006), those results are in common predicting significant buckling and post-buckling dynamics, either discussed here such as mode transition, snapping or discussed somewhere else like secondary bifurcation (Chen and Virgin, 2006).

The dynamic buckling in different structure members is not merely represented by mode change or snapping, but also by its intrinsic nature, like lateral vibrations in vibration buckling and axial waves in pulse buckling. The former are more common in a “slim” ad slender structure like column or thin plate; the latter are more seen in a massive rigid object. It is arbitrary to determine which type of buckling is more possible for creping process due to the lack of direct experiments which are difficult to implement, so the two types of dynamic buckling would be reviewed together for creping model in the following paragraphs.

In the investigation of dynamic buckling, impact, which sheet must undergo with during creping, is the necessary loading type. A common method is to apply impact to the test specimens assumed or preloaded with small imperfections. As an early research, Hoff (1951) implemented the experiment with impact over an initially slightly curved column along the longitudinal direction. The author designed a control parameter that was related to the geometry of the specimen and the relative impact speed. A vibration of deflection was observed around its static position together with the mass inertia effect, but, as the author argued, the results based on small deflection theory would not be reliable if the deflection becomes very large. Some expansions to Hoff’s results were referred by Sevin (1960) and Ari-Gur *et al.* (1982) in axial responses (inertia, strains) to impact.

The researches above also reveal that imperfections in vibration buckling seem to have great influences on the results. Compared to the imperfections used above, they were assumed like an analytical factor as white noise by Lindberg (1965). His work (1987, 1988,

1991, 1992a, 1992b) concentrated more on pulse buckling behaviors since applying this assumption to wave propagation study was more convenient.

As for structures like composites and laminates close to those in creping model, the dynamic buckling features were presented either in layered plates (Bottega and Maewal, 1983) or in matrix with fibers embedded (Kwon and Serttunc, 1993), etc. Studies of delamination and buckling behaviors have shown, especially in the results of Bottega and Maewal (1983), that the static method is more appropriate for the delamination of thin layer with impact type close to the case in creping process.

However, we have the reason to believe the dynamic effects in creping process should more associate with adhesive layer rather than the debonded sheet that seems to be under impact directly. Because the Yankee dryer's rotation speed, which must be treated as a measurement of the impact scale in creping process, has shown itself to be the dominant factor in determining the fracture toughness of adhesive layer according to the commercial test results.

The moisture and residual stress are the other factors that could effect on delamination and buckling for creping process. Waters and Volinsky (2007) induced moisture from the outermost surface to the very thin film coated over a thicker but still a thin plate substrate. Compressive residual stress was also induced.

From the two types of experiments with different materials, they pointed out moisture could take effect on adhesion strength only when the water reaches the interface between thin film coating and thin plate substrate. If the water does reach the interface, it would largely

reduce the adhesion strength (i.e., dozens of times according to the results), which means the delamination should grow much faster than those without moisture. Compressive residual stress is an active factor for delamination too. By applying the residual stress to the coated film, the delamination is more prominently observed.

1.3 Overview of the Chapters in Dissertation

The dissertation contains six chapters, including the introduction, the basic study of delamination and buckling, stress analysis for creping mechanics, fracture analysis in creping process, simulation in experiments, and conclusions. The outlines for all chapters are described below:

Chapter 1: Introduction. This chapter gives a brief background and literature review on fracture and failure research relevant to the creping process. The review is further divided into four topics subjectively by the author in consideration of their relations to creping problem: (1) delamination and buckling of thin surface layers; (2) delamination in composites and adhesive joints; (3) interfacial crack problem in bi-materials; (4) post-buckling, dynamic buckling, and other aspects.

Chapter 2: Fundamental Study of Delamination and Buckling Mechanism Applied to Creping Problem. The basic properties of delamination and buckling and their applications to creping model assumptions are discussed. The verifications in analytical and numerical methods are demonstrated for those basic characters.

Chapter 3: Stress Analysis of the Creping Mechanics. A stress analysis for adhesive layer and stress failure criterion for the delamination of creping process are proposed. Some analytical results are presented in the aspects of material properties and physical conditions.

Chapter 4: Fracture Analysis of Delamination and Buckling in Creping Process. A fracture energy based method is developed for creping process. The creping length is calculated by evaluating the energy release rate in mixed-mode condition. The method is compared with Finite Element Analysis in different control factors. Parametric study is also considered and exhibited.

Chapter 5: A Brief Introduction to Creping Experiment. The micro scale creping simulator for laboratory experiment is demonstrated. The working principle and test functions corresponding to commercial creping machine are discussed. Prior results are shown to verify the analytical results.

Chapter 6: Conclusions and Prospects. A summary for the dissertation and its conclusions on creping analysis are drawn. Some prospective suggestions are included as well.

CHAPTER 2

FUNDAMENTAL STUDY OF DELAMINATION AND BUCKLING MECHANISM APPLIED TO CREPING PROBLEM

Delamination is a kind of failure mechanism that usually happens in laminated materials by impacting force or alternating stresses. It can also happen in concrete materials with strong reinforcement. When there is a delamination generated, it means the stresses in the material in the delaminated area reaches or exceeds the strength of the material and it would fail or break as a consequence. However, different materials, structures and loading conditions influence greatly on the origins and propagation of delamination according to a long history of application and observations. Hence an insight study of delamination is necessary to understand the basics of delamination and determine critical factors involved in delamination of structures under a variety of service conditions.

Buckling is a failure mode happening abruptly under large compressive stresses which however have not exceeded the limit or the strength of the material's capability. It can appear in a member of a structure like bar or column. Buckling is also described as elastic instability. When the compressive force or load is applied on a member like column that is slender enough, and is continuously increased, the column should finally become unstable and undergo a sudden unpredictable lateral deflection. Mathematically, buckling is a phenomenon described by different solutions of the equations expressing the dynamics and equilibrium mechanics. In the beginning, the number of static state equilibrium solution

remains one. With the increasing load, the static state equilibrium will have more than one solution by any extra load after certain load value is approached. This certain load is called critical load for buckling.

Because the paper creping process is a complex phenomenon that combines several failure processes including delamination and buckling together, it is necessary to resolve this process into several fundamental parts with appropriate boundary conditions to obtain a basic understanding of the creping process from mechanics point of view. In this chapter, literature closely related to paper creping problem is presented to provide an understanding of failure mechanisms in creping.

2.1 The Delamination Study for Creping Problem

2.1.1 Discussion and Application of a Prior Fracture Model

The delamination in creping process occurs due to interfacial cracking. Similar situations could be found in the delamination of thin films and coatings over a solid and thick substrate. The thin film delamination study by Evans and Hutchinson (1984) using energy release rate method is considered as one of the theoretical foundations to this dissertation. So it is worthwhile discussing their work here on the intrinsic principle of fracture work and proposing some basic ideas on how to apply this fracture work to the creping model.

A circular delamination area of thin film with radius a was assumed by Evans and Hutchinson (1984). When the film was under biaxial compression forces, the study indicated that, the delaminated area should buckle and there would be a strain energy difference or say energy release δU from the unbuckled situation. This energy release appeared because the relative edge stress slope against the relative edge shortening displacement would decrease certain amount from that in the unbuckled state after the delaminated film buckled. And so the energy release rate was obtained by plate delamination theory (Lawn and Wilshaw, 1974). Figure 2.1 depicts the sketch of this model as a clamped circular plate over the delaminated area (Evans and Hutchinson, 1984).

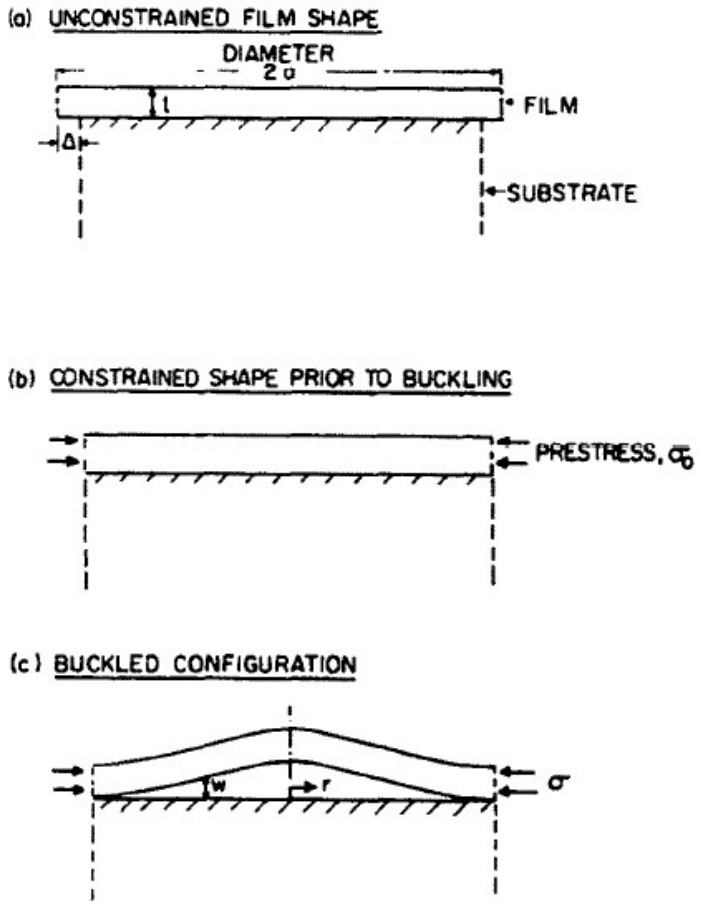

Figure 2.1 Schematic illustration of the film delamination, compressing pre-stress and the resultant stress in the buckled configuration (Evans and Hutchinson, 1984)

Here, Δ is the shortening of the diameter $2a$ of the circular area caused by pre-stress σ_0, t is the thickness of the film, σ is the resultant stress, w is the vertical displacement of buckled shape, and r is the radius direction.

According to the *Fracture of Brittle Solids* (Lawn and Wilshaw, 1974), the general form of energy release rate in this circular delamination model is calculated as equation (2.1) defined by the total energy released per unit length of crack edge.

$$G = \frac{1}{2\pi a}\left(\frac{d\delta U}{da}\right) \tag{2.1}$$

This result could also be derived from the theory in *Delamination buckling of composite materials* by Kachanov (1988) in the case of simply changing the crack edge from a straight line to a circle.

It was also argued that the strain energy change in substrate was relatively small to that of buckled part of film, therefore it was reasonably neglected. The deflection of substrate was also neglected for the same reason. Then by assuming the delaminated area of film separated from its neighboring area, the radius expansion when the biaxial compression σ_0 is removed, should be calculated as

$$\delta a = (1-\nu)\frac{\sigma_0 a}{E} \tag{2.2}$$

where ν and E are Poisson's ratio and elastic modulus, respectively. Based on the buckling theory of a clamped circular plate (Timoshenko and Gere, 1961), the critical buckling stress is

$$\sigma_c = \frac{kE}{12(1-\nu^2)}\left(\frac{t}{a}\right)^2 \tag{2.3}$$

Here k is a constant already known. Therefore the corresponding critical shortening of the film's diameter is developed as

$$\Delta_c = \frac{k}{12(1+\nu)}\frac{t^2}{a} \tag{2.4}$$

After the critical buckling stress and critical shortening of diameter are obtained, the strain energy in buckled delaminated film in Figure 2.1(c) could be calculated by the work done from the edge force against resultant force extending the edge of film back to the diameter $2a$ in Figure 2.1(a).

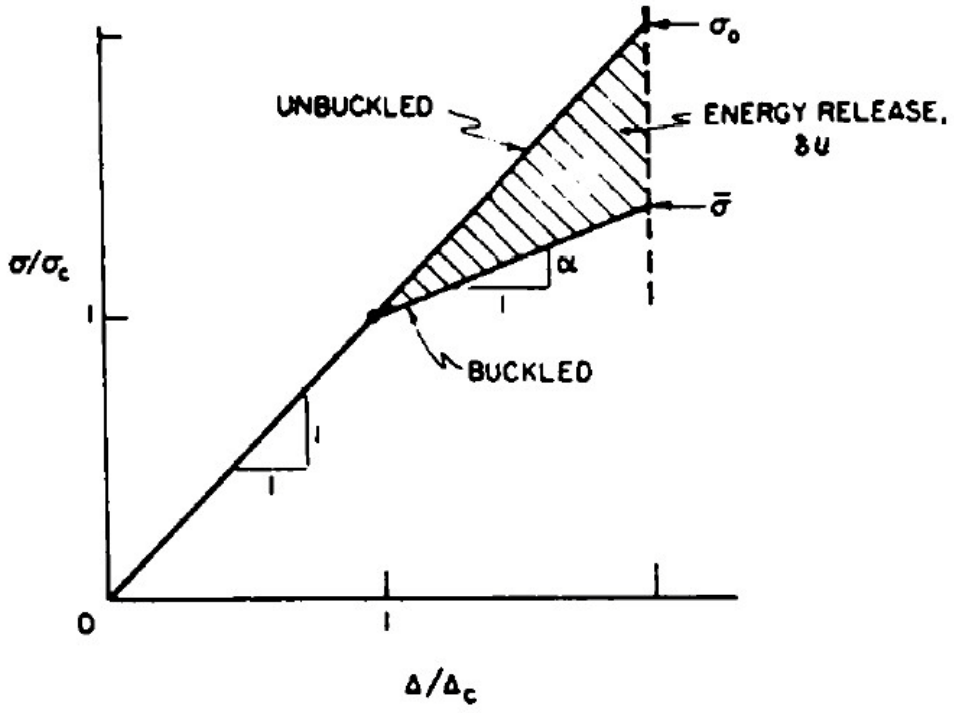

Figure 2.2 Relative edge stress against the relative shortening displacement for a clamped circular plate indicating the energy release between buckled and unbuckled states (Evans and Hutchinson, 1984)

The relative edge stress σ/σ_c against relative edge shortening displacement Δ/Δ_c over critical values is plotted in Figure 2.2 (Evans and Hutchinson, 1984) before the edge stress reaches the biaxial compression stress σ_0. The buckling of the delaminated thin film appears

if σ / σ_c larger than 1. The decreased slope of relative edge stress in buckled state is determined as

$$\alpha = \frac{1}{1+1.207(1+\nu)} \tag{2.5}$$

by Evans and Hutchinson (1984). The relative edge stress slope is unit 1 in unbuckled state. Apparently, $\alpha < 1$, so there is a decreased slope in buckled branch of the relative stress curve in the plot. This generates a total energy difference δU in the shaded area in Figure 2.2 when the edge stress σ is greater than the critical buckling stress σ_c in equation (2.3). Thus the energy release δU for the delaminated circular region of thin film is derived as

$$\delta U = \frac{\pi(1-\nu)(1-\alpha)ta^2(\sigma_0 - \sigma_c)^2}{E} \tag{2.6}$$

Applied with equation (2.1), the energy release rate of thin film in circular region is obtained as

$$G = \frac{(1-\nu)(1-\alpha)t(\sigma_0^2 - \sigma_c^2)}{E} \tag{2.7}$$

2.1.2 Significance of the Compressed Film Study for Creping Analysis

The fracture work calculated by Evans and Hutchinson (1984) reveals a stress decreasing trend when buckling happens in a delaminated thin film. They also employed the method of energy release rate to describe the delamination behavior in such a model. These results have served as a meaningful reference to the creping research in this dissertation.

The primary significance of the compressed thin film study is the adoption of an energy release rate method to the creping problem. It has the advantage of straightforwardly determining the delamination progress of fracture problem by avoiding complex mechanical analysis over the dynamic and multi-parametric creping system. Introducing the energy release rate method should be able to reduce a lot of computational work. The energy release rate also has the advantage of evaluating a crack across a buckled delamination by combining both the elastic fracture mechanics and the post-buckling in plate theory.

The next significance is that the compressed thin film model is a problem quite similar to creping process in terms of mechanics. The sheet is also a slender thin layer delaminated over a solid and thick substrate and subject to lateral compression. Although there is boundary geometry difference (i.e., linear delamination boundary in paper creping problem against circular boundary (Evans and Hutchinson, 1984)), the energy release rate in equation (2.1) can be conveniently changed to equation (2.8) in creping analysis according to the delamination buckling theory by Kachanov (1988)

$$G' = \frac{1}{w}\left(\frac{d\delta U}{dl}\right) \tag{2.8}$$

where w is the width of the sheet, l is the delamination length. Since w is constant for a rectangular sheet, equation (2.8) is chosen as the theoretical foundation of calculating energy release rate for 1-D creping model in later chapters.

The third significance is that the concept of edge shortening (i.e., see figure 2.1(a)) was used by this thin compressed film model. The creping model can apply such a variable to

calculate energy release rate by associating with the strain loading rather than with stress loading. The latter has some drawbacks when investigating on a continuously dynamic problem like creping process.

It is difficult to validate the model experimentally since the stresses in paper are not easy to measure. The stress based analysis explains the debonding behavior of paper and shows parametric effects during creping but it is less capable to address buckling and post-buckling behaviors of paper which are important to know in order to optimize the process.

It is true that there are some differences in the model structure and loading type between this model and creping process. But such differences would be weakened by the following reasons. The thin film delamination by Evans and Hutchinson (1984) did not include the adhesive layer underneath the sheet. If energy release rate method is still employed in creping model, the appearance of adhesive stress effect in creping model would not result in a basic change but adjust the method by adding energy terms for the adhesive layer. This would be verified in the section 2.1.4.

Besides, another difference is the loading condition. The model by Evans and Hutchinson (1984) is bi-axially loaded compared to the uniaxial loading condition in creping model. It can be simplified as an axisymmetric one-dimensional model due to the symmetry in both loading and structure's geometry.

Therefore, the model and method in the delamination of circular film developed by Evans and Hutchinson (1984) encourage this dissertation to employ fracture energy based approach. It helps resolve the above mentioned issues by addressing buckling and

delamination behaviors of the bonded paper during creping process. It complements the framework of computational analysis that explains the delamination and buckling of paper.

2.1.3 Validation of Chai's Fracture Energy Method in Creping Condition

In practice, the creping process of paper is a 3-D problem on the surface of the Yankee dryer which is a cylinder. Such problems could be numerically simulated by one of highly developed commercial software such as ABAQUS^{TM} or ANSYS^{TM}. However, we have several reasons to simplify the calculation method for creping process into 1-D analysis instead of 3-D analysis, because the latter could greatly increase the amount of computation and require large computational resource once run by the commercial software.

The first advantage to one-dimensional modeling reason is the simplicity of geometry. The creping process is carried out on the Yankee dryer's cylinder (i.e., the drum) surface. Meanwhile, the creping blade is a rigid flat plate and its edge contacted with sheet is parallel to the axis of the cylinder. In addition, the sheet thickness is very small compared to the length of contact edge with blade. So the geometric feature of creping process is relatively uniform in two dimensions (i.e., axial direction and radius direction of Yankee dryer cylinder) of 3-D space.

Second, the paper is an orthotropic material with the principal directions in the circumferential direction (i.e., creping direction), and in the cross section perpendicular to the circumferential direction. Because the circumferential direction is also perpendicular to axis direction, the cross section is parallel to axis of cylinder. So the material property of paper in the axial direction dominates the creping process and the sheet is assumed to be isotropic for

simplicity. Also, the adhesive could be treated as an isotropic material. Hence from the above, the sheet-adhesive structure is uniform in axis direction of the cylinder surface of Yankee dryer.

Third, the thickness of sheet-adhesive structure is quite small compared to the radius of the cylinder, thus the curvature of the cylinder could be relative infinite which makes it a flat surface for analysis purposes.

Based on these three features, creping model can be reasonably reduced as a 1-D problem within which most of sheet end shortening and delamination takes place.

A 1-D modeling of the delamination buckling mechanism in laminated plates has been developed by Chai *et al.* (1981). The loading was in terms of strain instead of stress for the case of fixed grip. The concept of three stages for delamination buckling was proposed and would also be applied in the paper creping model of this dissertation.

Let's review the three stages in delamination buckling demonstrated in Figure 2.3. Stage i is the uncompressed medium of thin film and substrate, stage ii indicates the medium is compressed uniformly with strain ε_0, and stage iii shows the delaminated film is buckled. The delamination of the thin buckled film then could be decided by the energy release rate calculated from the elastic energy stored in the system together with the critical energy release rate required to produce new crack surface.

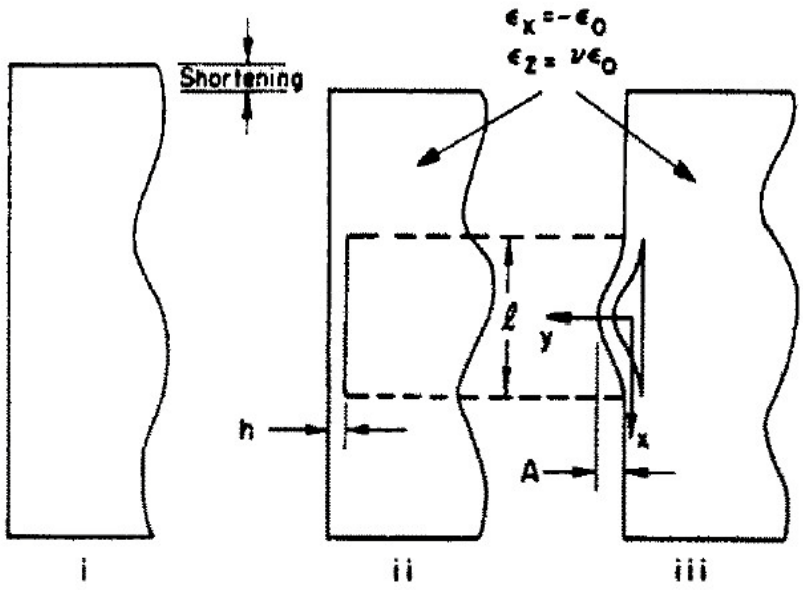

Figure 2.3 Three stages of thin film model (Chai *et al.*, 1981)

The derivation of energy release rate is based on strain and buckling shape's function. According to the beam/plate theory, the authors calculated the critical strain ε_{cr} for buckling state as

$$\varepsilon_{cr} = \frac{\pi^2}{3(1-\nu^2)}\left(\frac{h}{l}\right)^2 \tag{2.9}$$

where h, l, and ν are film thickness, delamination length and Poisson's ratio, respectively. Using the x-y coordinates in stage iii of Figure 2.3, the post-buckling shape is also calculated in a small buckling displacement assumption which yields

$$y = A\frac{1}{2}(1+\cos 2\pi x / l) \tag{2.10}$$

where A is the amplitude of the buckling. The author used the assumption that the delamination length l would not change at the very beginning of buckling from stage ii to stage iii, also used the membrane stress in buckled laminate, and then got

$$(\varepsilon_0 - \varepsilon_{cr})(1-\nu^2)l = \int_{-l/2}^{l/2} \frac{1}{2}\left(\frac{dy}{dx}\right)^2 dx \tag{2.11}$$

So the amplitude is

$$A^2 = (\varepsilon_0 - \varepsilon_{cr})\left(\frac{2l}{\pi}\right)^2 (1-\nu^2) \tag{2.12}$$

The strain energy in stage iii containing membrane and bending energy is given per unit width by

$$U_{iii}(l) = \frac{Ehl(1-\nu^2)}{2}\left(2\varepsilon_0\varepsilon_{cr} - \varepsilon_{cr}^2 + \frac{\nu^2}{1-\nu^2}\varepsilon_0^2\right) \tag{2.13}$$

And the strain energy in laminate in stage ii is calculated as

$$U_{ii}(l) = \frac{1}{2}Ehl\varepsilon_0^2 \tag{2.14}$$

In the case of the delamination introduced prior to the application of strain loading, there exists the energy decrease in stage iii from stage ii when the laminate buckles (i.e., $\varepsilon_0 > \varepsilon_{cr}$) shown in Figure 2.4 (Chai *et al.*, 1981).

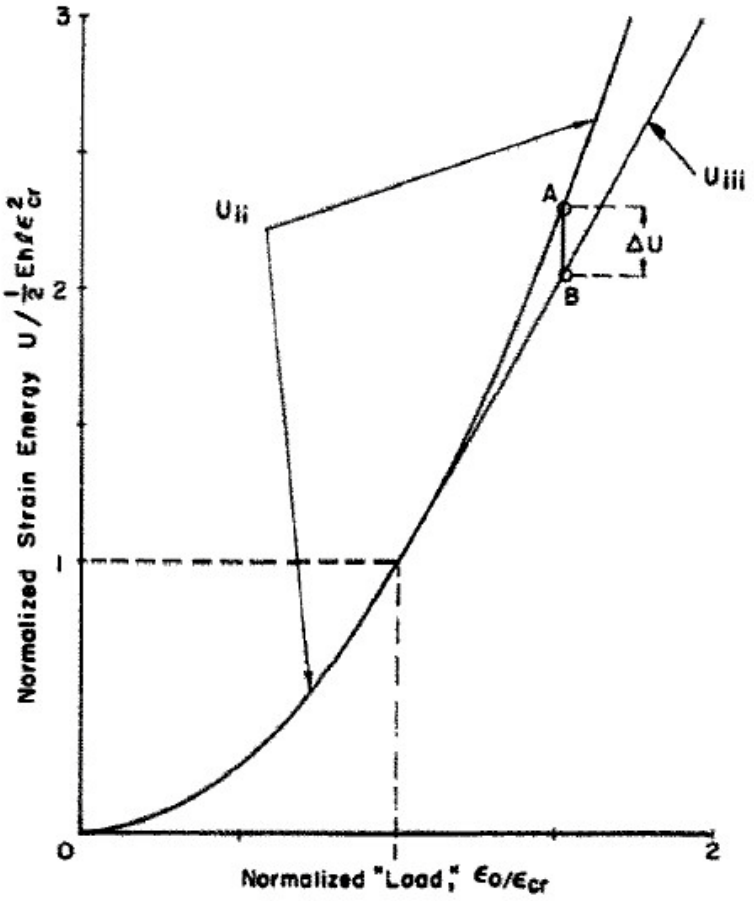

Figure 2.4 Strain energies of the delaminated thin film against the function of strain load (Chai *et al.*, 1981)

The decrease in strain energy of the system after buckling happens is mentioned by Evans and Hutchinson (1984) as well. In this figure, the energy difference ΔU increases if the strain loading continues to increase. The new laminated area would be generated once ΔU reaches or greater than the fracture energy Γ_0 to create new delamination. The fracture energy Γ_0 is only related to the medium property of the thin film in model of Chai *et al.* (1981) here.

Using the definition, the energy release rate is obtained by taking the derivative of system strain energy over the delamination length l

$$G = \frac{Eh(1-\nu^2)}{2}(\varepsilon_0 - \varepsilon_{cr})(\varepsilon_0 + 3\varepsilon_{cr}) \tag{2.15}$$

2.1.4 Validation and Application of Chai's Laminated Plate Model for Creping Analysis

In order to apply the above result to the creping problem, we need to examine the phenomenon of energy decrease in a 1-D validation model for creping problem using Chai's theory and method (Chai *et al.*, 1981). Considering a paper sheet (i.e., equivalent to thin laminate) with a portion delaminated and the rest bonded by adhesive onto a flat substrate, the dissertation presents the validation model in Figure 2.5.

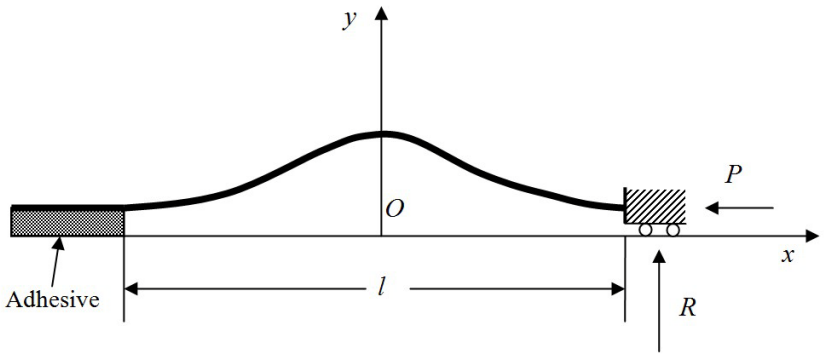

Figure 2.5 1-D validation model for creping analysis

The model is in accordance with the case of the delamination introduced prior to the application of strain loading (Chai *et al.*, 1981). The coordinates and boundary conditions in the thin sheet (laminate) should be the same with those of Chai's model in last section,

except that additional shear and normal stresses effects from adhesive layer are included here. The axial and resultant forces are P and R respectively. The total energy in the validation model would be that of delaminated thin film only added with extra energy in adhesive layer, since the strain in the bonded sheet should be very small and can be reasonably neglected. Chai's concept of three stages is also employed here. The strain in delaminated sheet before buckling could be obtained by

$$\varepsilon_0 = \frac{u}{l+u} \tag{2.16}$$

where u is the shortening of the sheet tip in stage ii. And the critical buckling strain is still given by equation (2.9).

For the energies in stage ii and iii, notations U_{ii}_v and U_{iii}_v are used in difference with U_{ii} and U_{iii} (Chai *et al.*, 1981). U_{ii}_v could be calculated as

$$U_{ii}\_v(l) = \frac{1}{2} Ehl\varepsilon_0^2 + U_{adhesive} \tag{2.17}$$

where E, h, l and ε_0 are in the same definitions with Chai's model, $U_{adhesive}$ is the energy in adhesive layer obtained from the stress solutions (Ramasubramanian *et al.*, 2011). Similarly, U_{iii}_v is calculated as

$$U_{iii}\_v(l) = \frac{Ehl(1-\nu^2)}{2}\left(2\varepsilon_0\varepsilon_{cr} - \varepsilon_{cr}^2 + \frac{\nu^2}{1-\nu^2}\varepsilon_0^2\right) + U_{adhesive} \tag{2.18}$$

The curves of normalized strain energies versus normalized strain load are displayed in Figure 2.6. The normalizing factors for strain energies and strain load are $Ehl\varepsilon_{cr}^2/2$ and ε_{cr}

respectively. It clearly shows that energy of buckled state (stage iii) also decreases from the unbuckled state (stage ii) in the validation model for creping problem using the same assumptions and method in Chai's model. As the strain load ε_0 increases, once the relative strain load $\varepsilon_0 / \varepsilon_{cr} > 1$, there appears an energy difference between unbuckled and buckled states. The difference becomes greater allowing it to approach any critical energy value required to generate new delamination, if the critical value exists.

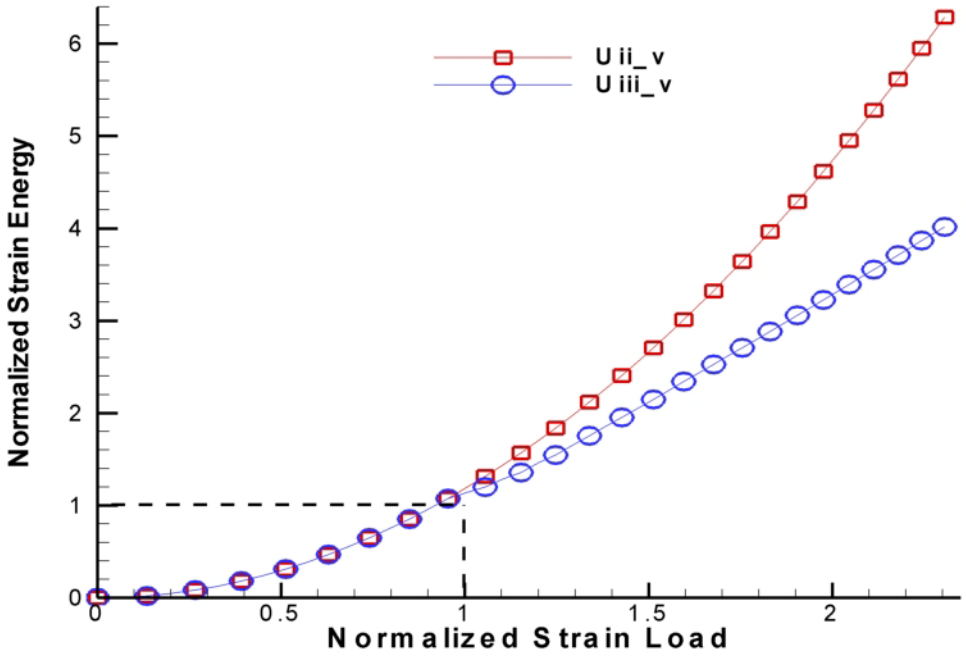

Figure 2.6 Relative strain energies of delaminated area against the relative strain load in validation model

2.1.5 Summary

In this section, a study of compressed thin film by Evans and Hutchinson is reviewed firstly, outlining a fracture based method in solving the problem of thin layer delamination similar to creping process. The study provides a foundation for the energy release rate method for thin layer delamination problem. Some contributions to the theoretical foundation of creping study are explained by comparing the similarities and differences in geometry, structure and loading. Reasons and the need for a fracture energy based method for modeling the creping process are also described.

Then a 1-D modeling of failure in laminated plates by Chai *et al.* (1981) is carefully reviewed and applied as the computational foundation of creping study. The creping model is simplified from the 3-D problem in industry to 1-D in calculation. A validation model with adhesive layer added to Chai's model is presented by this dissertation in order to verify the energy decrease from unbuckled stage to buckled stage in a thin laminated layer. The result shows the consistent energy decrease trend with that of Chai's model.

2.2 Study of Buckling for Creping Problem

Buckling is a failure mode happening abruptly under large compressive stresses. However the stresses in the structure have not exceeded the strength of the material. It can appear in a member of a structure like column or plate. Buckling is also described as elastic instability. When the compressive force or load is applied on a member that is slender enough, and is continuously increased, the member should finally become unstable and undergo a sudden unpredictable lateral deflection. Mathematically, the buckling is a phenomenon generated from the different solutions of the static mechanics equilibrium at that moment. In the beginning, the number of static state equilibrium solution remains one. With the increasing load, the static state equilibrium will have more than one solution by any extra load after certain load value is approached. This certain load is called critical load for buckling.

2.2.1 Simulation of Different Buckling States in the Sheet as Thin Plate

The bucking of a structure member usually has different buckling states represented by buckling mode. If the buckling mode is different, the member's buckling shape should also be different. In order to have a first understanding of how the buckling shape varies from different buckling modes and how the physical variables like displacements, stresses distributed in buckled member, some simulations are demonstrated in FEA results for the different buckling states of a thin plate long enough in compression direction.

Figure 2.7 Von Mises stresses distribution of buckled sheet for different buckling mode.
(a) n=1; (b) n=2; (c) n=3

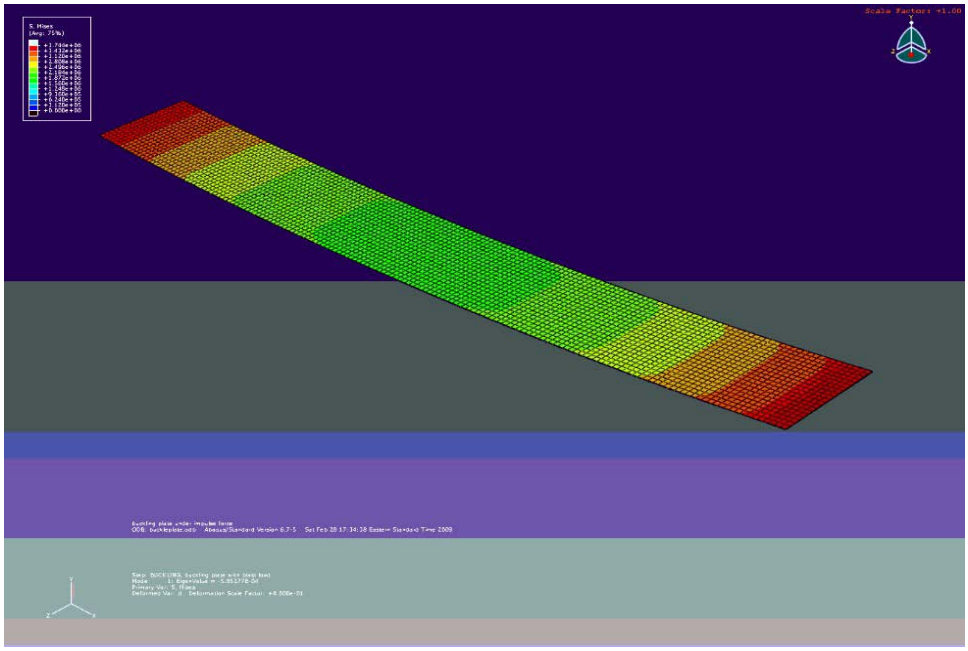

(a)

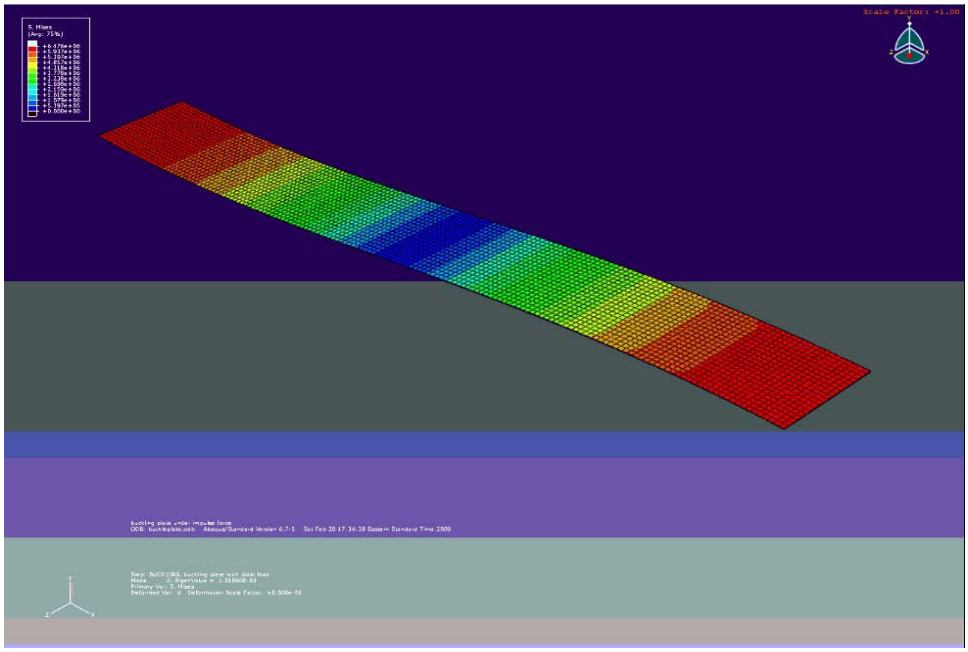

(b)

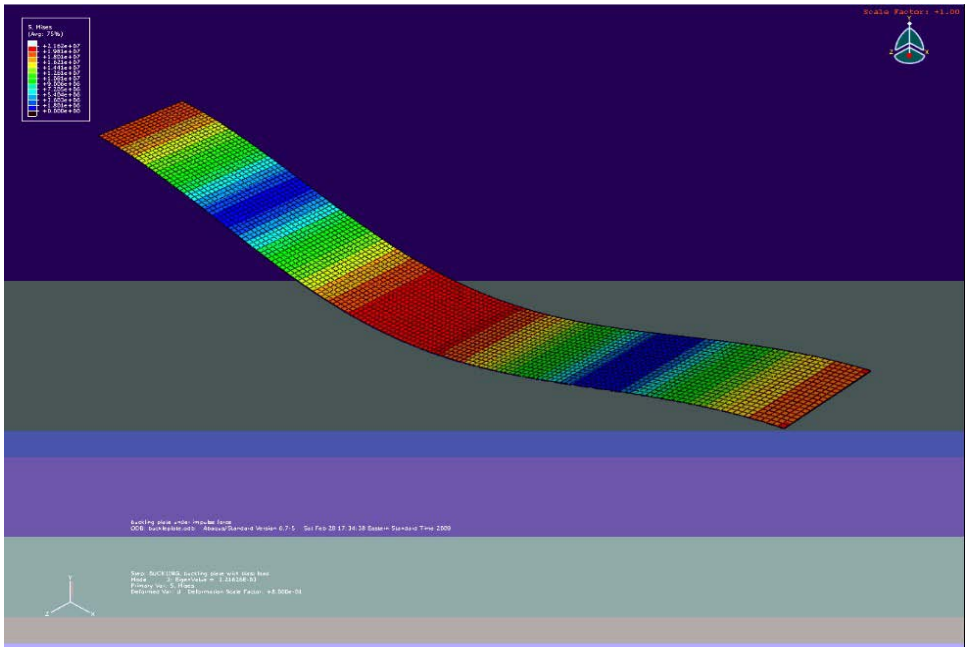

(c)

Figure 2.7 shows the deformations and stresses of a rectangular thin plate simulated by ABAQUS^{TM} FEA model. As a simulation model for the creping sheet, the plate has one side fixed and the opposite side uniformly loaded with critical buckling force. The rest of sides are free. The buckling of plate is conducted in buckling mode $n = 1, 2, 3$ respectively.

In the aspect of deflections, it is verified by this numerical simulation that the buckled sheet plate could have different buckling shapes by different buckling modes. It should be pointed out that higher compressive force generates higher buckling mode with other conditions the same. This indicates the compressive loading is important to determine the buckling shape.

In the aspect of physical parameters, higher stress, strain and strain energy tend to appear near the two opposite edges applied with boundary conditions for all buckling modes. This indicates the significant influences of boundary conditions on the results of buckling analysis. Therefore, the boundary conditions should be defined reasonably and accurately for a creping model which is close enough to the real creping process. The type of boundary conditions would be discussed and developed in the following section.

2.2.2 The1-D Buckling Analysis for Creping Model

Besides the reasons of simplifying the practical 3-D creping problem to a 1-D model mentioned in section 2.1.3, two more assumptions are discussed here to apply the 1-D buckling analysis to the creping model.

The first one is that buckling analysis is still valid in initial condition of creping process. In the industrial production, there is no or very small delamination between the sheet and

Yankee dryer at the beginning of creping process, but as long as the blade hits on the edge of bonded sheet, an original crack across the sheet width would be created. The formation speed of any crack on the interface of adhesive and sheet (i.e., order of sonic speed) should possibly be much faster than the drum surface speed (i.e., order of meters or feet per second) according to the results from both theory (Yu and Yang, 1995; Huang *et al.*, 1998) and experiment (Lambros and Rosakis, 1995; Rosakis *et al.*, 1998). That is to say, the delamination of sheet should have already extended to a very large distance compared to the sheet thickness before the sheet is significantly compressed in the moving direction of drum surface. Therefore, the buckling of the sheet should be possible as long as the sheet is debonded quite a bit at first.

Second, buckling in a long-column is assumed for the sheet in 1-D creping model. Because the sheet is light weight paper (i.e., 32 g/m^2) (Ramasubramanian and Shmagin, 2000) with high slenderness, the ratio of sheet thickness (i.e., equivalent to cross section in 1-D) to sheet debonding length could easily approach to the definition of a long-column. Compared to short-column or medium-column often appears with elastic-plastic property during buckling, long-column assumption would maintain the elastic property in 1-D creping model.

The simplified buckling study for creping process starts with a critical buckling load from Euler's formula (Timoshenko and Gere, 1961) for the column with both ends pinned. The general form of the Euler's formula is given by

$$P^* = \frac{(2n-1)^2 \pi^2 EI}{4l^2}, n = 1, 2, 3, \cdots \tag{2.19}$$

These P^* are actually the series of solutions to the critical loads P_{cr} in different buckling mode n. The buckling shape of column also changes according to different mode number n. Obviously, the smallest critical load P_{cr} is obtained when the mode $n = 1$ as

$$P_{cr} = \frac{\pi^2 EI}{4l^2} \tag{2.20}$$

However, the equations above are limited to only one type of boundary condition. In many cases, especially in the creping process, the boundary conditions are different.

Consider the boundary conditions of 1-D sheet column in simplified creping structure. For the free end of the sheet column, the contact point of creping blade and sheet tip does not have the freedom of motion in transverse direction, because the angle between creping blade surface and drum surface is acute, generating a force that pushes the sheet tip downward onto the drum surface. Meanwhile, the sheet tip is continuously compressed so its longitudinal position is subject to the blade position. However, because the sheet tip is free originally without attached on any surface, it has the rotational freedom of motion at the contact point, which means the moment here is zero. Concluded from the above analysis, the boundary condition type at the contact point of sheet tip should be a pinned end.

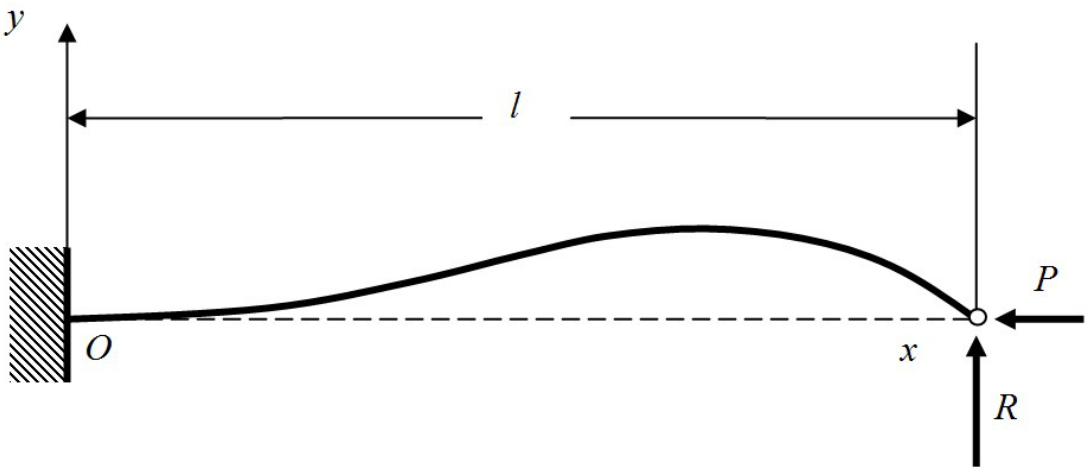

Figure 2.8 Buckling in 1-D sheet column with one end fixed the other pinned

For the other end at the delamination or crack tip, all of sheet beyond that tip is always attached firmly on the drum surface by adhesive. Although adhesive is also assumed as elastic material that should have deformations during creping process, the thickness of adhesive is too small to result in any significant displacement at this end of sheet. So there should not be any freedom of motion. The boundary condition can be assumed as the fixed end.

Figure 2.8 demonstrates the type of boundary conditions of creping model 1-D column assumption, with one end pinned and the other fixed. The column length is l, axial force is P and the reaction for at the pinned end is R.

Except for the boundary conditions at two ends, there are no other external constraints along the column to form a higher buckling mode, so the buckling mode in sheet column is $n=1$.

By applying the extended Euler's formula (Timoshenko and Gere, 1961; Beer *et al.*, 2002) to the creping model, the critical load for sheet column in buckling mode $n = 1$ is

$$P_{cr} = \frac{\pi^2 EI}{(0.699l)^2} = \frac{20.19EI}{l^2} \tag{2.21}$$

where E is elastic modulus, and I is moment of inertia.

The equation (2.21) is valid at the critical state of sheet buckling. However, the buckling shape of sheet should undergo a large deflection before a complete creping length is formed. This strong post-buckling character no longer satisfies the small buckling condition on which the equation (2.21) is based. A detailed adjustment and complement to critical buckling force for creping model would be described later in Chapter 4.

2.3 Conclusions

The fundamental studies of delamination and buckling are presented in this chapter in order to contribute their applications to creping process. In the first part, the two typical models of thin layer delamination buckling using fracture energy method are carefully investigated and validated for application to the creping sheet-adhesive structure problem, suggesting the feasibility in adopting fracture energy method as the basis for creping calculation. In the second part, buckling modes in different shapes are discussed and mode 1 is reasonably selected for solving buckling problems in creping model. Buckling boundary condition type is established based on the known geometry and conditions of the process.

CHAPTER 3

STRESS ANALYSIS OF THE CREPING MECHANICS

3.1 Principle and Assumptions

The creping process can be treated as repeating cycles of delamination and buckling procedure that happen in the thin sheet bonded to a rigid substrate by adhesive layer according to industrial data and experiments. As indicated before, both the sheet and adhesive layer are assumed as elastic media. Out-of-plane shear and Young's modulus, shear and tensile strengths and adhesive thickness are used as parameters to describe the physical properties of adhesive layer. In a similar way, the in-plane Young's modulus, Poisson's ratio, and sheet thickness are the parameters describing paper sheet. In this case, some further assumptions may apply including the in-plane compressive stresses developed in sheet, and the out-of-plane shear stress and normal stresses (opening stress) developed in adhesive layer. All these assumptions could also be traced back to the classic work on cemented joints stress analysis (Goland and Reissner, 1944), and tapered bonded joints and doublers (Duong, 2006). Plane strain is also assumed since the out-of-plane width of creping sheet is very large compared to the in-plane sheet thickness. Therefore applying a stress based approach is a quite straightforward way to start with the creping process study in this dissertation in common computational point of view and would be a necessary foundation to the energy based analysis described in later chapters.

Based on the assumptions above, a description of creping procedure as the framework of stress analysis in a quasi-static manner can be achieved (Ramasubramanian *et al.*, 2011). Once the sheet hits the blade, stresses instantly appear and rapidly increase in both sheet and adhesive layer; meanwhile the maximum stresses in sheet and adhesive should be at the contact position with blade and decrease along the sheet. Then adhesive layer begins to fail at the maximum point as long as the stresses there reach the stress failure criterion. As the blade moves further along the sheet direction the delamination length in sheet-adhesive structure would increase (i.e., crack extends) and the debonded portion of the sheet would probably buckle due to the increasing compressive pressure. After the debonded sheet buckles, the blade continues to move forward and thus increases the amplitude of the buckled sheet without further delamination. The blade would push the end of buckled sheet more and more close to the tip area of delaminated sheet till they meet together. Hence one creping length is formed.

3.2 Mathematical Model in Stress Analysis

3.2.1 Analytical Solutions to Stresses in Adhesive Layer

The stresses in adhesive layer are critical to the study of creping issues, because they are not only directly related to the stress criteria as the determination of delamination in stress analysis but also the basic factors in strain energy calculation for energy based method in the following chapters of this dissertation.

To begin with the stress analysis in adhesive layer, infinitesimal elements of sheet-adhesive system should be introduced first (Ramasubramanian *et al.*, 2011). In Figure 3.1(a), M , F_C and V are the bending moment, axial compressive force and vertical force in the sheet over adhesive layer, respectively. Point O is the geometric center of the infinitesimal sheet element. τ_a is the shear stress on the interface between infinitesimal sheet element and infinitesimal adhesive layer element which is the same value but in opposite direction in Figure 3.1(a) and (b) respectively. The moment equilibrium regarding to point O with high order terms neglected could be (Ramasubramanian *et al.*, 2011),

$$\frac{dM}{dx} - V + \frac{\tau_a t_s}{2} = 0 \tag{3.1}$$

where t_s is the sheet thickness. The axial compressive force equilibrium and the vertical force equilibrium could be investigated as equation (3.2) and (3.3),

$$\frac{dF_C}{dx} - \tau_a = 0 \tag{3.2}$$

$$\frac{dV}{dx} + \sigma_a = 0 \tag{3.3}$$

where, σ_a is the out-of-plane normal stress in the adhesive layer.

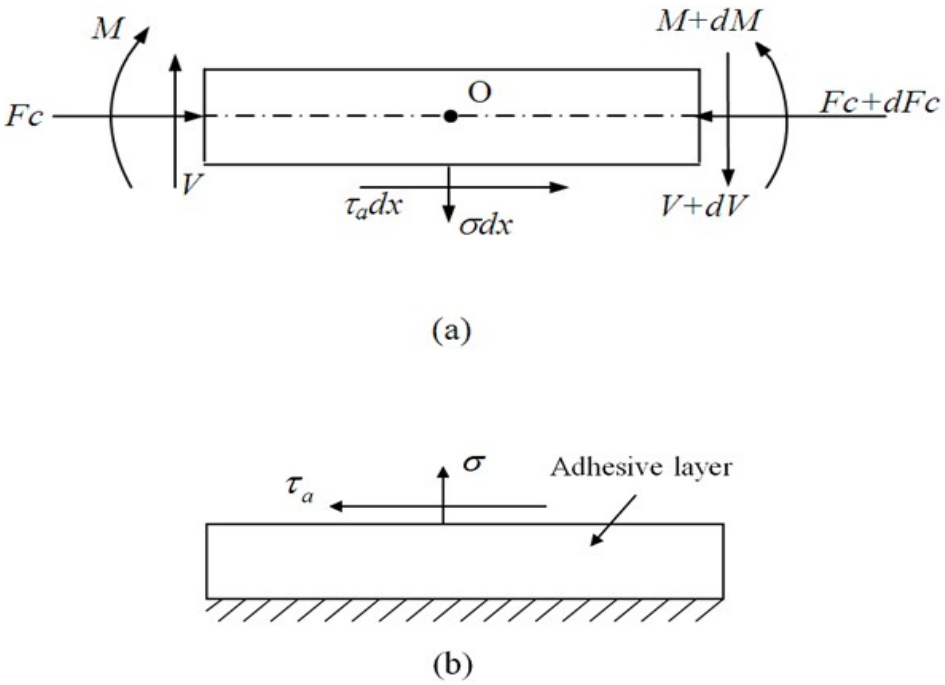

Figure 3.1 Isolated sheet element and the adhesive layer element (a) infinitesimal sheet element and (b) infinitesimal adhesive layer element

In Figure 3.1(b), the thickness of adhesive layer is quite small, meanwhile the displacements of lower surface of adhesive layer should be zero since it is directly adhered to the rigid substrate (i.e., Yankee dryer) surface, so the stresses could be approximately assumed as constant value along the vertical direction in adhesive layer. In this way the vertical and horizontal displacements on the upper surface of adhesive layer (i.e., interface

between sheet and adhesive layer) can be defined as v and u to create the relationship between stresses and moduli which are described in equation (3.4) and (3.5) as

$$\frac{\sigma_a}{E_a} = \frac{v}{t_a} \tag{3.4}$$

$$\frac{\tau_a}{G_a} = \frac{u}{t_a} \tag{3.5}$$

where E_a, t_a, G_a are the Young's modulus, thickness, and shear modulus of the adhesive layer, respectively.

The bending moment on the interface between sheet and adhesive layer could also be derived assuming the sheet is a large out-of-plane thin plate as equation (3.6)

$$\frac{d^2v}{dx^2} = \frac{M}{D} \tag{3.6}$$

where $D = \frac{E_s t_s^3}{12(1-\nu^2)}$ is the flexural rigidity, and E_s, t_s and ν are the Young's modulus, thickness and Poisson's ratio of the sheet, respectively.

The strain of sheet element can be represented on the interface between sheet and adhesive layer and be described in terms of axial force F_C and bending moment M as

$$\frac{du}{dx} = \frac{(1-\nu^2)}{E_s}\left[\frac{F_C}{t_s} - \frac{6M}{t_s^2}\right] \tag{3.7}$$

Two governing equations for the stress analysis are derived through the interface shear and normal stresses in the followings by combining equations from (3.1) to (3.7),

$$\frac{d^3\tau_a}{dx^3} - \frac{4G_a(1-\nu^2)}{E_s t_s t_a}\frac{d\tau_a}{dx} - \frac{6G_a(1-\nu^2)}{E_s t_a t_s^2}\sigma_a = 0 \tag{3.8}$$

$$\frac{d^4\sigma_a}{dx^4} + \frac{E_a}{Dt_a}\sigma_a + \frac{E_a t_s}{2Dt_a}\frac{d\tau_a}{dx} = 0 \tag{3.9}$$

The stress distributions can therefore be obtained by solving the ODEs in equations (3.8) and (3.9), with constant coefficients and appropriate boundary conditions.

For convenience, let $a = \frac{4G_a(1-\nu^2)}{E_s t_s t_a}$, $b = \frac{6G_a(1-\nu^2)}{E_s t_s^2 t_a}$, $c = \frac{E_a}{Dt_a}$, $d = \frac{E_a t_s}{2Dt_a}$, and $e = (bd - ac)$. Eliminating τ_a, the two governing equations can be reduced to a linear seventh order equation in terms of σ_a as

$$(L^7 - aL^5 + cL^3 + eL)\sigma_a = 0 \tag{3.10}$$

where $L = \frac{d}{dx}$. Solving it analytically, the general solution should be in the form of

$$\begin{aligned}\sigma_a = {} & A_0 + A_1 e^{-\beta x} + B_1 e^{-\gamma x}\cos(\delta x) + C_1 e^{-\gamma x}\sin(\delta x) \\ & + A_1' e^{\beta x} + B_1' e^{\gamma x}\cos(\delta x) + C_1' e^{\gamma x}\sin(\delta x)\end{aligned} \tag{3.11}$$

where $\pm\beta$, $\pm(\gamma + i\delta)$, and $\pm(\gamma - i\delta)$ are the eigenvalues of the characteristic equation (3.10). A_0, A_1, A_1', B_1, B_1', C_1, and C_1' are the undetermined coefficients.

Replacing σ_a in equations (3.8) by its solution (3.11), the general solution to τ_a in equation (3.8) should be expressed as

$$\tau_a = A_2 + B_2 e^{-\sqrt{a}x} + C_2 e^{\sqrt{a}x} + (\tau_a)_p \tag{3.12}$$

where A_2, B_2, and C_2 are also the undetermined coefficients, $(\tau_a)_p$ is the particular solution that can be solved as

$$(\tau_a)_p = \frac{-bA_1 e^{-\beta x}}{\beta(\beta^2 - a)} + e^{-\gamma x}\frac{\delta \sin \delta x - \gamma \cos \delta x}{\gamma^2 + \delta^2}\left(\frac{bB_1 A - bC_1 B}{A^2 + B^2}\right) - \frac{bA_0}{a}x - e^{-\gamma x}\frac{\gamma \sin \delta x + \delta \cos \delta x}{\gamma^2 + \delta^2}\left(\frac{bC_1 A + bB_1 B}{A^2 + B^2}\right) \tag{3.13}$$

and here $A = (\gamma^2 - \delta^2) - a$, $B = -2\gamma\delta$.

In order to specify those coefficients in (3.11) and (3.12) and the particular solution of τ_a, some additional conditions need to be included. The general solutions to σ_a and τ_a are required to satisfy not only the governing equations (3.8) and (3.9) but also the boundary conditions (3.14) and (3.15) assuming the bonded sheet is infinite long in *x* direction:

$$\tau_a \to 0 \; as \; x \to \infty \tag{3.14}$$

$$\sigma_a \to 0 \; as \; x \to \infty \tag{3.15}$$

Applying the boundary condition (3.15) in equations (3.11)

$$A_0 = A_1' = B_1' = C_1' = 0 \tag{3.16}$$

and also substituting the general solutions (3.11) and (3.12) back to governing equations (3.8) and (3.9), we have

$$A_2 = B_2 = C_2 = 0 \tag{3.17}$$

The solutions of σ_a and τ_a are then reduced to

$$\sigma_a = A_1 e^{-\beta x} + B_1 e^{-\gamma x}\cos(\delta x) + C_1 e^{-\gamma x}\sin(\delta x) \tag{3.18}$$

$$\tau_a = (\tau_a)_p = \frac{-bA_1 e^{-\beta x}}{\beta(\beta^2 - a)} + e^{-\gamma x}\frac{\delta \sin \delta x - \gamma \cos \delta x}{\gamma^2 + \delta^2}\left(\frac{bB_1 A - bC_1 B}{A^2 + B^2}\right) - e^{-\gamma x}\frac{\gamma \sin \delta x + \delta \cos \delta x}{\gamma^2 + \delta^2}\left(\frac{bC_1 A + bB_1 B}{A^2 + B^2}\right) \tag{3.19}$$

where A_1, B_1 and C_1 are the only three unknown coefficients that need to specify later.

3.2.2 Stress Criteria and Determination of Coefficients

As we know, the stress based failure criteria can be expressed as

$$\left(\frac{\sigma_a}{\sigma_{allow}}\right)^2 + \left(\frac{\tau_a}{\tau_{allow}}\right)^2 = 1 \tag{3.20}$$

where σ_{allow} and τ_{allow} are the normal and shear strengths of the adhesive, respectively. Usually, this criterion is applied at the zone where failure would happen. For convenience, assuming the crack tip in Figure 3.2 is the failure point and is at the origin of the *x* coordinate (i.e., *x*=0) in the creping model, we can get horizontal and vertical equilibriums as

$$F_C = \int_0^\infty \tau_a dx \tag{3.21}$$

$$F_T = \int_0^\infty \sigma_a dx \tag{3.22}$$

where F_C and F_T are the axial compressive force and vertical force generated from the blade impacting against the sheet. The moment which is expressed in equation (3.23) at the crack tip can be related to the product of vertical force F_T and the delamination length l_{cr} as shown in Figure 3.2.

$$M\big|_{x=0} = D\frac{d^2v}{dx^2}\bigg|_{x=0} = \frac{t_a D}{E_a}\frac{d^2\sigma_a}{dx^2} = F_T l_{cr} \tag{3.23}$$

According to the geometry of creping blade, sheet and adhesive layer in stress model, the vertical F_T force can also be described by compressive force F_C

$$F_T = F_C \tan(\theta - \frac{\pi}{2} - \theta_F) \tag{3.24}$$

where μ is friction coefficient, $\theta_F = \tan^{-1}\mu$ is the friction angle, and θ is the creping angle (Ramasubramanian and Shmagin, 2000).

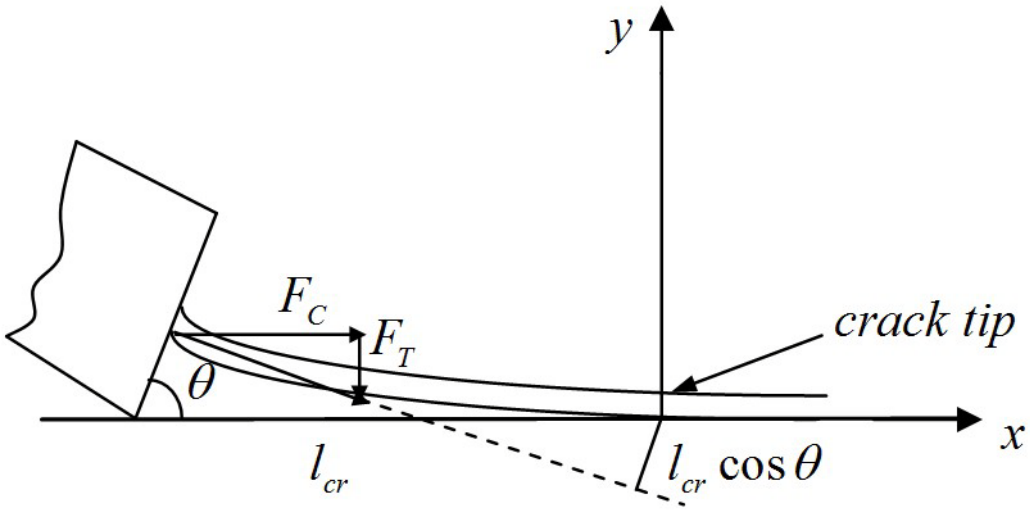

Figure 3.2 Schematic diagram of geometry in stress based creping model and forces applied to the sheet by the blade in stress analysis

Experiments of creping process show that the debonded sheet would experience buckling and continue to collapse in post buckling (Ramasubramanian and Shmagin, 2000).

Because the fiber bonding at the post-buckling stage should probably get ruptured, paper sheet is physically ascribed to the highly inelastic medium under large deformation. But the sheet-adhesive structure in stress based analysis can still be assumed as elastic with small deformations when the buckling in the debonded sheet is about to happen. With this assumption, the post-buckling behavior of sheet and its influences over the sheet-adhesive structure is not investigated here in this stress method. Therefore Euler critical load is applied conveniently to the crack tip as the critical axial compressive (Ramasubramanian *et al.*, 2011). With the fix-free ends boundary conditions applied and also sheet density included to adjust to the fact of a flat heavy lying sheet (Wang, 1984), the buckling load per unit width of the sheet is derived as

$$F_e = \frac{\pi^2 D}{4l_{cr}^2} + \frac{3}{2}\left(1-\frac{2}{\pi}\right)^{\frac{2}{3}}\left(\frac{\rho}{D}\right)^{\frac{2}{3}} D \tag{3.25}$$

where ρ is the density defined by the sheet weight per unit area. Based on the buckling geometry, the shear deformation needs to be incorporated to the sheet buckling in terms of shear modulus G_s of sheet. By this way, the critical buckling load in different buckling modes should be achieved (Timoshenko and Gere, 1961)

$$F_{cr} = \frac{\sqrt{1+4nF_e / t_s G_s} - 1}{2n / t_s G_s} \tag{3.26}$$

where $n = 1, 2, 3, \cdots$ is the buckling mode corresponding to each critical buckling load, respectively. Therefore the buckling condition is obtained as

$$F_C = F_{cr} \tag{3.27}$$

Now to determine the three unknown coefficients A_1, B_1 and C_1 in stress solutions of adhesive layer, several equilibrium equations regarding to stress failure criteria, axial compressive force F_C, vertical force F_T and bending moment M in equation (3.21) through (3.23) are necessarily specified by substituting σ_a, τ_a with their solutions in equation (3.18) and (3.19). Stress criteria and bending moment M should be applied only at the crack tip (i.e., x=0).

For the stress criteria, the normal and shear stresses in adhesive layer at the crack tip can be specified making $x = 0$ in equation (3.18) and (3.19),

$$\sigma_a\big|_{x=0} = A_1 + B_1 \tag{3.28}$$

$$\tau_a\big|_{x=0} = \alpha_{11}A_1 + \alpha_{12}B_1 + \alpha_{13}C_1 \tag{3.29}$$

where

$$\begin{aligned} \alpha_{11} &= \frac{-b}{\beta(\beta^2 - a)}, \\ \alpha_{12} &= \frac{-\gamma bA - \delta bB}{(\gamma^2 + \delta^2)(A^2 + B^2)}, \\ \alpha_{13} &= \frac{\gamma bB - \delta bA}{(\gamma^2 + \delta^2)(A^2 + B^2)} \end{aligned} \tag{3.30}$$

and hence the stress criteria applying at the crack tip is in the form of

$$\left(\frac{A_1 + B_1}{\sigma_{allow}}\right)^2 + \left(\frac{\alpha_{11}A_1 + \alpha_{12}B_1 + \alpha_{13}C_1}{\tau_{allow}}\right)^2 = 1 \tag{3.31}$$

Similarly, the forces and moment equilibrium equations are achieved as,

$$\int_0^\infty \sigma_a dx = \alpha_{21} A_1 + \alpha_{22} B_1 + \alpha_{23} C_1 = F_T \tag{3.32}$$

$$\int_0^\infty \tau_a dx = \alpha_{31} A_1 + \alpha_{32} B_1 + \alpha_{33} C_1 = F_{cr} \tag{3.33}$$

$$\left|M\right|_{x=0} = \left| D \frac{d^2 v}{dx^2} \right|_{x=0} = \left| \frac{t_a D}{E_a} \frac{d^2 \sigma_a}{dx^2} \right|_{x=0} = \alpha_{41} A_1 + \alpha_{42} B_1 + \alpha_{43} C_1 = F_T l_{cr} \tag{3.34}$$

where

$$\alpha_{21} = \frac{1}{\beta}, \alpha_{22} = \frac{\gamma}{\gamma^2 + \delta^2}, \alpha_{23} = \frac{\delta}{\gamma^2 + \delta^2} \tag{3.35}$$

$$\begin{aligned} \alpha_{31} &= \frac{-b}{\beta^2(\beta^2 - a)}, \\ \alpha_{32} &= \frac{(\delta^2 - \gamma^2)bA - 2\gamma\delta bB}{(A^2 + B^2)(\gamma^2 + \delta^2)^2}, \\ \alpha_{33} &= \frac{-(\delta^2 - \gamma^2)bB - 2\gamma\delta bA}{(A^2 + B^2)(\gamma^2 + \delta^2)^2} \end{aligned} \tag{3.36}$$

$$\alpha_{41} = \frac{\beta^2}{c}, \alpha_{42} = \frac{A + a}{c}, \alpha_{43} = \frac{B}{c} \tag{3.37}$$

Obviously, all coefficients α_{ij} are constants from the physical and material properties together with the eigenvalues of the characteristic equation (3.10).

Using Cramer's rule in linear algebra, A_1, B_1 and C_1 are then extracted from equation series (3.32)-(3.34) as the followings:

$$A_1 = \begin{vmatrix} F_T & \alpha_{22} & \alpha_{23} \\ F_{cr} & \alpha_{32} & \alpha_{33} \\ F_T l_{cr} & \alpha_{42} & \alpha_{43} \end{vmatrix} / \det|\alpha| \tag{3.38}$$

$$B_1 = \begin{vmatrix} \alpha_{21} & F_T & \alpha_{23} \\ \alpha_{31} & F_{cr} & \alpha_{33} \\ \alpha_{41} & F_T l_{cr} & \alpha_{43} \end{vmatrix} / \det|\alpha| \tag{3.39}$$

$$C_1 = \begin{vmatrix} \alpha_{21} & \alpha_{22} & F_T \\ \alpha_{31} & \alpha_{32} & F_{cr} \\ \alpha_{41} & \alpha_{42} & F_T l_{cr} \end{vmatrix} / \det|\alpha| \tag{3.40}$$

$$\det|\alpha| = \begin{vmatrix} \alpha_{21} & \alpha_{22} & \alpha_{23} \\ \alpha_{31} & \alpha_{32} & \alpha_{33} \\ \alpha_{41} & \alpha_{42} & \alpha_{43} \end{vmatrix} \tag{3.41}$$

From the solution procedure we can find that the coefficients A_1, B_1 and C_1 are all functions with respect to simply one variable l_{cr}, which means if l_{cr} is specified, A_1, B_1 and C_1 are automatically obtained. The delamination length l_{cr} could be solved non-linearly by substituting A_1, B_1 and C_1 in stress criteria equation (3.31) with their solution expressions (3.38)-(3.40), and further numerically calculated in MATLAB™ software. As long as l_{cr} is solved, all the forces indicated are ready to know in this analysis and hence the stress distribution functions in adhesive layer are finally determined.

3.3 Results and Discussion

The stress analysis is a pre-study as well as the foundation for the energy based approach in creping calculation. By applying the stress criteria and the solved stresses in adhesive layer, the creping process could be now simulated only if the parameters in those constants and coefficients obtained above are known. These parameters include material properties such as Young's modulus and stress strengths in sheet and adhesive, physical properties such as thicknesses of sheet and adhesive layer, density of sheet, and geometry in stress model which is the blade angle. Some other parameters are also included like Poisson's ratio and friction factor.

Table 3.1 shows the parameters in details (Ramasubramanian *et al.*, 2011). Three parameters can be easily measured (i.e., the Young's modulus of sheet, the sheet density, and creping angle) from experiments and referential data. The rest of parameters are evaluated in an appropriate range so as to make the calculated results fit the experimental results as good as they can.

The details of instructions on experiment and some experimental results are described in Chapter 5. All the material properties in this table are marked with $\_ref$ to indicate them as benchmark values in the computational analysis. In the following section, parametric study is conducted to reveal how creping results are influenced by either changing in one parameter at a time or in combinations which should be more meaningful in practice. The crepe

wavelength (i.e., creping length) and the creping force (i.e., axial compressive force on sheet tip) are normalized by the results generated from reference parameters.

Table 3.1 Parameter values for simulation of creping process

Parameters	Notation	Reference values	Units
Paper sheet elastic modulus	E_{s_ref}	100	*MPa*
Adhesive elastic modulus	E_{a_ref}	25	*MPa*
Adhesive shear strength	τ_{allow_ref}	18	*MPa*
Adhesive normal strength	σ_{allow_ref}	18	*MPa*
Creping angle	θ_0	82	*Degree*
Paper sheet thickness	t_{s_ref}	100	μm
Adhesive thickness	t_{a_ref}	2	μm
Paper sheet weight/unit area	ρ	0.163	N/m^2
Poisson's ratio	ν	0.3	——
Friction coefficient	μ	0.3	——

In Figure 3.3, the creping force is F_y as in experimental data notation which is equivalent to F_C in stress model (Ramasubramanian *et al.*, 2011). The reason that creping angle effect was studied firstly is because changing the creping machine's blade angle was

the most convenient way of parameter adjustment in the creping experiment. In this figure, the crepe wavelength gradually decreases as the creping angle increases from 70 degree to its normal position of 90 degree while the creping force continuously increases. Generally speaking, crepe wavelength tends to shrink when creping angle becomes larger. Similar curves can be achieved in most conditions with different other material properties.

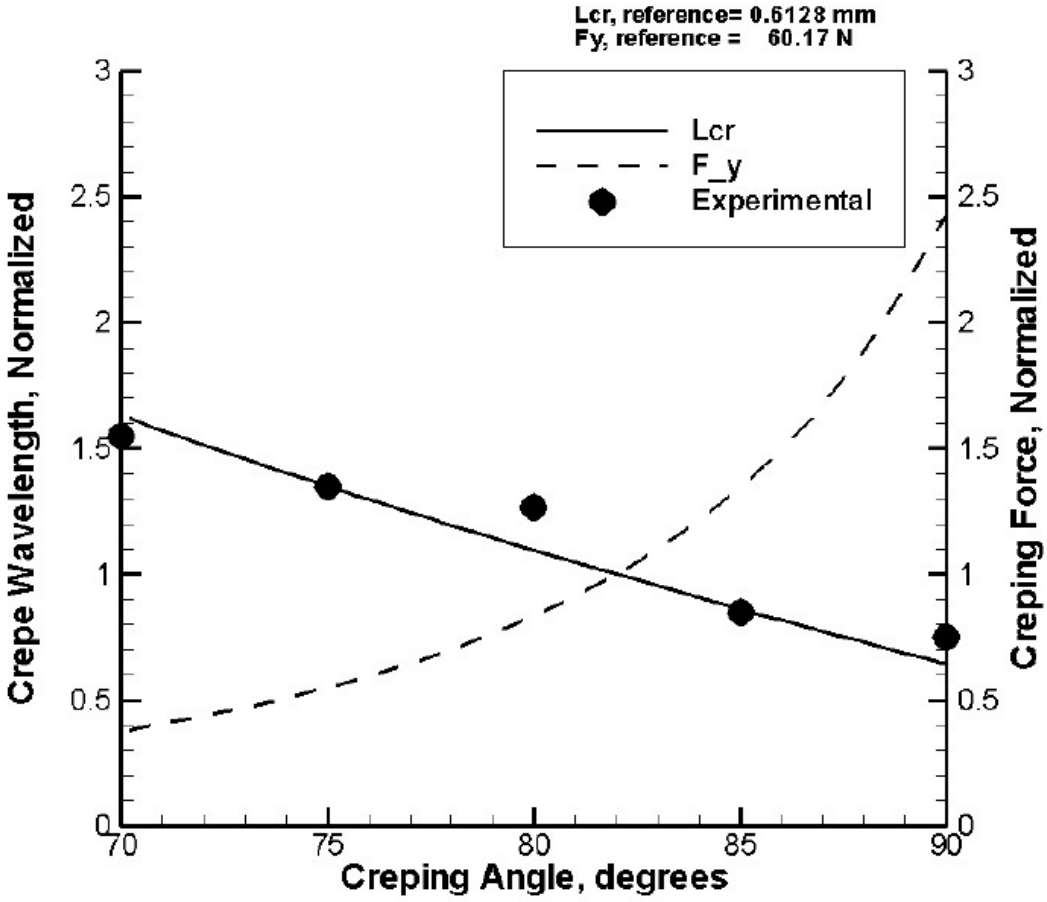

Figure 3.3 Normalized crepe wavelength and creping force w.r.t. creping angle

Figure 3.4 shows a plot of creping force and crepe wavelength versus sheet stiffness for increasing sheet thickness values (Ramasubramanian *et al.*, 2011). The sheet thickness and

the elastic modulus are independently controllable in manufacturing. For a given sheet thickness curve, the crepe wavelength increases when the stiffness of the sheet increases, solely by the increase in elastic modulus.

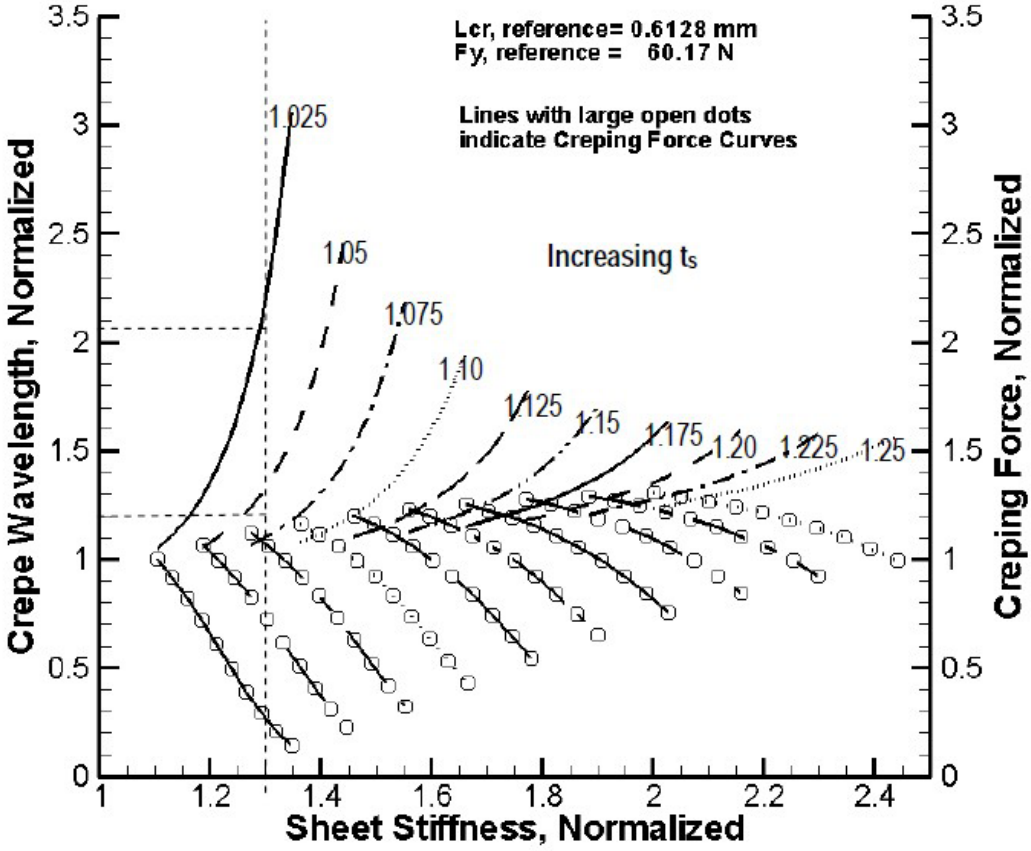

Figure 3.4 Influence of normalized sheet stiffness on crepe wavelength and creping force

As thickness of the sheet increases, the sensitivity of crepe wavelength to elastic modulus decreases, as seen by the gradual flattening of the curves. Further, the crepe wavelength itself decreases with increasing sheet thickness. If we look at values for the crepe wavelength for a normalized stiffness of 1.3, shown by vertical and horizontal markers, a

thicker sheet produces a smaller wavelength than a thinner sheet. There is about 40% reduction in crepe wavelength for only a sheet thickness increase of about 2.5%, if the stiffness is maintained constant. Smaller crepe wavelength is desirable in creped structures. An increase in sheet thickness (for same mass/unit area) while maintaining the same sheet stiffness (decreasing the modulus) is desirable to achieve smaller crepe wavelength.

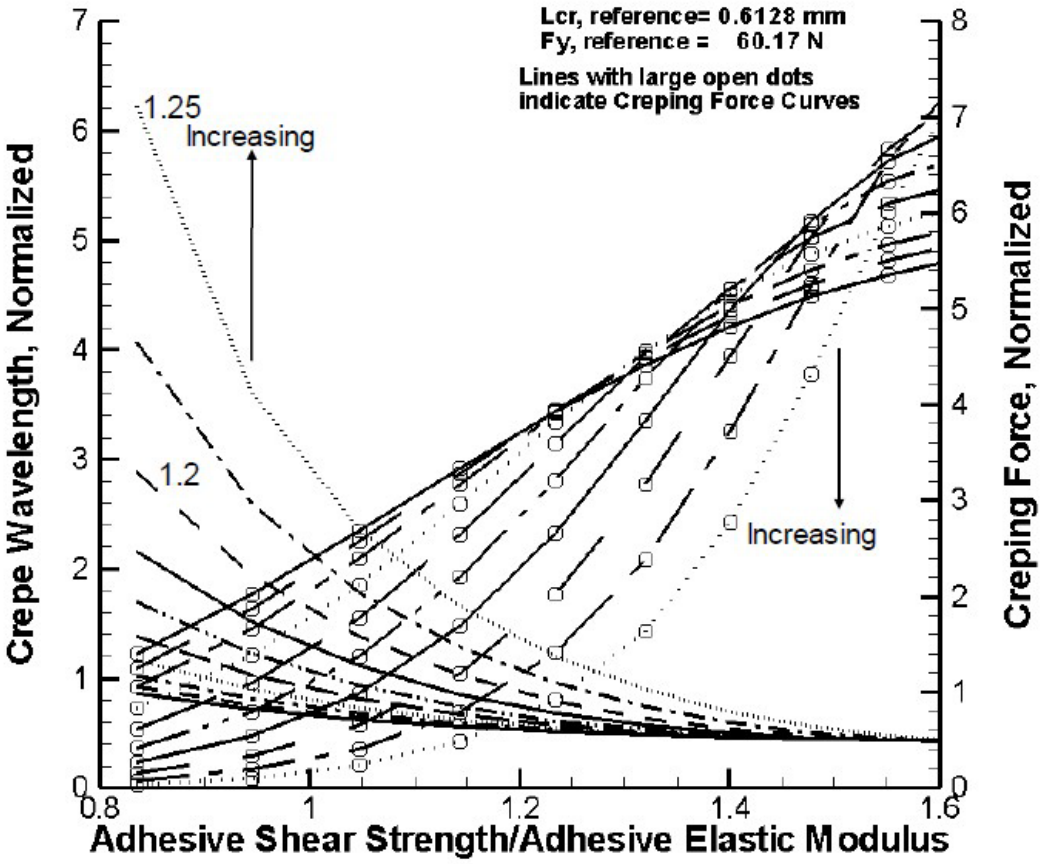

Figure 3.5 Influence of adhesive shear strength and elastic modulus on the crepe wavelength and creping force for different sheet moduli

Figure 3.5 shows the effects of changing adhesive shear strength and simultaneously increasing the adhesive elastic modulus (Ramasubramanian *et al.*, 2011). The non-dimensional adhesive shear strength is changed from 1 to 3 and the non-dimensional modulus is changed from 1 to 1.3. The plot only shows the "adhesive shear strength / adhesive modulus" ratio's range from about 0.85 to 1.6. Curves are plotted for constant sheet modulus, changing from 1.0 to 1.25, noted as "increasing" with arrows. As the sheet elastic modulus increases, crepe wavelength increases.

The sensitivity of crepe wavelength to sheet elastic modulus decreases as the adhesive shear strength / adhesive modulus is increased, indicated by converging lines. The creping force decreases with increasing sheet elastic modulus.

It was also found that the adhesive shear strength alone could not be increased independently without increasing the adhesive modulus. Therefore adhesive strength usually has to decrease together with adhesive modulus to produce a smaller crepe wavelength which is beneficial to the creping results.

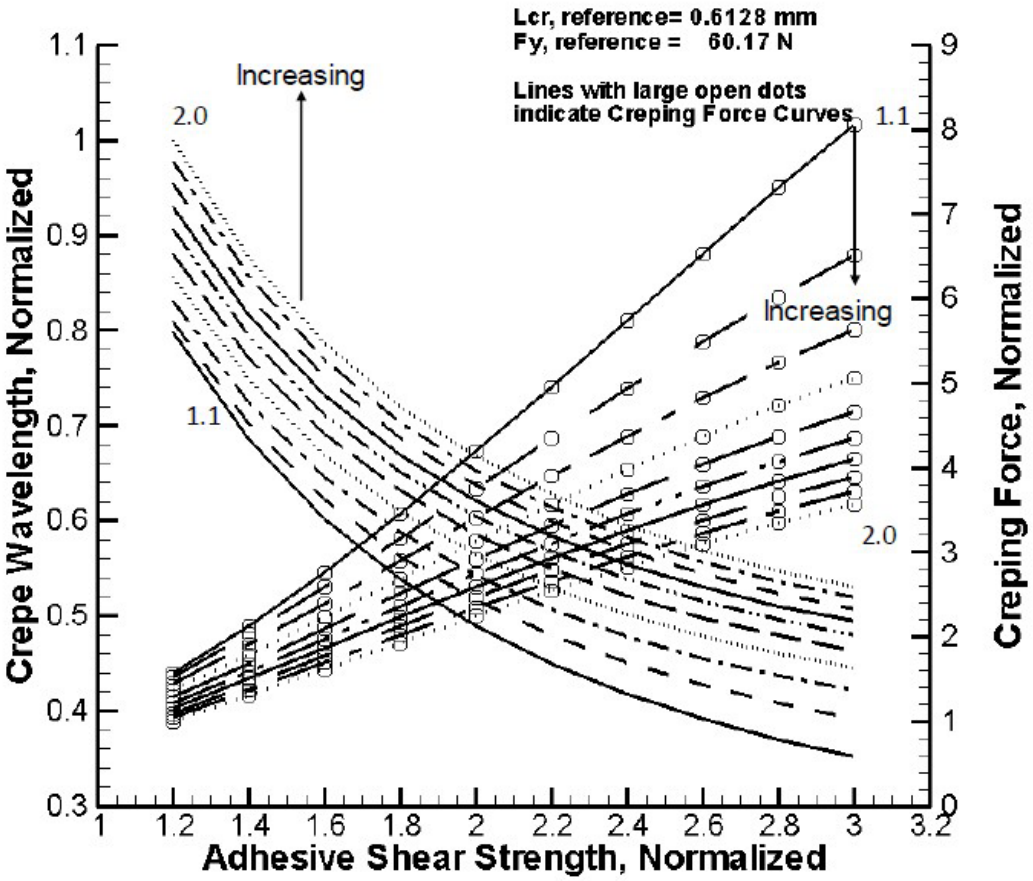

Figure 3.6 Influence of adhesive shear strength on crepe wavelength and creping force for different adhesive moduli

Figure 3.6 shows the effect of increasing adhesive modulus and adhesive shear strength independently while keeping the sheet modulus constant (Ramasubramanian *et al.*, 2011). It is seen that as adhesive modulus increases, the crepe wavelength increases and the creping force decreases. As the adhesive shear strength increases, the crepe wavelength decreases and creping force increases. Adhesive shear strength is changed over a range of 1.2 to 3.0 while

the adhesive modulus is changed from 1.1 to 2. It is observed that the adhesive shear strength has a strong influence in decreasing the crepe wavelength for all adhesive modulus values.

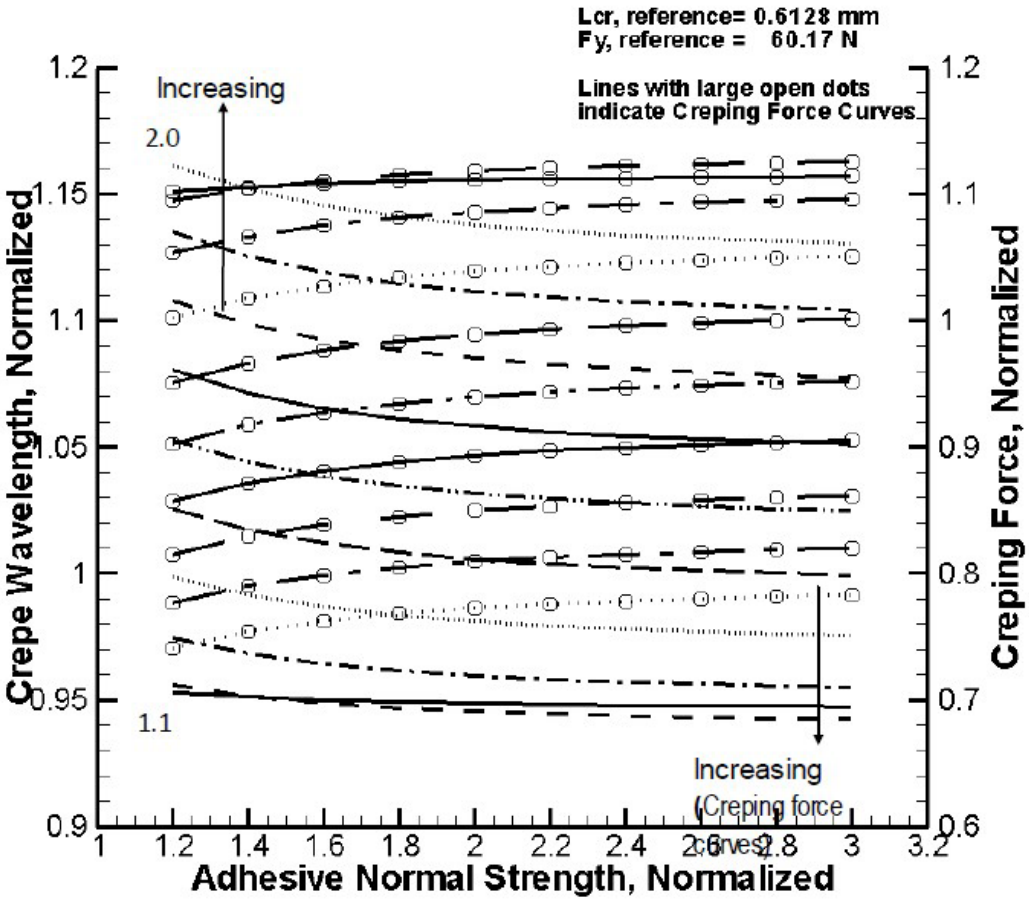

Figure 3.7 Influence of normalized adhesive normal strength on crepe wavelength and creping force for different adhesive elastic moduli

Figure 3.7 shows that the adhesive normal strength does not affect the crepe wavelength over a wide range, if the elastic modulus is kept constant (Ramasubramanian *et al.*, 2011). When elastic modulus of the adhesive increases, the crepe wavelength increases, but relatively small amount, about 20% increase for an increase in adhesive modulus by a factor

of 2. The tensile strength of the adhesive does not play a very important part in the creping process when compared to the shear strength effects discussed earlier.

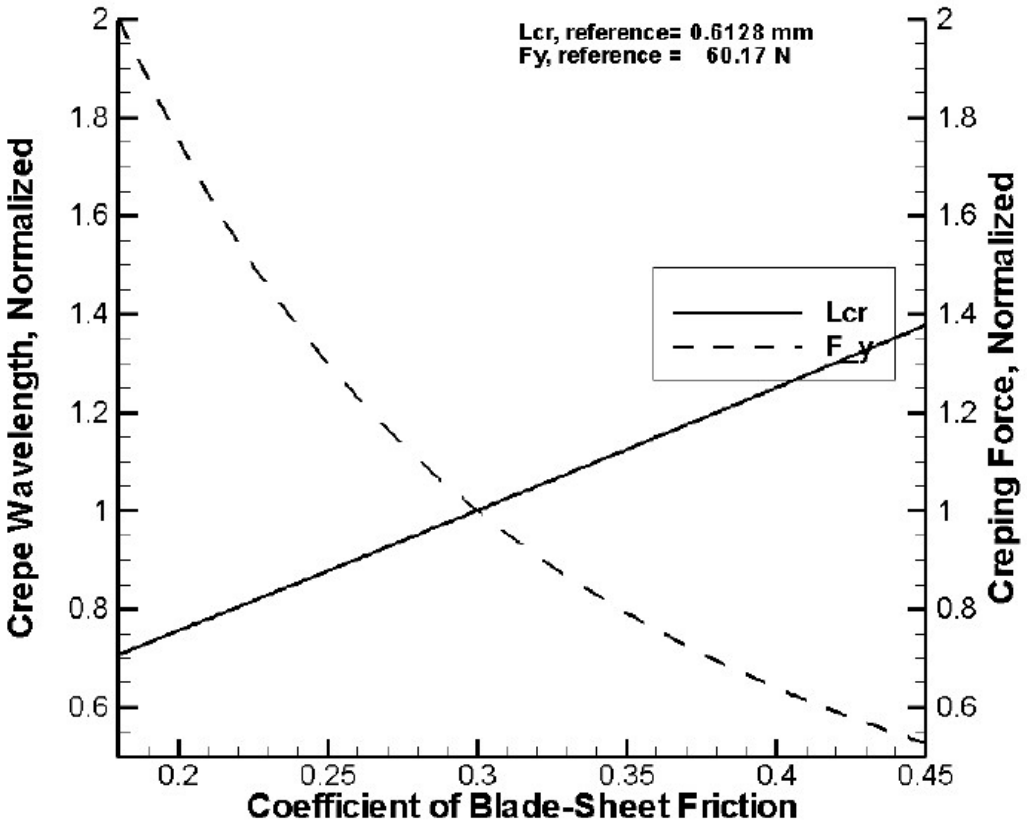

Figure 3.8 Influence of sheet-blade contact friction factor on crepe wavelength and also the creping force

Figure 3.8 shows the effect of blade sheet coefficient of friction on crepe wavelength and creping force (Ramasubramanian *et al.*, 2011). As the coefficient of friction is increased, the crepe wavelength increases and the creping force decreases.

In order to understand the adhesive stress distribution, the shear and normal stresses are plotted in Figure 3.9 as functions of distance from the delamination edge into the adhesive

bond for a range of shear and normal strength values (Ramasubramanian *et al.*, 2011). The adhesive shear stress is maximum at the tip and asymptotically reaches zero within a short distance (about 4×sheet thickness) into the joint. The normal stress starts near zero at the tip and within a very short distance (0.2×sheet thickness) reaches a positive maximum and reverses to a negative minimum within one sheet thickness and asymptotically reaching zero.

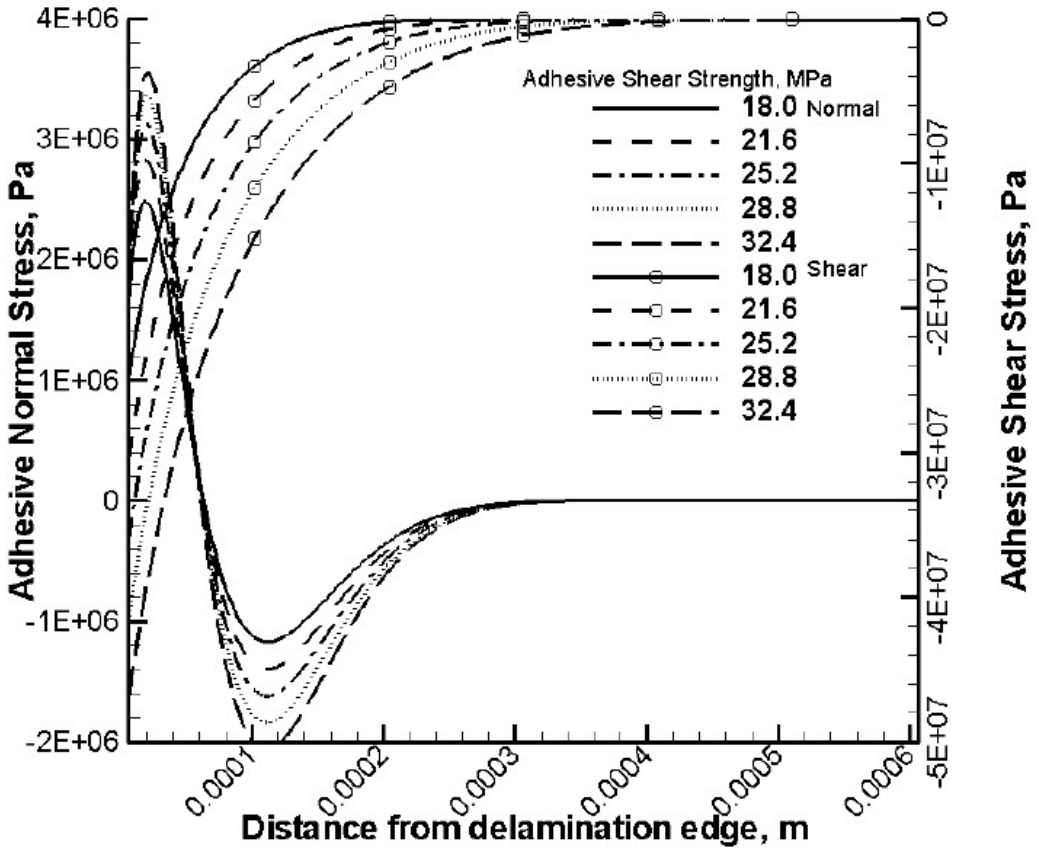

Figure 3.9 Stress functions in adhesive layer w.r.t. distance from the delamination edge (i.e., crack tip, x=0)

However, the peak values of normal stress are on order of magnitude smaller than the shear stress maximum values. These results are consistent with lap joint analysis for single

lap points and doublers (Duong, 2006), showing a peel stress reversal and sharply decreasing shear stress, and both stresses asymptotically reaching zero about $4\times$ adherend thickness. Increasing the shear strength simply increases peak stress levels and the stress decays over a longer bonded length.

3.4 Conclusions

This chapter provides the stress solutions in 1-D creping process as a pre-investigation and a part of theoretical foundation for energy based fracture analysis in the next chapter. The results from stress analysis show agreement with industrial data and observations. Effects of different parameters and their combinations on crepe wavelength are presented and predicted in the model. This is realized by parametric study near some reference values and the study shows that two important parameters influence on the crepe wavelength the most, which are adhesive shear strength and sheet stiffness. For a given sheet stiffness, crepe wavelength should be reduced if adhesive shear strength is higher.

There is also a dependency between adhesive elastic modulus and adhesive shear strength. A ratio of adhesive shear strength to adhesive elastic modulus is applied as a combined parameter in the parametric study of stress analysis. This is because the shear strength should have an overall influence on decreasing crepe wavelength and it can be simultaneously increased to greater values if adhesive elastic modulus also increases, though increased adhesive elastic modulus can also yield a decreased crepe wavelength. Changing the adhesive elastic modulus and its shear strength can be realized by mixing polymers in different proportions. Further, a holding back force on sheet is contributed by friction between the creping blade and the sheet. It results in a greater force applied onto the sheet and increases the crepe wavelength. Therefore a blade surface with low friction factor is necessary in producing finer and softer crepe paper.

CHAPTER 4

FRACTURE ANALYSIS OF DELAMINATION AND BUCKLING IN CREPING PROCESS

In previous chapter the equations for an analytical stress based methodology using a one-dimensional model were developed, and the effects of some process parameters such as creping angle, sheet stiffness, adhesive shear and normal strength, coefficient of blade-sheet friction, were calculated. Even though stress based model helps get an insight into the creping process, it has several disadvantages. It is difficult to validate the model experimentally since the stresses in paper are not easy to measure. The one-dimensional model explains the debonding behavior of paper during creping but it fails to address post-buckling behavior of paper which is important to know in order to optimize the process. Fracture based approach helps resolve the above mentioned issues by addressing buckling and delamination behaviors of the bonded paper during creping process. The fracture based method developed in this chapter complements the one-dimensional method that explains the debonding of paper in the previous chapter.

In the following sections, a physical model is built up and the principle of energy release rate (ERR) criteria (i.e., fracture criteria) is introduced using which the energy based method for the fracture analysis in creping process are developed. Subsequently, the 1-D fracture method is incorporated with axial force P, normal force V and bending moment M at the crack tip as the boundary conditions for the structure of sheet & adhesive. With the fracture criteria for delamination and the strain criterion for buckling, a numerical calculation

program is designed to get the creping length which we recall is the average span of the small waves along the crepe paper. The parameter influences (material properties, blade angle, etc.) on the creping length are studied.

4.1 Physical Model

The physical model is shown in Figure 4.1. Some assumptions are applied to simplify this problem. In geometry, since the Yankee dryer's radius is very large compared to the sheet-adhesive structure, the drum underneath the sheet-adhesive structure (i.e., area in $y < 0$) is assumed with a flat surface. In kinematics, although the sheet-adhesive structure together with rigid substrate (i.e., Yankee drum) is actually moving in a constant speed from right to left impacting onto the left stationary blade, the simulation procedure in this fracture analysis instead assumes the blade is moving from left to right onto the sheet tip while sheet-adhesive structure remains stationary for the convenience in coordinates.

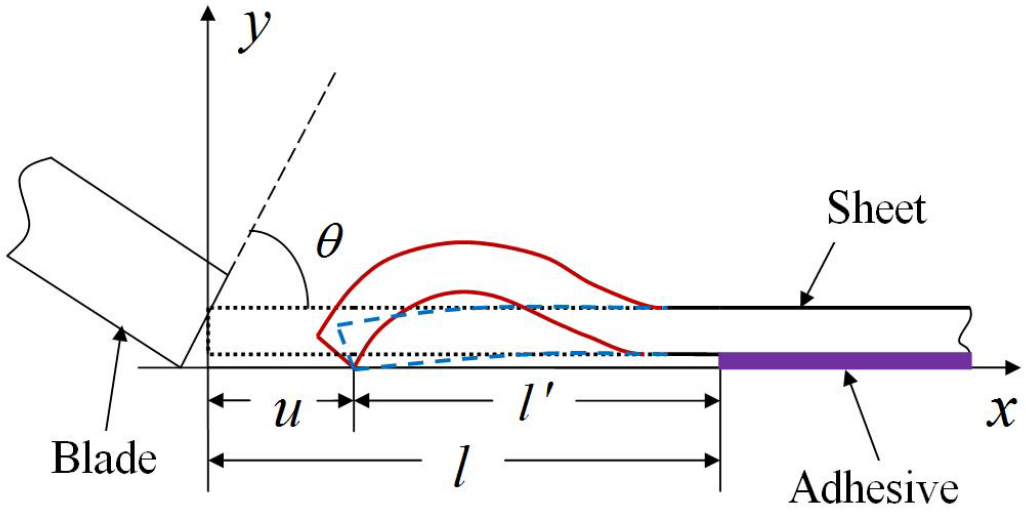

Figure 4.1 Creping model in three stages
• • • : stage i; - - -: stage ii; —: stage iii

The model simplifies the analysis by integrating all environmental factors that receive dissipated energy into itself without considering heat transfer. Hence the dissipated energy

remains in the model of an isolated conservative system which obeys the second law of thermodynamics. Frictionless contact surfaces are assumed in order to attribute all energy dissipation to the results of fracture by delamination and failure by buckling.

The beginning position of blade is set at $x = 0$ before any displacement happens. A debonding region of paper with crack length in *x*-direction and buckling direction in *y*-direction is defined. u is the debonded sheet end displacement, l is the crack length, and $l' = l - u$ is the buckling span of debonded sheet. θ is the blade angle that is fixed during creping process.

Because the dimension of paper width in the out-of-plane direction is very large compared to the paper or adhesive thickness, plane strain conditions apply. Meanwhile, a fixed end boundary condition is also assumed at the crack tip (i.e., $x = l$), since the bonded sheet is relatively infinite long compared to the debonded sheet. Also the elastic material is assumed in this model, and strains are quite small and vanished quickly beyond the crack tip in the bonded sheet since it is firmly attached on the adhesive layer which is very thin. Therefore it is reasonable to neglect the strain energy in bonded portion of the sheet.

According to most of the experiments and studies like laminated plates (Chai *et al.*, 1981), three stages of creping procedure can also be applied to this model: stage i, the debonded sheet is not compressed; stage ii, the structure of sheet-adhesive is compressed but the debonded sheet is not buckled; stage iii, the debonded sheet is buckled.

4.2 Analytical Analysis of Fracture Energy in Creping Process

The creping process in sheet-adhesive structure is generally summarized as delamination and buckling behaviors based on observations from experiments. Therefore the fracture and failure conditions are crucial to the creping analysis studied in this chapter. In the following part of this section, two criteria are presented: one is the fracture criteria that decide if the crack extends or not; the other is the buckling criterion that decides when the debonded sheet buckles with a certain crack length.

4.2.1 Buckling Criterion

In this study, a critical strain for buckling (Chai *et al.*, 1981) is used as buckling criterion in creping process. Firstly, since stage i is not under any compression, there is no force or any energy generated in this stage. Then for the axial strain in free flat sheet,

$$\varepsilon(u,l)=\frac{u}{l} \tag{4.1}$$

and the critical buckling strain can be obtained by assuming the beam/plate theory

$$\varepsilon_{cr}(u,l)=\frac{\pi^2}{3(1-\nu^2)}\left(\frac{t_s}{l'}\right)^2=\frac{\pi^2}{3(1-\nu^2)}\left(\frac{t_s}{l-u}\right)^2 \tag{4.2}$$

where t_s and ν are the sheet thickness and Poisson's ratio. Both $\varepsilon(u,l)$ and $\varepsilon_{cr}(u,l)$ are the functions of variables u and l. The judgment whether the debonded sheet buckles or not relies on which of the two strains is larger as u and/or l change during creping process. If $\varepsilon>\varepsilon_{cr}$, the debonded flat sheet buckles, and the model's stage moves to stage iii. It is necessary to point out that once the flat sheet buckles, the sheet should not recover to a flat

state based on prior observations from both experiments and simulations. This is also based on the thermodynamic assumption in physical model. Since the strain energy of compressed thin film decreases from unbuckled state to buckled state, which is validated in Chapter 2, the buckled sheet would stay at the lower strain energy level according to the minimum total potential energy principle in the isolated system.

4.2.2 Fracture Criteria

The fracture criteria are not applicable for stage i since no force or energy appears in paper-sheet system at this time yet. Fracture criteria are presented in mode I and mode II for stage ii and iii respectively by means of energy release rate in equation (4.3)

$$\frac{G_I}{G_{Ic}} + \frac{G_{II}}{G_{IIc}} = 1 \tag{4.3}$$

G_I, G_{II} are energy release rates of the model system in model I (opening effect) and mode II (shearing effect). Here G_{Ic}, G_{IIc} are the given values of critical energy release rates for mode I and II. In fracture criteria, G_{Ic} and G_{IIc}, which are found to be material properties independent of orientation and specimen geometry, and they could be directly measured from pure peeling or bending experiment or from previous industrial reference data. In this study, these values are assumed and not measured.

With the compressive strain from blade increasing, if the fracture criteria exceed one, the crack should extend to maintain the criteria no larger than one. In stages ii and iii, mode

II term always appears since there will always be shearing effect, but mode I term appears only in stage iii because buckling contributes an opening effect at the crack tip.

The energy release rate terms of G_I, G_{II} need to derive from strain energy terms in the sheet-adhesive structure according to the definition

$$G_{I,II} = -\frac{d(strain\ energy)}{dl} = -\frac{d(U)}{dl} \tag{4.4}$$

Next, the strain energy U should be calculated based on different stage conditions. As the strain energy in bonded sheet is left out, the whole strain energy in sheet-adhesive structure is reduced to separate terms in debonded sheet and adhesive layer. Meanwhile, in stage ii, because the shear effect is dominant in adhesive layer, the normal strain energy term in adhesive layer can also be neglected. So the strain energy U stored in the sheet-adhesive structure in stages ii and iii could be concluded respectively as

Stage ii: $$U_{ii} = U_{ii-sheet} + U_{ad-shear} \tag{4.5}$$

Stage iii: $$U_{iii} = U_{iii-sheet} + U_{ad-normal} + U_{ad-shear} \tag{4.6}$$

where $U_{ii-sheet}$ and $U_{ii-sheet}$ are the strain energies of debonded sheet in stage ii and stage iii, respectively. $U_{ad-shear}$ and $U_{ad-normal}$ are the strain energies calculated from shear and normal stresses in adhesive layer by employing the stress solutions (3.18) and (3.19) obtained in Chapter 3.

For the strain energy $U_{ii-sheet}$, since the debonded sheet undergoes a pure compressive deformation, the strain energy of debonded unbuckled sheet per unit width b is

$$U_{ii-sheet} = \frac{1}{2}\frac{E_s u^2}{l^2} lbt_s = \frac{1}{2}\frac{E_s u^2 t_s}{l} \tag{4.7}$$

where E_s is the sheet elastic modulus, t_s is the sheet thickness.

For the strain energy $U_{iii-sheet}$, it contains membrane energy and the bending energy. This energy term could be derived from buckled layer energy U_{iii} from the result by Chai *et al.* (1981). In the following "Chai" stands for this work and its authors in brief.

In Chai's calculation of U_{iii}, the delamination does not extend during the buckling of laminated layer. So the buckling span l' should be equal to delamination length l in Chai's result. Here only one notation l is used to represent both buckling span and delamination length. For convenience, the origin in Chai's method is adjusted to the left end of buckling span instead of the middle of the span. Also, E, h are the elastic modulus and thickness of the laminated layer in Chai's calculation, corresponding to E_s and t_s in this dissertation.

Firstly, buckling shape function can be obtained as

$$y = \frac{\delta}{2}\left[1 + \cos\frac{2\pi(x - l/2)}{l}\right] \tag{4.8}$$

where δ is the buckling amplitude. This satisfies the geometry and fixed boundary conditions at $x = 0$ and $x = l$ (i.e., $y = 0$ and $y' = 0$).

When $\varepsilon > \varepsilon_{cr}$ the buckling happens and develops. If the crack does not extend during buckling initiation or say l=const, this condition leads to

$$(\varepsilon-\varepsilon_{cr})(1-\nu^2)l=\int_0^l\frac{1}{2}\left(\frac{dy}{dx}\right)^2dx \tag{4.9}$$

where $(\varepsilon-\varepsilon_{cr})l$ is used to form buckled shape. In addition,

$$y'=\frac{\delta}{2}\left[-\frac{2\pi}{l}\sin\frac{2\pi(x-l/2)}{l}\right] \tag{4.10}$$

$$(y')^2=\frac{4\delta^2\pi^2}{4l^2}\sin^2\left[\frac{2\pi(x-l/2)}{l}\right] \tag{4.11}$$

$$(y'')^2=\left[-\frac{\delta\pi}{l}\left(\frac{2\pi}{l}\right)\right]^2\cos^2\frac{2\pi(x-l/2)}{l} \tag{4.12}$$

$$\int_0^l\frac{1}{2}\left(\frac{d}{dx}\right)^2y\,dx=\frac{4\pi^2\delta^2}{8l^2}\int_0^l\sin^2\frac{2\pi(x-l/2)}{l}dx=\frac{4\pi^2\delta^2}{8l^2}\int_0^l\frac{1}{2}\left[1-\cos\frac{4\pi(x-l/2)}{l}\right]dx$$

$$=\frac{4\delta^2\pi^2}{16l^2}\left\{l-\left[\frac{l}{4\pi}\sin\frac{4\pi(x-l/2)}{l}\right]\Bigg|_0^l\right\}=\frac{4\delta^2\pi^2}{16l^2}l=\frac{\delta^2\pi^2}{4l} \tag{4.13}$$

$$\therefore(\varepsilon-\varepsilon_{cr})(1-\nu^2)l=\frac{\delta^2\pi^2}{4l} \tag{4.14}$$

So the buckling amplitude in Chai's result would be

$$\delta^2=(\varepsilon-\varepsilon_{cr})(1-\nu^2)\left(\frac{2l}{\pi}\right)^2 \tag{4.15}$$

Because the buckled laminated plate is assumed to contain membrane energy and bending energy in stage iii of Chai's model, strain energy term U_{iii} on a unit width basis in the buckled laminated layer is

$$U_{iii} = \frac{Ehl}{2}\left[\varepsilon_{cr}^2(1-\nu^2)+\nu^2\varepsilon^2\right]+\int_0^l \frac{Eh^3}{24(1-\nu^2)}\left(-\frac{\delta\pi}{l}\right)^2\left(\frac{2\pi}{l}\right)^2\cos^2\frac{2\pi(x-l/2)}{l}dx \quad (4.16)$$

where E and h are the elastic modulus and the thickness of laminated plate in Chai's model respectively.

The integral part is:

$$\int_0^l \cos^2\frac{2\pi(x-l/2)}{l}dx = \int_0^l\left[\frac{1}{2}+\cos\frac{4\pi(x-l/2)}{l}\right]dx$$

$$= \frac{l}{2}+\frac{l}{4\pi}\sin\frac{4\pi(x-l/2)}{l}\Bigg|_0^l = \frac{l}{2} \quad (4.17)$$

Then we get

$$U_{iii} = \frac{Ehl}{2}\left[\varepsilon_{cr}^2(1-\nu^2)+\nu^2\varepsilon^2\right]+\frac{Eh^3}{24(1-\nu^2)}\left[\left(\frac{2\pi}{l}\right)^2\frac{\pi^2}{l^2}\delta^2\right]\frac{l}{2}$$

$$= \frac{Ehl}{2}\left[\varepsilon_{cr}^2(1-\nu^2)+\nu^2\varepsilon^2\right]+\frac{Eh^3}{24(1-\nu^2)}\left[\frac{2\pi^4}{l^3}\right]\delta^2$$

$$= \frac{Ehl}{2}\left[\varepsilon_{cr}^2(1-\nu^2)+\nu^2\varepsilon^2\right]+\frac{Eh^3}{24(1-\nu^2)}\left[\frac{2\pi^4}{l^3}\right]\left\{(\varepsilon-\varepsilon_{cr})(1-\nu^2)\left(\frac{2l}{\pi}\right)^2\right\}$$

$$= \frac{Ehl}{2}(1-\nu^2)\left[\varepsilon_{cr}^2+\frac{\nu^2}{1-\nu^2}\varepsilon^2\right]+\frac{Eh^3}{24}\left[\frac{2\pi^4}{l^3}\right]\left\{(\varepsilon-\varepsilon_{cr})\left(\frac{2l}{\pi}\right)^2\right\}$$

$$= \frac{Ehl}{2}(1-\nu^2)\left[\varepsilon_{cr}^2+\frac{\nu^2}{1-\nu^2}\varepsilon^2\right]+\frac{Ehl}{2}\frac{\pi^2}{3}\frac{h^2}{l^2}(\varepsilon-\varepsilon_{cr})\cdot 2$$

$$= \frac{Ehl}{2}(1-\nu^2)\left[\varepsilon_{cr}^2+\frac{\nu^2}{1-\nu^2}\varepsilon^2+\frac{\pi^2}{3(1-\nu^2)}\left(\frac{h}{l}\right)^2(\varepsilon-\varepsilon_{cr})\cdot 2\right]$$

$$= \frac{Ehl}{2}(1-\nu^2)\left[\varepsilon_{cr}^2 + \frac{\nu^2}{1-\nu^2}\varepsilon^2 + 2\varepsilon_{cr}(\varepsilon - \varepsilon_{cr}) \right]$$

$$= \frac{Ehl}{2}(1-\nu^2)\left[2\varepsilon_{cr}\varepsilon - \varepsilon_{cr}^2 + \frac{\nu^2}{1-\nu^2}\varepsilon^2 \right] \tag{4.18}$$

By replacing E, h and l with E_s, t_s and l', in this dissertation, the strain energy term $U_{iii-sheet}$ per unit width of sheet should be obtained as

$$U_{iii-sheet} = \frac{E_s t_s l'}{2}(1-\nu^2)\left[2\varepsilon_{cr}\varepsilon - \varepsilon_{cr}^2 + \frac{\nu^2}{1-\nu^2}\varepsilon^2 \right] \tag{4.19}$$

For the strain energy U_{ad} in adhesive, after getting the solutions of σ_a and τ_a, one can obtain the shear and normal strain energies per unit width in the adhesive layer beyond crack tip $x = l$ to the infinite by equation (4.20) and (4.21):

$$U_{ad-shear} = \int U_0 dV = \int_l^\infty \frac{\tau_a^2 t_a}{2G_a} dx \tag{4.20}$$

$$U_{ad-normal} = \int U_0' dV = \int_l^\infty \frac{\sigma_a^2 t_a}{2E_a} dx \tag{4.21}$$

Now applying these energy terms in equation (4.4) yields the energy release rates in stage ii and stage iii respectively:

Stage ii: $$G_{II} = -\frac{d(U_{ii-sheet} + U_{ad-shear})}{dl} = G_{ii-sheet} + G_{ad-shear} \tag{4.22}$$

Stage iii: $$\begin{cases} G_I = -\dfrac{d(U_{iii-sheet} + U_{ad-normal})}{dl} = G_{iii-sheet} + G_{ad-normal} \\ G_{II} = -\dfrac{d(U_{ad-shear})}{dl} = G_{ad-shear} \end{cases} \tag{4.23}$$

where the energy release rate G corresponds to the energy term U with the same subscript.

Then the calculations of energy release rates per unit width are quite straightforward. For brevity, only $G_{ii-sheet}$ and $G_{iii-sheet}$ are calculated here:

For the calculation of $G_{ii-sheet}$, we can get

$$G_{ii-sheet} = -\frac{dU_{ii-sheet}}{dl} = \frac{1}{2}\frac{E_s u^2 t_s}{l^2} \tag{4.24}$$

For the calculation of $G_{iii-sheet}$, we should begin from the strain ε and critical buckling strain ε_{cr}, and apply them to the derivative of $U_{iii-sheet}$ with respect to l.

As we know,

$$\varepsilon_{cr} = \frac{\pi^2}{3(1-\nu^2)}\left(\frac{t_s}{l'}\right)^2 = \frac{\pi^2}{3(1-\nu^2)}\left(\frac{t_s}{l-u}\right)^2 \qquad \varepsilon = \frac{u}{l} \tag{4.25}$$

and $\varepsilon'_{cr} = d\varepsilon_{cr} / dl$, $\varepsilon' = d\varepsilon / dl$, which can be written as:

$$\varepsilon'_{cr} = \frac{\pi^2 t_s{}^2}{3(1-\nu^2)}\left(\frac{-2}{l'^3}\right)\frac{dl'}{dl} = \frac{\pi^2}{3(1-\nu^2)}\left(\frac{t_s}{l'}\right)^2\left(\frac{-2}{l'}\right)\cdot 1 = -\frac{2\varepsilon_{cr}}{l'} \tag{4.26}$$

$$\varepsilon' = -\frac{u}{l^2} = -\frac{\varepsilon}{l} \tag{4.27}$$

Applying equation (4.19) to its derivative with respect to l then yields

$$
\begin{aligned}
-\frac{\partial U_{iii-sheet}}{\partial l} &= -\frac{E_s t_s l'}{2}(1-\nu^2)\left[2\varepsilon\varepsilon'_{cr} + 2\varepsilon'\varepsilon_{cr} - 2\varepsilon_{cr}\varepsilon'_{cr} + \frac{2\nu^2}{1-\nu^2}\varepsilon\varepsilon'\right] \\
&\quad -\frac{E_s t_s}{2}(1-\nu^2)\left[2\varepsilon_{cr}\varepsilon - \varepsilon_{cr}^2 + \frac{\nu^2}{1-\nu^2}\varepsilon^2\right] \\
&= -\frac{E_s t_s l'}{2}(1-\nu^2)[2\varepsilon\left(\frac{-2\varepsilon_{cr}}{l'}\right) + 2\varepsilon_{cr}\left(\frac{-\varepsilon}{l}\right) \\
&\quad -2\varepsilon_{cr}\left(\frac{-2\varepsilon_{cr}}{l'}\right) + \frac{2\nu^2}{1-\nu^2}\varepsilon\left(\frac{-\varepsilon}{l}\right)] \\
&\quad -\frac{E_s t_s}{2}(1-\nu^2)\left[2\varepsilon_{cr}\varepsilon - \varepsilon_{cr}^2 + \frac{\nu^2}{1-\nu^2}\varepsilon^2\right] \\
&= -\frac{E_s t_s}{2}(1-\nu^2)[-4\varepsilon\varepsilon_{cr} - 2\frac{l-u}{l}\varepsilon\varepsilon_{cr} + 4\varepsilon_{cr}^2 - \frac{2\nu^2}{1-\nu^2}\frac{l-u}{l}\varepsilon^2 \\
&\quad +2\varepsilon\varepsilon_{cr} - \varepsilon_{cr}^2 + \frac{\nu^2}{1-\nu^2}\varepsilon^2] \\
&= \frac{E_s t_s}{2}(1-\nu^2)\left[\frac{4l-2u}{l}\varepsilon\varepsilon_{cr} - 3\varepsilon_{cr}^2 + \frac{\nu^2}{1-\nu^2}\frac{l-2u}{l}\varepsilon^2\right] \qquad (4.28)
\end{aligned}
$$

$$
G_{iii-sheet} = -\frac{\partial U_{iii-sheet}}{\partial l} = \frac{E_s t_s (1-\nu^2)}{2}\left[\frac{4l-2u}{l}\varepsilon\varepsilon_{cr} - 3\varepsilon_{cr}^2 + \frac{\nu^2}{1-\nu^2}\frac{l-2u}{l}\varepsilon^2\right] \qquad (4.29)
$$

The result of energy release rate calculated in equation (4.29) is an application and widespread use of the energy release rate in a laminated plate (Chai *et al.*, 1981), because in this dissertation the delamination length l is a variable of the strain function $\varepsilon(u,l)$ and critical buckling strain function $\varepsilon_{cr}(u,l)$ whereas l is assumed constant which yields $\varepsilon' = d\varepsilon / dl = 0$, $\varepsilon'_{cr} = d\varepsilon_{cr} / dl = 0$ in Chai's model. If applying $\varepsilon' = 0$, $\varepsilon'_{cr} = 0$ into equation (4.28), the energy release rate for the thin laminated plate in the same medium of a thick substrate could be reduced to

$$G = \frac{E_s t_s (1-\nu^2)}{2}(\varepsilon - \varepsilon_{cr})(\varepsilon + 3\varepsilon_{cr}) \tag{4.30}$$

which is the same form in Chai's result. Hence the calculation of energy release rate in this fracture model should be consistent with that by Chai *et al.* (1981).

4.2.3 Boundary Conditions

The boundary conditions are expressed by axial force P, vertical force V, and bending moment M at the crack tip. Once the mechanics equilibrium satisfied, they can be easily set up for stage ii in equation (4.31)-(4.33) and stage iii in equation (4.34)-(4.36) respectively.

BCs in Stage ii:

$$P = \frac{E_s u b t_s}{l} \tag{4.31}$$

$$V \cong 0 \tag{4.32}$$

$$M \cong P \cdot (t_a + \frac{1}{2} t_s) \tag{4.33}$$

where t_s, t_a are the thicknesses of sheet and adhesive layer, respectively.

BCs in Stage iii:

$$P \cong P_{cr} \tag{4.34}$$

$$V = \frac{M}{l'} = \frac{M}{l-u} \tag{4.35}$$

$$M = D \cdot \left. \frac{d^2 v}{dx^2} \right|_{x=l} \tag{4.36}$$

where $D = \frac{E_s t_s^3}{12(1-\nu^2)}$, v is the vertical displacement of buckled sheet.

In 1-D buckling, sheet is assumed as a column with crack tip end fixed and the blade contact end pinned, and the critical axial force P_{cr} of an Euler column can be calculated using the expression $P_{cr} = K(p)^2 E_s I_s / L_e^2$, assuming that paper undergoes large buckling deflection (Timoshenko and Gere, 1961). $K(p)$ is the complete elliptic integral of the first kind, $p = \sin(\theta/2)$, effective buckling length $L_e = 0.699l/2$, E_s is the sheet modulus , I_s is the moment of inertia of sheet, and b is the unit width of sheet.

4.2.4 Creping Procedure in Computational Model

The 1-D computational model is built up as an iterative approach. An initial crack length l_0 with a small value as an imperfection in the numerical model is assumed in order to help give the original condition where the calculation could start. During the iteration cycles, after an increase of u by a constant step Δu in each cycle, a new crack length l would be calculated and transmitted to the next cycle until the sheet buckling span $l' = l - u$ reaches $2t_s$ which is two times of sheet thickness. In physics this means the buckled sheet is overlapped by itself forming a large buckling deflection at the crack tip.

The whole process can be schematically displayed in Figure 4.2 and summarized as the following four typical periods consequently,

(1) Pre-buckling. There is no buckling and no crack extension but only the elastic shortening in debonded sheet.

(2) Crack extension. The crack begins and continues to extend inward the bonded area (i.e., new crack is in area marked by horizontal line pattern near crack tip in Figure 4.2(b)) meanwhile the debonded sheet may remain flat.

(3) Buckling. The debonded sheet buckles, and buckling shape keeps changing.

(4) Approaching creping length. Once l' reaches $2t_s$, the creping length is approached.

Figure 4.2 Sketches of the four periods in creping process. (a): period (1); (b): period (2); (c): period (3); (d): period (4).

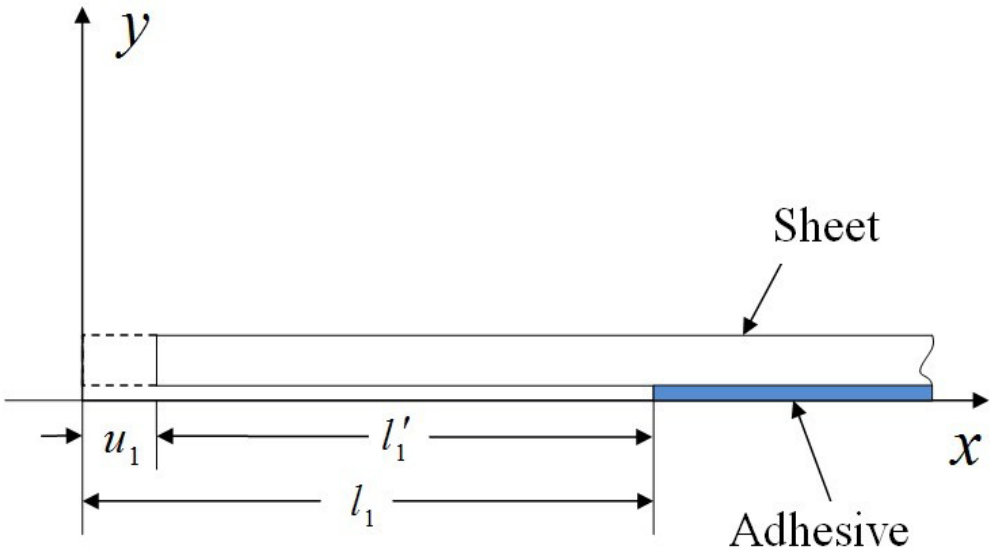

(a)

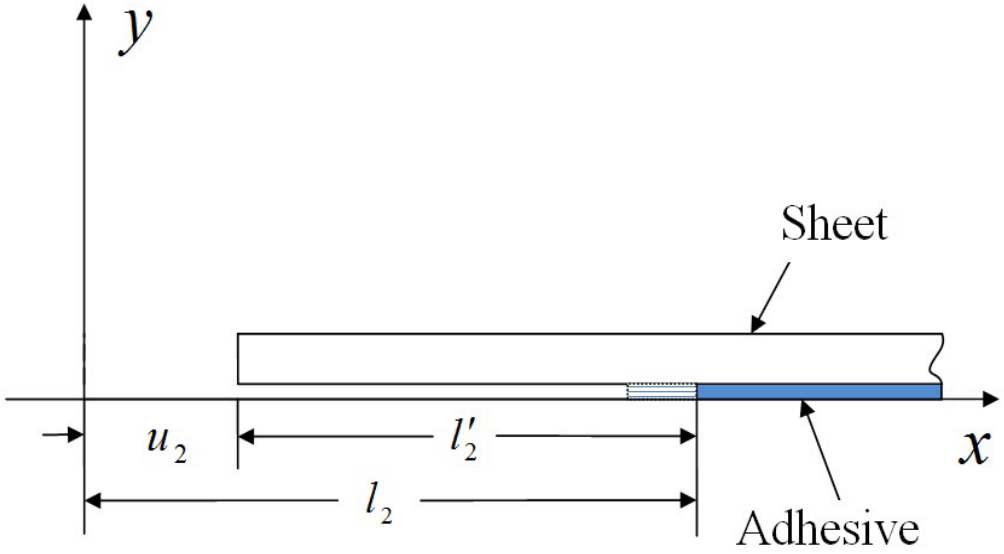

(b)

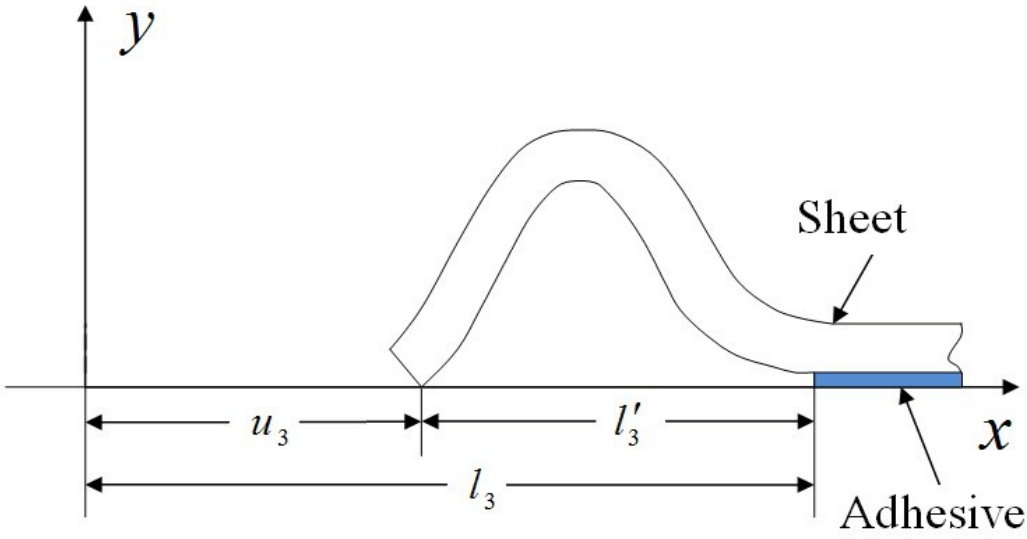

(c)

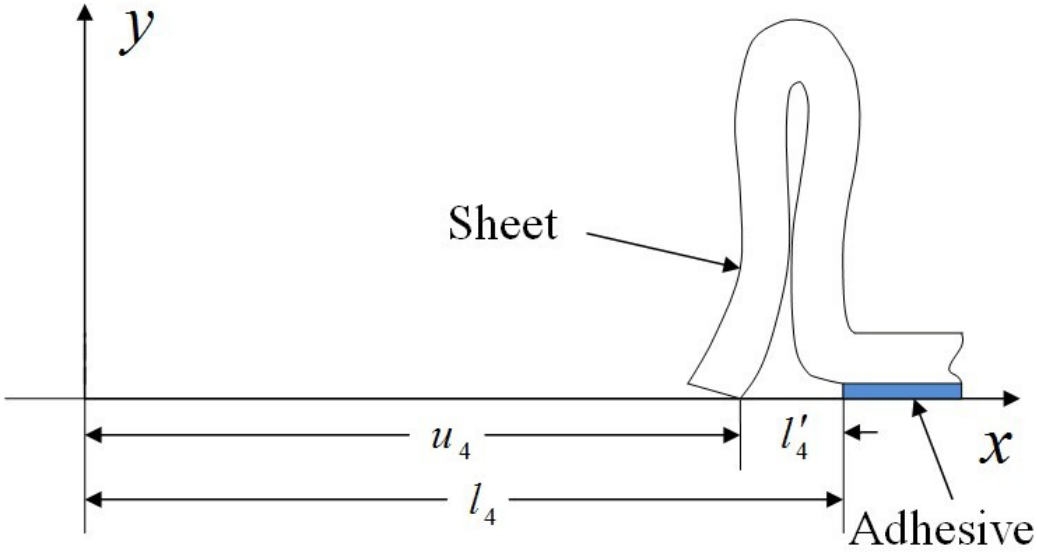

(d)

Now we can design a program to simulate this process and get the final creping length. The program is developed in MATLAB™ code. In order to refer to the three stages of physical model that have been mentioned above, the code is also designed into mainly three parts, which are: Part(a): Initial condition definition (stage i); Part(b): Compression in unbuckled sheet and crack extension (stage ii, period (1), (2)); Part(c): Sheet buckles and keeps changing shape until creping length is reached (stage iii, periods(3), (4)).

The following is a summary of the designed program. There is a line mark in front of each command line for clear instruction.

**********Program begins**********

Part(a):

00……an initial crack length l_0 is assumed, u begins with $u = l_0$, increment is Δu .

Continues to Part(b):

01……while $\varepsilon(u,l) < \varepsilon_{cr}(u,l)$

02……increase u to $u + \Delta u$

03……calculate $G_{II}(u + \Delta u, l)$ only

04……...if $G_{II}(u + \Delta u, l) \big/ G_{IIc} > 1$, calculate Δl to satisfy $G_{II}(u + \Delta u, l + \Delta l) \big/ G_{IIc} = 1$

05……update l to $l + \Delta l$

06……end

Continues to Part(c):

07……while $l-u<2t_s$

08……increase u to $u+\Delta u$

09……calculate $G_I(u+\Delta u,l)$ and $G_{II}(u+\Delta u,l)$

10……if $G_I(u+\Delta u,l)/G_{Ic}+G_{II}(u+\Delta u,l)/G_{IIc}>1$,

calculate Δl to satisfy $G_I(u+\Delta u,l+\Delta l)/G_{Ic}+G_{II}(u+\Delta u,l+\Delta l)/G_{IIc}=1$

11……update l to $l+\Delta l$

12……end

13……export final creping length

14……export data history of ε, ε_{cr}, l .vs. u ,etc.

**********Program ends**********

Detailed MATLAB™ code is provided only with the main program which can be found in the Appendix A.

4.3 Results and Discussion

The computational model is evaluated in three steps: the first step is the delamination history in a single creping wave formation and understanding the influence of fracture criteria on creping length; the second step is the parametric study to determine how different material and physical properties affect the creping length; and the third step is to compare with FEA model developed in ABAQUS™. In this dissertation, numerical algorithms of energy based fracture analysis on creping process is developed by a MATLAB™ coding environment and the results are demonstrated and discussed below. All of the reference parameters used here are the same as in Table 3.1, except for specific instructions.

4.3.1 Delamination History and Critical Fracture Values Study

Earlier numerical or analytical analysis (Sun, 2000; Ramasubramanian *et al.*, 2011) has shown that computational results are consistent with experimental observations: the creping process is a combination of crack extension and buckling. In this process the crack extension usually happens first and then or meanwhile the debonded sheet buckles and continues to change the buckling shape until reaches the creping length without ever becoming flat again.

In order to simulate this process more thoroughly and to obtain the creping length, the numerical calculation of fracture energy method induces a step length Δu for the sheet end displacement. It simulates blade's constant and continuous movement onward the sheet. Every time when the sheet end displacement increases with Δu , the sheet is compressed by a distance of the same length. The step length is mandatorily decided and kept constant during

each creping simulation. The step length discretizes the practically continuous blade movement into discontinuous points for numerical calculation along the moving direction. Obviously, if the step length is smaller, the number of scattered points is greater in the same blade moving distance. That is to say the numerical result is closer to physical fact with a smaller step length. But the calculation amount would be increased if the points are too many. Therefore it is necessary to investigate what value of step length is appropriate for an efficient but also accurate numerical calculation in the following studies.

Different values of step length are attempted in the same numerical program in order to know their effects on creping length result.

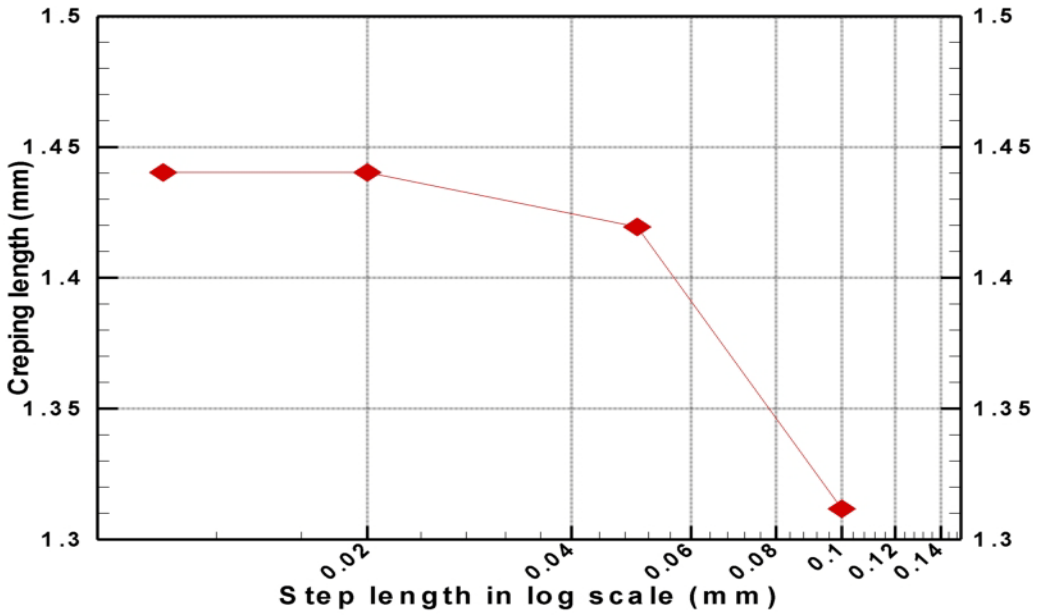

Figure 4.3 Creping length converges to stable value with step length decreases

Figure 4.3 demonstrates the creping length result versus different numerical step length Δu . The parameters are all reference values in Table 3.1 except that the sheet thickness t_s is 60 μm. The critical energy release rates G_I and G_{II} are both set at 32N/m. The imperfection of initial crack length l_0 is chosen at 0.33 mm as small as possible for nontrivial solutions. As plotted in this figure, a convergent behavior of creping length appears as the step length decreases. The creping length gradually changes to a stable value about 1.44 mm if the step Δu decreases below 0.02mm. Therefore it is confident to choose $\Delta u = 0.01$ mm as the greatest step length for acceptable creping length result that is accurate enough. In the following studies, all results are calculated with a step length of 0.01 mm.

Next, the results of crack extension history in one creping length together with the strain ε and critical buckling strain ε_{cr} are calculated to demonstrate the crack extension process controlled by the fracture criteria and buckling states controlled by buckling criterion. And finally, a complete study of creping length over different critical fracture values is concluded.

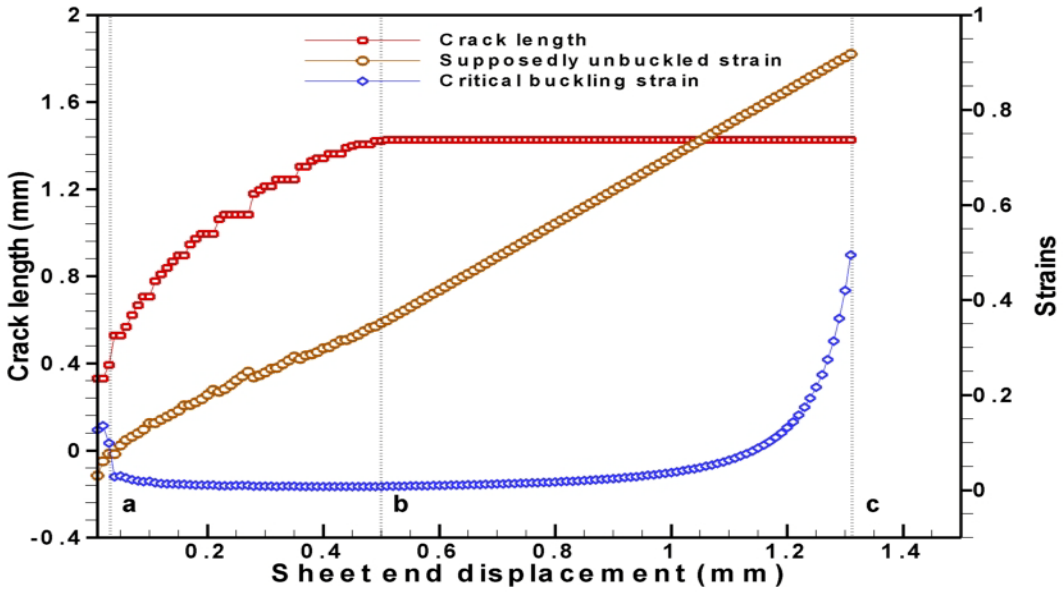

Figure 4.4 Crack extension process and buckling states in one creping length history

Figure 4.4 shows the crack extension history and buckling state in the single creping length. The supposedly unbuckled strain ε in equation (4.1) and the critical buckling strain ε_{cr} in equation (4.2) are calculated with the same sheet end displacement u and crack length l . Whether the sheet satisfies the critical buckling condition is reflected by comparing which strain's curve is above the other. All the input material and physical parameters are the same with Figure 4.3, so the calculated creping length is still 1.44mm.

In this sample creping length history, it can be found that along the end displacement u axis, $[0, a)$ is the interval corresponding to period (1); $[a, c)$ corresponds to period (2) and (3); and point c corresponds to period (4). The initial crack extends abruptly near $u = a$ soon

after the beginning of creping process. Correspondingly, the curve of critical strain ε_{cr} drops suddenly below that of strain ε near position a, indicating the sheet buckles there because of the first jump of crack length. Following that, the uptrend pattern of crack length curve in $[a, b)$ could be concluded as a staggering delamination interrupted by a series of small crack jumps and short crack pauses, displaying both continuity and discontinuity characters during the delamination procedure. The crack length then gradually increases up to a stable level in $[b, c)$ which means the crack extension stops there. While the sheet end displacement is increasing with constant iteration step, the buckling span l' of sheet finally shrinks to $2t_s$ at point c thus the corresponding l yields the creping length after many iterating calculations.

It is also noticed from the strains in Figure 4.4 that once the critical strain ε_{cr} is surpassed by the strain ε, it would not catch up with strain ε again thereby keeping the sheet in buckling shape till the creping length is reached. The reason that creping structure with buckled state would not return to its former unbuckled state could be explained in the following.

On one hand, it is shown (Chai *et al.*, 1981; Evans and Hutchinson, 1984) that the buckled sheet contains less energy than unbuckled sheet. On the other hand, the energy in adhesive should also decrease after buckling. According to the experiments (Beacham, 1998; Ramasubramanian and Shmagin, 2000), once the sheet buckles, there is a rapid decrease in creping force. This should result in similar decrease of shear stress which is the main stress in adhesive with sheet compressed laterally. Therefore the potential energy in the whole sheet-

adhesive structure decreases after buckling. As long as isolated system is assumed, the creping process should obey the minimum total potential energy principle that any structure shall deform or displace to a position that minimizes the total potential energy. The calculation result keeps in consistence with this fact.

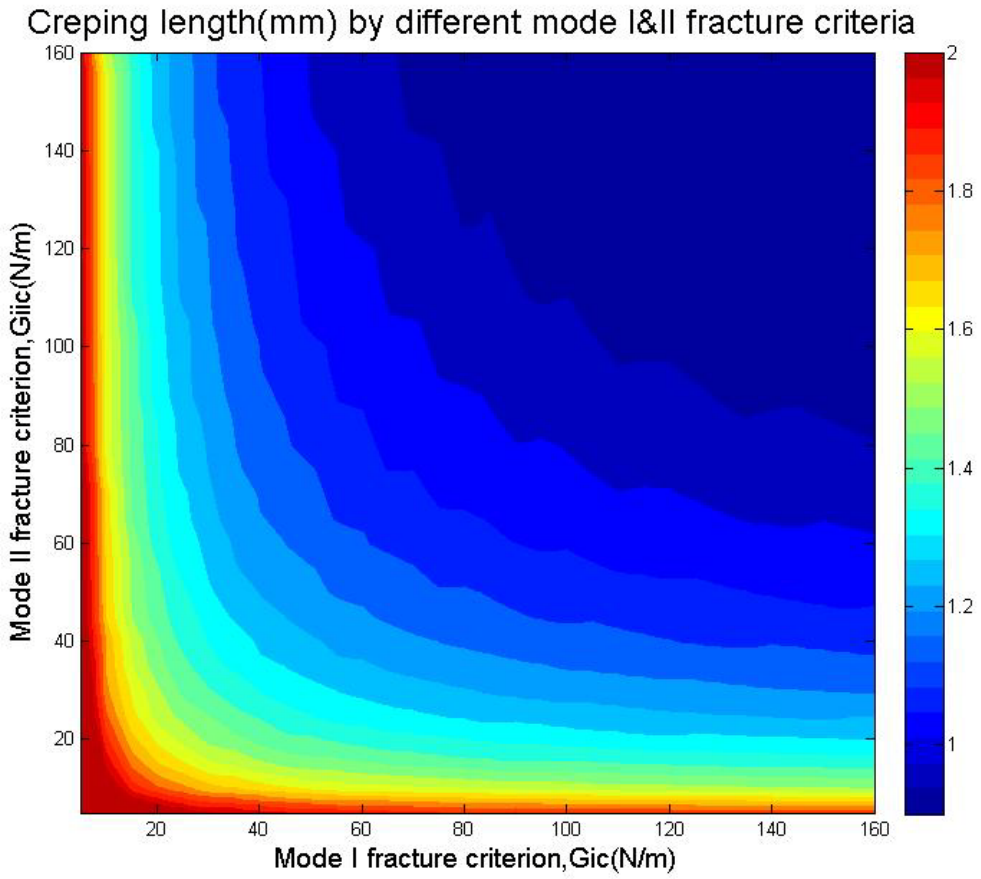

Figure 4.5 Creping length in 2-D domain of mode I and II critical energy release rates

The critical energy release rates G_{Ic} and G_{IIc} are important fracture critical values since the delamination procedure is highly dependent on that of mode I and II. These critical values

are related to the properties of the sample of test paper sheet in experiments and also the working conditions such as the rolling speed of drum, temperature, and moisture of sheet sample, etc. However, in advance of the experiments, these values could be assumed as input data. To investigate the relations between these critical values and creping lengths, a calculation for creping lengths by different G_{Ic} and G_{IIc} in 2-D domain has been carried out.

Figure 4.5 is the 2-D contour plot showing how the creping length varies with different G_{Ic} and G_{IIc}. All other parameters are chosen the same as in Figure 4.3. The unit of creping length in the legend is millimeter. In this plot, a creping length is calculated at each combination of G_{Ic} and G_{IIc}.

Creping length, as plotted in Figure 4.5, demonstrates high dependence over fracture criteria values. In general, creping length decreases as the critical energy release rates increase. In the case with higher critical values of fracture energy, creping structure requires more strain energy in order to delaminate. As a result, the structure should be more difficult to have any crack extension, reducing the crack extension pace. If the sheet end displacement increases in the constant rate, the crack tip should be caught up by the sheet end in a shorter distance, which forms a shorter creping length. In the energy point of view, a creping structure that generates smaller creping length is usually capable to store more energy before it fails, since the critical fracture energy is a material property to evaluate how much energy is required to break the material. This figure also clearly reveals that creping length should decrease more and more slowly as critical energy release rates increase to greater values. The

non-linear relation between the fracture criteria values and creping length indicates that creping length not only reduces its value to smaller one but also reduces its sensitivity to critical fracture energies, as the critical fracture energies increase.

Further, in mixed-mode condition, if the critical fracture energy in one of the two modes is relatively very small, the creping length would be very large no matter how critical fracture energy in the other mode changes. For example, if critical fracture energy of mode I is relatively very small, the opening mode effect by itself alone should make the fracture criteria easily satisfied and generate much longer creping length. Similarly, if critical fracture energy of mode II is relatively very small, the shearing mode effect could break the material directly no matter how strong the material is in opening direction.

The conclusion over the effects of critical energy release rates should be meaningful for the deep understanding of the creping process from the energy aspect, and be directive for generating acceptable quality of crepe paper in industrial production using appropriate combination of sheet and adhesive that yields desired creping length.

4.3.2 Parametric Study

The parametric study is an important part in creping analysis, since it is an approach to understand how the material properties and physical conditions influence on the creping results and how those influences can be a direct guidance to the production control of crepe paper. Prior results from experimental tests obtained some knowledge of the creping parameters' effects on the final crepe paper (Ramasubramanian and Shmagin, 2000). In this dissertation consistent results with those similar effects have also been achieved. The

parameters that are studied here include blade angle θ (i.e., creping angle), sheet Young's modulus E_s, sheet thickness t_s and adhesive Young's modulus E_a. During each parameter's study, one of the above selected parameters changes evenly while the others remain constant. G_{Ic} and G_{IIc} are always set at 32N/m.

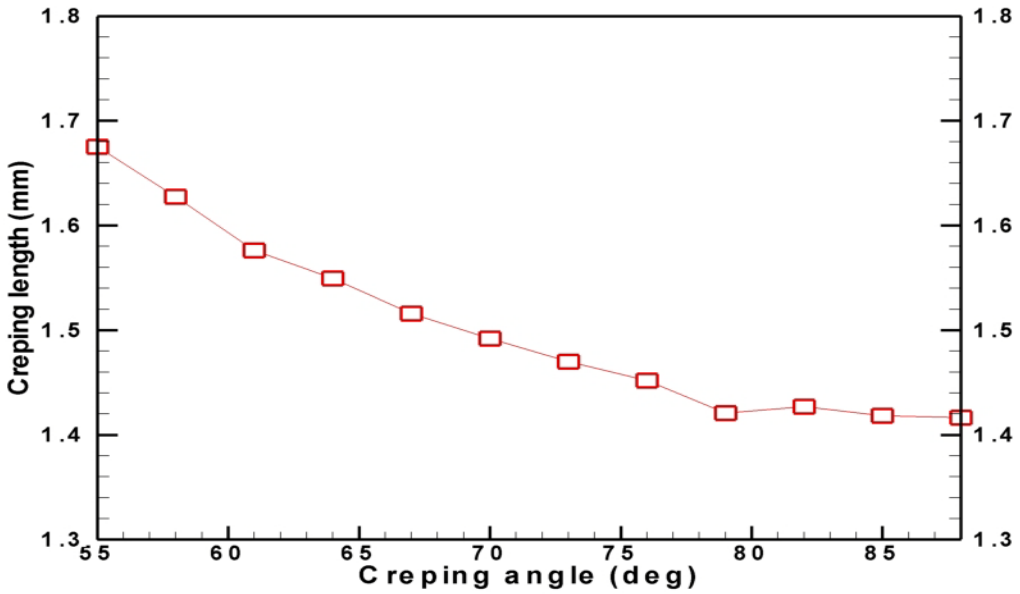

Figure 4.6 Creping length versus blade angle

In Figure 4.6, the blade angles from 55 up to 88 degree are selected to calculate different creping lengths. The sheet Young's modulus E_s is 100MPa that is the reference value, sheet thickness t_s is $60\mu m$, and adhesive Young's modulus E_a is also the reference value of 25MPa. As shown in this plot, the creping length is in decreasing trend as blade angle increases. Generally, the creping length always tends to decrease as the blade angle increases in most

cases while other parameters are held constant. This is consistent with the result from stress analysis and the result from earlier experiments (Ramasubramanian and Shmagin, 2000). One possible explanation for this effect is that a larger blade angle reduces the curvature of buckled sheet near the crack tip. Consequently, the bending moment at crack tip to cause mode I effect is diminished.

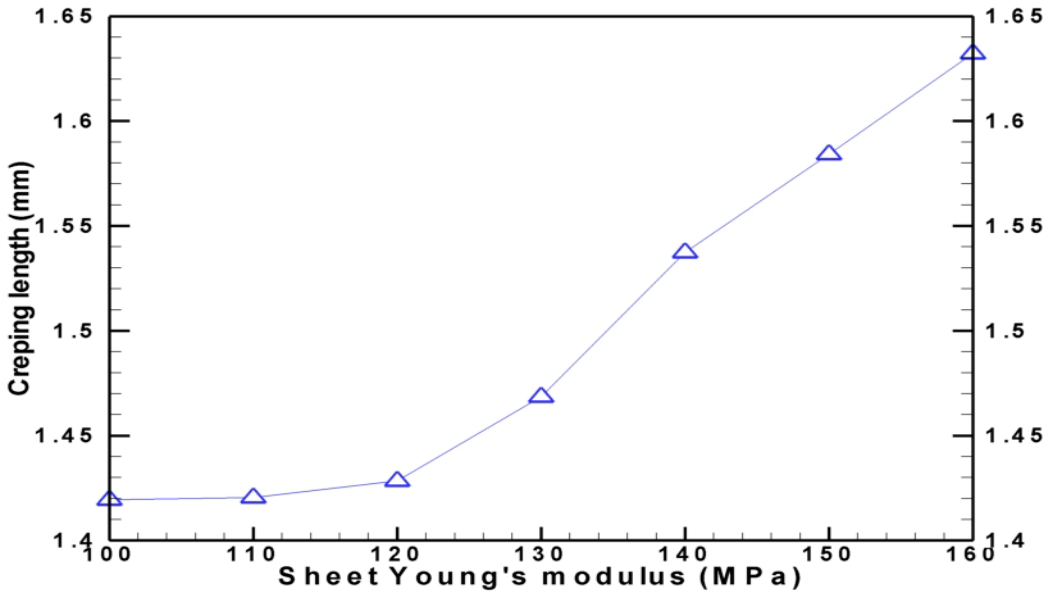

Figure 4.7 Creping length versus sheet Young's modulus

Figure 4.7 reveals the effect of the sheet Young's modulus on the creping length. Seven E_s values from 100MPa to 160MPa with an increment of 10MPa are used to calculate creping lengths in this study. θ, t_s and E_a are maintained at reference values. The creping length is in ascending trend from over 1.4mm to over 1.6mm as E_s increases, which means

the stiffer sheet generates more opening mode I deformation at the crack tip after it buckles and thus the crack extends easier. From the energy point of view, the stiffer sheet needs to release more strain energy during crack extension, so the crack should grow longer and faster compared to the condition with softer sheet. In this way, when the creping process is finished, the creping length is obviously longer with larger E_s .

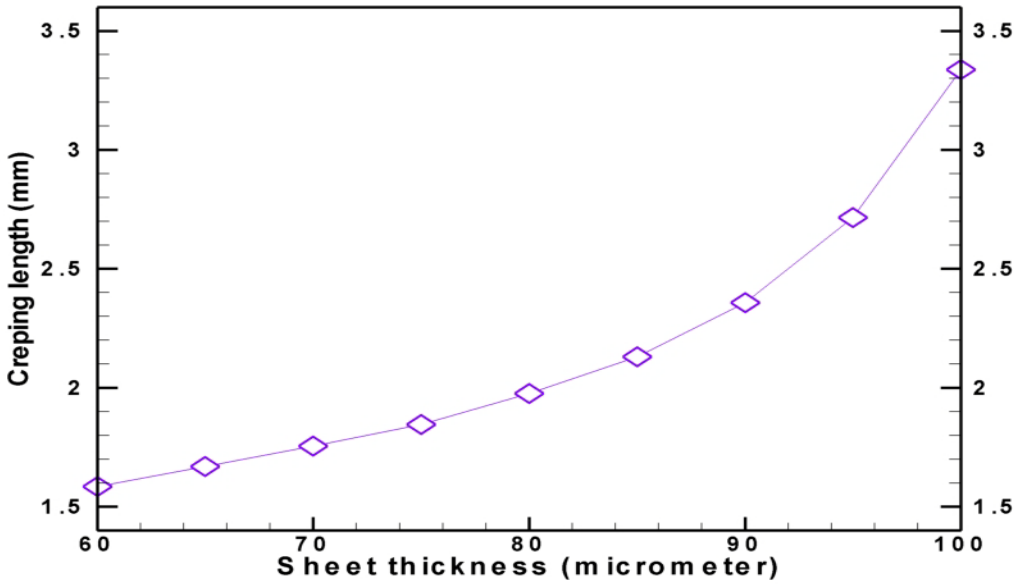

Figure 4.8 Creping length versus sheet thickness

Figure 4.8 demonstrates that sheet thickness t_s also positively influences on creping length. Here, E_s is chosen at 150MPa, and the other parameters remain as reference values. The larger t_s makes the sheet stiffer and so with higher strains. Therefore the crack also

extends faster to achieve a larger creping length which is in a similar way as in sheet Young's modulus E_s study.

Actually, both sheet thickness and sheet Young's modulus define the sheet stiffness. In addition, because the creping model has 1-D column assumption in the formulation, the sheet thickness is equivalent to the cross section of sheet and crack length is equivalent to the column length. Therefore t_s should not be too large compared to crack length.

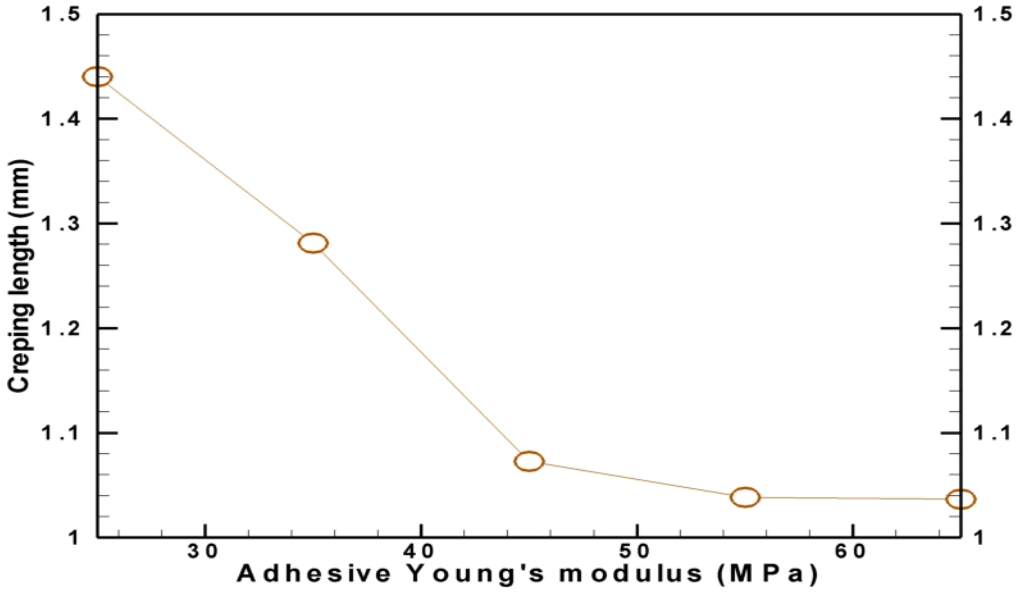

Figure 4.9 Creping length versus adhesive Young's modulus

Because the delamination mostly happens in adhesive layer, the crack extension should also definitely affected by adhesive property. The adhesive Young's modulus effect is displayed in Figure 4.9. It shows that the creping length drops as the modulus E_a increases in

adhesive layer. The creping length decreases slower when E_a is getting large, especially after 45MPa. The explanation for this downtrend effect by E_a is that stiffer adhesive is capable to store more strain energy before it breaks. Correspondingly, more strain energy is required to break the adhesive, leading to the sheet more difficult to peel off. For the same rate of sheet end displacement, the front of delamination should be caught up by sheet end in a shorter distance, thereby forming a shorter creping length.

In summary of the parametric study, larger blade angle makes the creping length shorter within appropriate range (i.e., less than 90 degree), and the parameters of sheet stiffness factors (E_s, t_s) have positive influences on creping length while the parameter of adhesive stiffness factor (E_a) has the opposite effect.

4.3.3 Comparisons with FEA Model

In the area of computational modeling of the creping process, other methods are also being developed parallel to the fracture analysis described in this chapter. Finite Element Analysis (FEA) is one of those capable methods in simulating a variety of problems in structure and solid mechanics, including the paper creping problem. The advantage of FEA compared to the fracture analytical method is that it can simulate the process vividly in a model very close to the physical facts without making too many assumptions. However, FEA also requires much larger computational resource, and usually it is also highly dependent on the mesh and accuracy level that sometimes increase the difficulty in obtaining results which are good enough. In this dissertation, the FEA results from a 2-D model are compared with

the results of this energy based fracture analysis. The FEA model is developed in ABAQUS^{TM} by Gupta (2011).

The comparisons are mainly conducted on creping length results in two parts. The first part is the primitive comparison by changing the critical energy release rate to pick out a value of G_c (i.e., assuming $G_c = G_{Ic} = G_{IIc}$) that generates the best matched creping length from the two models. Applying the picked G_c, the second part is the comparison of creping length with different values of sheet Young's modulus E_s and sheet thickness t_s by keeping the ratio of E_s / t_s in several constants.

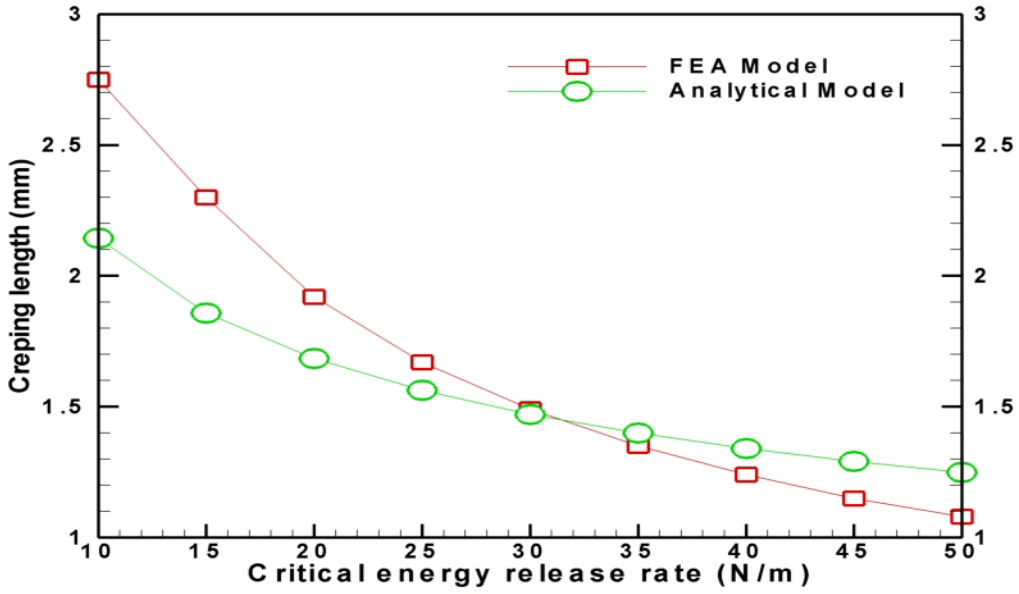

Figure 4.10 Comparison of creping lengths in different critical fracture energy

The 1-D fracture method developed by this dissertation is marked as analytical method in following comparisons. In part one, Figure 4.10 shows the creping length comparison with FEA method by increasing critical fracture energy value $G_c = G_{Ic} = G_{IIc}$ from 10N/m to 50N/m. All the rest parameters are the same with those in Figure 4.3. As indicated in the figure, both of creping length curves from the two methods decrease non-linearly as G_c increases. The decrease amount of creping length by analytical method result is from 2.15mm to 1.25mm while the decrease amount of FEA result is a little greater from 2.75mm to 1.08mm. Both the two curves by the two methods are consistent with prior experiments and physical theory in creping process and they have achieved a good match in this range of G_c. Especially, there is a cross point between the two curves near G_c=32N/m where the analytical model and FEA model reach the best match of creping length.

Based on part one's conclusion, part two would continue comparing analytical method with FEA method at G_c=32N/m in the aspect of material properties. Current comparisons within this aspect are conducted mainly on sheet properties (i.e., sheet Young's modulus and sheet thickness) since they directly impact on the choice of sheet sample which is an important concern in industry. As investigated in parametric study, greater sheet Young's modulus E_s and sheet thickness t_s should both increase the creping length. However, only this information is not enough in further comparison. Different increasing scales of E_s and t_s may also effect on creping length and the comparison between analytical and FEA methods,

because the scales of E_s and t_s could associate with different bending radius, different flexibility or different compatibilities with 1-D model assumptions. The ratio of E_s / t_s would provide a more profound point of view to study whether and how the two computational methods are matched with different E_s, t_s increasing pace.

Figure 4.11 displays the comparison between this analytical model and FEA model, with constant ratios of sheet modulus over sheet thickness for 1.4, 1.5, and 1.6 respectively. The unit of ratio is MPa/μm. In this study, this ratio is designed to reflect the relative relationship between sheet elastic modulus and sheet thickness instead of sheet stiffness $E_s t_s^3$. The ratio's effect on the comparison result is shown below. The comparison is much better with larger ratios of E_s / t_s as the ratio increases. Usually lower ratio of E_s / t_s means greater sheet thickness and softer sheet, and this situation should inevitably weaken the long-column assumption for the debonded sheet over an initial crack, as the sheet thickness (i.e., equivalent to cross section of the column) is relatively large compared to the initial crack length (i.e., equivalent to column length).

Figure 4.11 Comparisons with constant ratio of sheet elastic modulus over sheet thickness. (a) ratio=1.4; (b) ratio=1.5; (c) ratio=1.6.

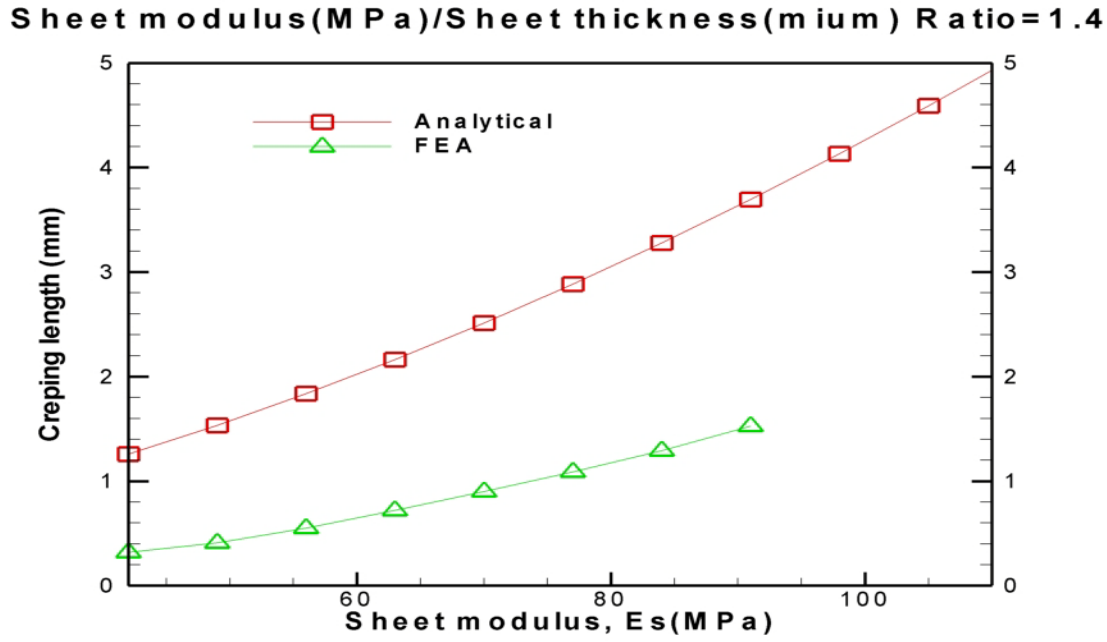
Sheet modulus(MPa)/Sheet thickness(mium) Ratio=1.4
Analytical
FEA
Creping length (mm)
Sheet modulus, Es(MPa)
0
1
2
3
4
5
60
80
100

(a)

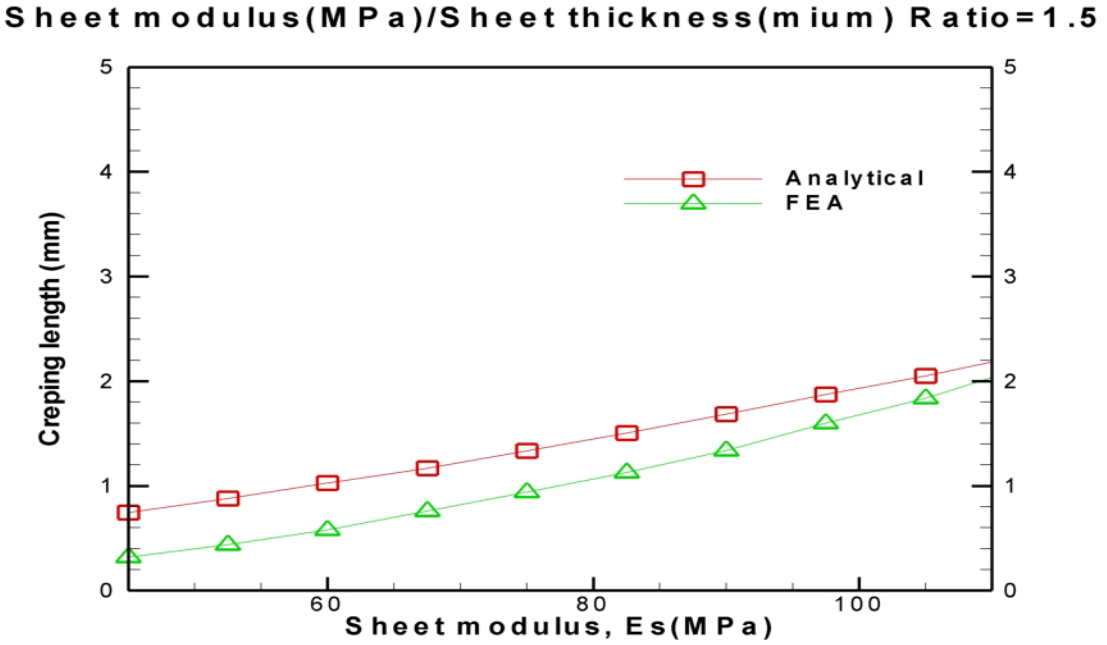
Sheet modulus(MPa)/Sheet thickness(mium) Ratio=1.5
Analytical
FEA
Creping length (mm)
Sheet modulus, Es(MPa)
0
1
2
3
4
5
60
80
100

(b)

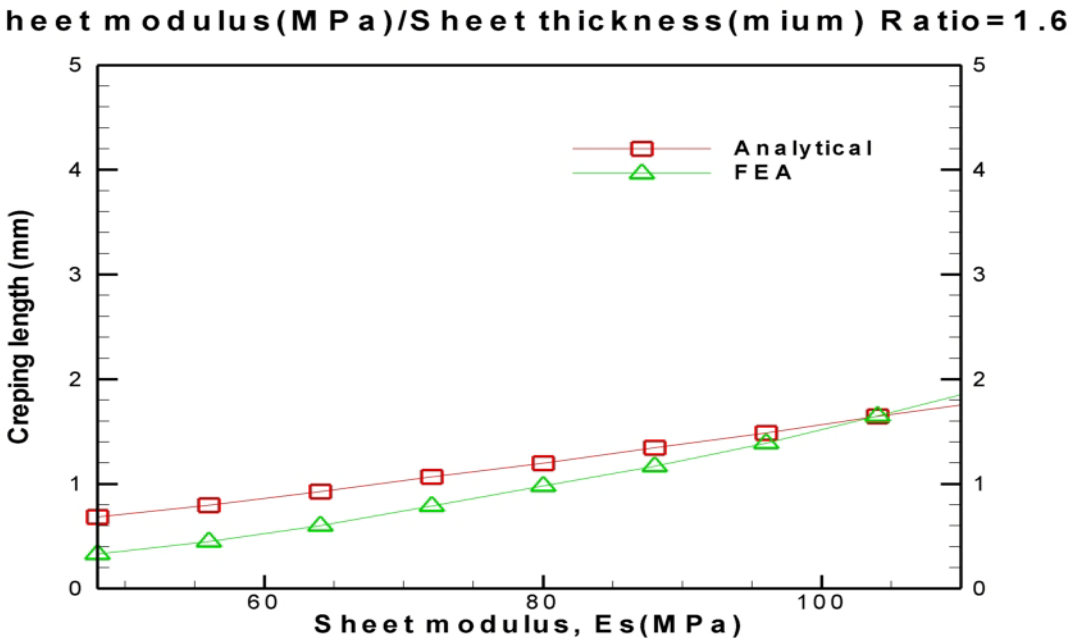
Sheet modulus(MPa)/Sheet thickness(mium) Ratio=1.6
Creping length (mm)
Sheet modulus, Es(MPa)
Analytical
FEA
0
1
2
3
4
5
60
80
100

(c)

Besides, thicker and softer sheet should also bring in obvious 2-D effects of shear stress and strain in the sheet layer, because the shear deformation along sheet thickness direction becomes larger in such kind of sheet. This factor weakens the 1-D assumption that confines the model only in creping direction. Meanwhile, the bending radius of this kind of sheet is no longer uniform along the thickness direction, destroying the boundary condition of uniform bending moment in 1-D assumption. The results of creping length under such a condition are more unreliable or unstable usually appearing as very high values.

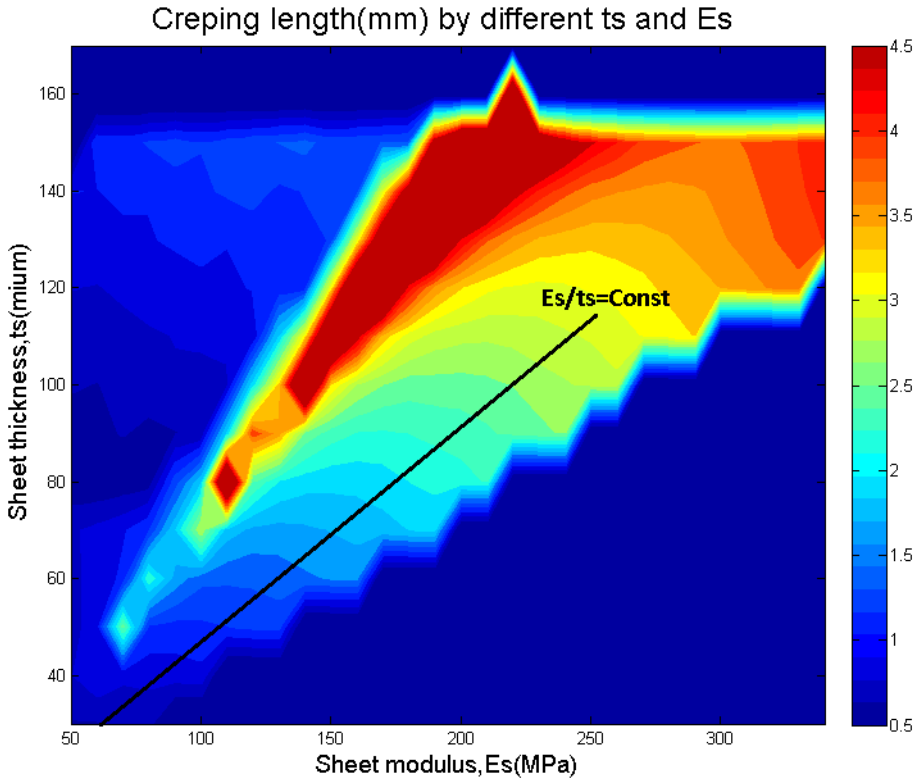

Figure 4.12 Creping length in 2D contour plot with different sheet elastic modulus and sheet thickness, marked with a sample trace of constant modulus/thickness ratio

To demonstrate valid and stable solution area by sheet elastic modulus E_s and sheet thickness t_s in this fracture analytical model, a creping length study over 2-D domain of E_s and t_s is shown in Figure 4.12. It investigates the relations between creping length and basic factors (E_s, t_s) in sheet stiffness and how those factors together effect on the creping length in this analytical model. E_s is increased from 50MPa to 340MPa with a 10MPa step and t_s is increased from $30\ \mu m$ to $170\ \mu m$ with a $10\ \mu m$ step. The trace of E_s / t_s with constant ratio should be a straight line with a certain slope goes from bottom left to top right corner in the 2-D domain. Apparently, there exists a boundary of valid creping length values. Beyond this boundary the creping length would become trivial solutions reflected by very low and uniform value area in this figure where it means the sheet does not make any significant delamination.

In addition, it is found that below certain ratio of E_s / t_s, the creping length results seem to be unstable and tend to yield very high values that are not acceptable according to commercial production. The reason was explained by the second part of comparison with FEA model in prior section. On the contrary, in the area with higher ratio of E_s / t_s, the creping length values are stable, reasonable and consistent with physical fact therefore generates a better agreement with FEA results.

4.4 Conclusions

This study presents a one-dimensional computation model for paper creping process, and develops an analytical method based on energy release rate using fracture criteria and buckling criteria to predict the creping length. The research starts with stress solutions in the creping stress analysis of Chapter 3 and then derives the fracture analysis for the sheet-adhesive structure.

In this way, a numerical iteration calculation program to decide the creping length is developed in MATLAB^{TM}. This program generates the crack extension history during one creping length, the strains change, the creping lengths over 2-D domain of critical fracture work G_{Ic} and G_{IIc}, and the creping lengths over 2-D domain of sheet elastic modulus and sheet thickness. Meanwhile, a parametric study has been carried out to study the effects from material properties (sheet elastic modulus, sheet thickness, and adhesive elastic modulus), and working condition (blade angle). The results are compared with those of FEA, and achieve good agreements in greater ratios of sheet modulus to sheet thickness.

CHAPTER 5

A BRIEF INTRODUCTION TO CREPING EXPERIMENT

One important independent approach for the study of creping process is the creping experiment on a mini creping machine called micro Yankee dryer, reproducing the characteristics of a creping machine in commercial production mentioned in Chapter 1. The experiment of creping process on this laboratory device is a convenient method to learn fracture failure phenomena and the effects of control parameters in creping process and also provides the basis for computational analysis in current and future studies.

At NC State University, in particular, Dr. Ramasubramanian's laboratory, several students (Beacham, 1998; Sun, 2000; Ramasubramanian and Shmagin, 2000) have worked continuously for several years on developing an accurate crepe process simulator. Currently, we have a mature experimental system and vast amounts of test data. Following their prior work, this dissertation employs the creping experiment together with some selected results from past work as a reference source for validating, adjusting and improving the creping model.

5.1 The Creping Simulator — Micro Yankee Dryer

The commercial scale creping machines use in regular tissue production are very large (drum diameters can be up to 5.5 meters, and 8.3 meters wide) and run very fast (surface speeds in excess of 7000 feet per minute). In addition, Yankee dryers are pressure vessels with steam pressures up to 10.9 bars, and covered by a hood that impinges hot air jets on the paper to dry it quickly. Given this enormity in size scale it is almost impossible to instrument the machine to measure tiny creping forces. Furthermore, at these operating speeds, the lost production will be great while experimenting with the machine. For these reasons, it has been necessary to find a way to simulate the creping process in a realistic manner in the laboratory. A micro scale creping machine has been designed and built in our laboratory by past graduate students (Shmagin, Swecker, Beacham). The device has been recognized worldwide as a true simulator of the creping process and the uniqueness of the design allows discrete paper samples and minimizes the need for large quantities of paper and the reel mechanisms needed if this was a continuous paper creping machine. The size scale of this micro Yankee dryer in terms of diameter is about $1/15^{th}$ of a commercial drum. The width, however is much smaller, about $1/100^{th}$ of the width of a large commercial drum. .

In 1995, Dmitry Shmagin started the original design and installation of the simulator. Later on, this experiment was continued by Beacham (1998). He investigated on the electro-mechanical system and structure of the creping device, and studied the creping control factors and their effects on the creping results. In the aspects of electro-mechanical device

system and structure, he described several improvements for the earlier work in drum speed, data analysis and drum coating with adhesive. Then the coating method and creping procedure were presented. He also gave the results of creping frequency and creping force. Ramasubramanian and Shmagin (2000) further demonstrated the creping experimental results with improved and refined measurements.

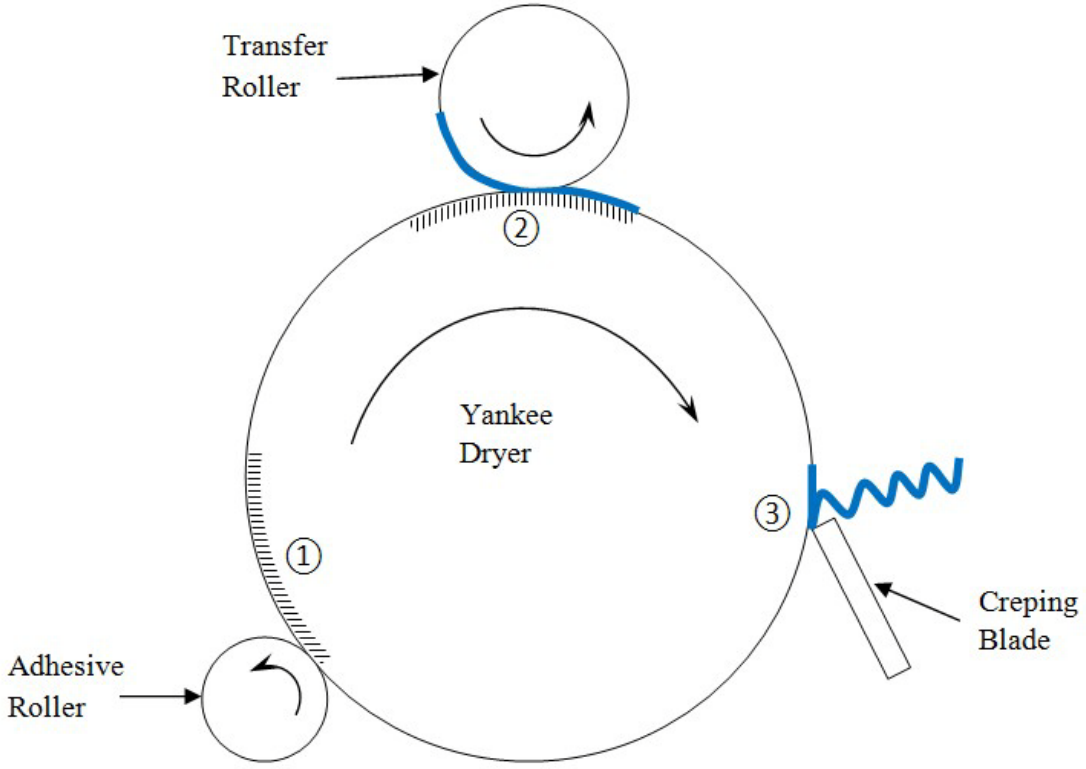

Figure 5.1 Sketch of the experimental micro creping device

Figure 5.1 demonstrates the sketch of the experimental micro scale creping device. In the experimental simulation of creping process implemented by micro Yankee dryer, the

loading of sheet is done through a transfer roller designed to load and press short paper samples onto the drum. The high velocity hood and the steam heating in industrial scale Yankee dryer (see Figure 1.1) is replaced by an electrical heating unit assembled underneath the drum's surface. The cleaning after creping process could be done by hand easily so the cleaning blade is not installed to reduce the complexity of the system. The adhesive spray nozzle in industrial device is replaced by an adhesive applicator (i.e., adhesive roller) for a similar reason. Prior experiments (Beacham) have shown that the roller application in the case of the laboratory simulator results in more uniform application compared to spray application or dipping of the sample in adhesive and applying to the drum.

In figure 5.1, as the Yankee dryer rotates at a slow rate of speed, first the adhesive roller applies adhesive over the shaded surface area in position ①. When the adhesive area rotates to position ②, the transfer roller would press down and attach wet sheet sample from itself onto the adhesive. Finally, when the attached sheet rotates to position ③, it would be scraped off by the creping blade while the drum rotates at full speed with the attached sample.

To control the micro scale creping device in accordance with commercial creping process as much as possible, the input control parameters are designed as heating temperature, drum rotation speed, paper thickness, number of adhesive applications, curing time of adhesive, drying time of wet paper, and installation of creping blade angle, etc., including most of those main influential factors in crepe paper production. According to commercial testing data and other prior work (Beacham, 1998; Ramasubramanian and Shmagin, 2000)

the drum rotation speed is related to critical fracture energy that are usually obtained from experiments like peeling or bending tests. The number of adhesive applications actually decides the thickness of adhesive layer. The temperature together with curing time decides the material property of elastic modulus in adhesive during creping, and the temperature with drying time determines the density or moisture of the paper sheet. The outputs of the micro Yankee dryer are mainly loading forces in different axes, measured by a load cell holding the creping blade, and the creping length (or crepe wavelength) of the crepe paper sample.

The overview of the micro Yankee dryer is shown in Figure 5.2. The main rotating part of the device is the creping drum located in the center in Figure 5.2(a) labeled as “1”. The drum is made of cast iron with the diameter about 39.37 cm (15.5 inches) and width 8.25 cm (3.25 inches). The drum is driven by rotary servo motors installed in the back of the drum (“7”in Figure 5.2(b)). On the top of the drum is the transfer roller (“2” in both Figure 5.2 (a) and (b)) pressing wet sheet onto the drum surface, and to the left of drum is the adhesive roller (“4” in Figure 5.2 (a) or “8” in Figure 5.2 (b)) applying adhesive onto the drum surface. Both of the two parts are driven by compressed air supply (“5” in Figure 5.2 (a)). The creping blade (“9” in Figure 5.2(a) or “5” in Figure 5.2 (b)) is fixed with a certain angle ahead of the smaller rotary servo motor (“6” in Figure 5.2 (a) and (b)) on the down right side in Figure 5.2(a).

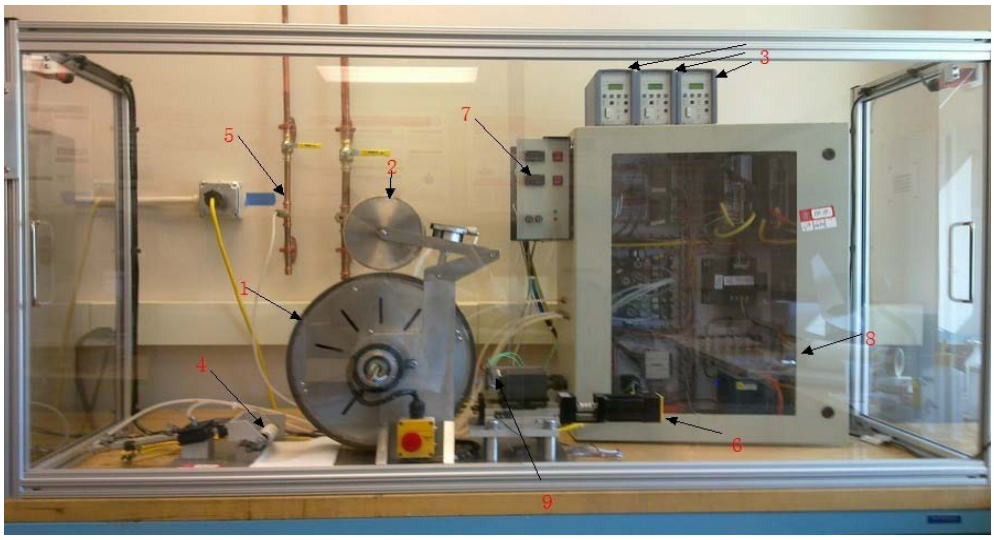

(a)

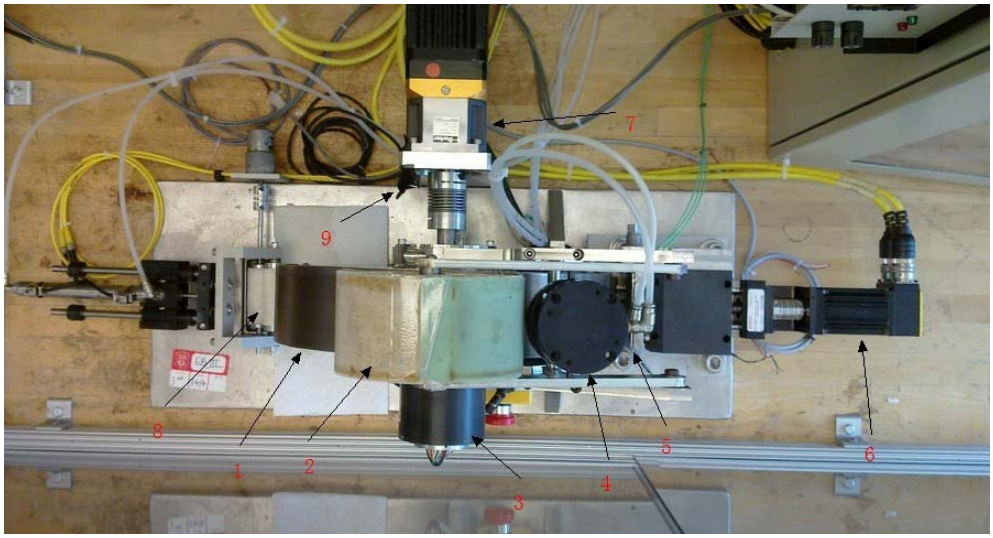

(b)

Figure 5.2 The overview of micro scale creping simulator device. (a) the side-view (1. Drum; 2. Transfer roller; 3. Charge amplifiers; 4. Adhesive roller; 5. Air supply; 6. Blade servo; 7. Temperature control; 8. Cabinet; 9. Creping blade); (b) the top-view (1. Drum; 2. Transfer roller; 3. Heating unit; 4. Air pump; 5. Creping blade; 6. Blade servo; 7. Drum servo; 8. Adhesive roller; 9. Homing sensor)

The motor control card, acquisition card and other electronic control systems are installed in the cabinet on the right. There can also be mounted a high speed camera (not installed in this figure for a clearer display of the device) in front of the contact area between the creping blade and drum to take the video of the creping process for a limit length of attached sheet in a very short moment. To the left of the creping device is the computer which is not included in Figure 5.2. Over the top of the cabinet are three charge amplifiers measuring Voltage data related to forces in three axis directions X, Y and Z, which would be indicated later in the next section.

The micro Yankee dryer is a reasonable simulator for the commercial scale creping machine because of several points listed below. First, the micro device is still large enough to make the same physical assumptions as for commercial device when developing creping analysis, since the differences of dimensions which are most related to creping process (i.e., paper and adhesive thicknesses, drum's diameter and width, sample sheet length, etc.) between the micro device (i.e., diameter of 39.37 cm and width of 8.25 cm) and the paper-adhesive structure (i.e., sheet thickness around 100 μm and one layer adhesive thickness of 2 μm) is far greater than those between the micro device and the commercial device (i.e., diameter of 2.4~7.0 meters (Ramasubramanian and Shmagin, 2000)). Second, if the dimensions of micro scale device are reasonable for simulation, then the material properties like elastic modulus would also have very little or no influence on creping process when applied in different scales of devices. Third, most of other control parameters like

temperature and density of paper sheet are independent with device dimensions. For the speed in the rotational direction of drum's surface in micro device, it can be easily calculated as input control parameter and adjusted to the equivalent speed of commercial device based on the scale proportion.

In this dissertation, most of the studies are carried out based on the micro creping machine, and a physical model would be assumed in the effort of trying to understand the delamination procedure in the paper creping process and its mechanism. Also, the control parameters and their effects on the creping results are investigated in the experimental study of creping process, since they are critical to the success of production and process optimization for industry.

5.2 Working Principle of the Micro Yankee Dryer

A sketch of the control and data acquisition system in creping machine is demonstrated in Figure 5.3. In this figure, the red double arrows indicate the moving directions of those assemblies. The area in the dashed line box is displayed in 3D to demonstrate the XYZ 3-axis load cell directions for the measurement of loads installed on the creping blade. Here, X-axis is the contact force direction (i.e., perpendicular to tangential direction of the blade contact point on drum's surface), Y-axis is the creping (force) direction (i.e., tangential direction), and Z-axis is the drum's axial direction.

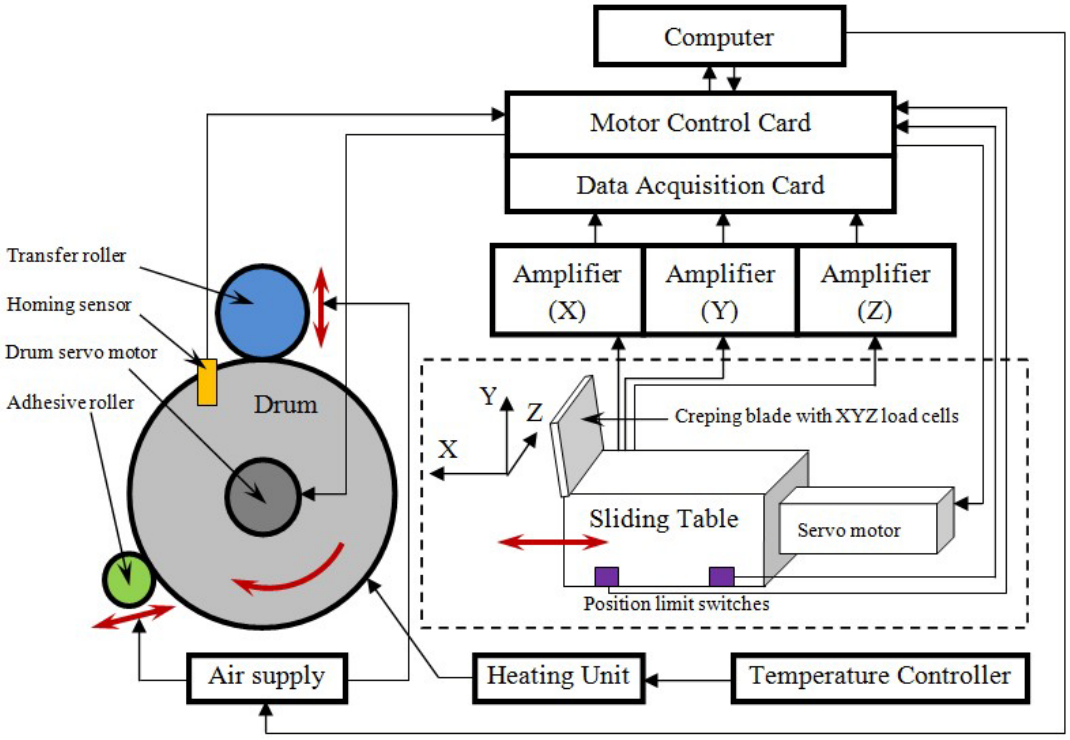

Figure 5.3 Electro-mechanical control system of the creping simulator

The loading force data in XYZ axis are correspondingly collected from XYZ channels of charge amplifiers to the computer end. They are saved and converted as excel documents. The recorded data are in Voltage units. In order to change the data to forces in Newton that could be meaningful to the creping analysis, the following conversion method must be used using the formula

$$\text{loading force (N)} = \text{scale(N/Volt)} \times \text{loading data (Volt)} \tag{5.1}$$

where the scale of X,Y axis is 20 N/Volt that is preset in creping experiment and can be directly read from the charge amplifiers in Table 5.1. Notation "MU" stands for the mechanical unit that represents Newton force here, and "pC" stands for Pico-Coulomb.

Table 5.1 Scales and sensitivities on the charge amplifiers

Channel (Axis)	Sensitivity (pC/MU)	Scale (MU/Volt)
X	8.10	20
Y	8.10	20
Z	3.90	3000

In general, the whole system can be divided into three parts.

The first one is the motion control system implemented in the motor control card. This system executes the motion control commands from the computer to the moving of drum and creping blade installed on a sliding table. Both the drum and sliding table are driven by rotary

motors. Meanwhile it also receives the signals from the sensors of drum position homing and creping blade position limits to control the starting and ending points of motions.

The second one is the data acquisition system which mainly contains three units: load cell mounted on creping blade, charge amplifiers, and data acquisition card. The loading signals are firstly collected through the charge amplifiers. They are converted to the usable values and uploaded to the data acquisition card connected at the PC end.

The third one is the compressed air supply system that provides the moving power of transfer roller and adhesive roller. The transfer roller is used to load sheet samples and press is on the drum, and the adhesive roller is used to marinate and spread adhesive glue on the drum surface. All the three main systems are finally controlled in the computer end through the Motion Planner™ and Labview™ graphical user interfaces. There are other independent parts such as heating system including temperature controller and heating unit for the drum, and also the measuring part of creping blade angle.

The working principle of this creping device is briefly described below.

1. When everything is ready, the computer delivers the setup command to motor control card and receives signals from homing sensor and position limit switches, moving the drum's rotational position and creping blade's x-directional position to their home positions (i.e., original positions).

2. Transfer roller is lifted by compressed air waiting to load with any sheet sample. Adhesive roller is also held by compressed air in the position where it can be soaked with adhesive glue solution (i.e., usually PolyVinyl Alcohol (PVA)).

3. The drum begins to rotate slowly (i.e., dozens of feet per minute in circumferential direction of the drum surface) and heated gradually to a steady temperature (i.e., $200^{\circ}F$) maintained throughout the whole creping process.

4. After the sheet sample moisturized by water is loaded on the transfer roller, the adhesive roller is pushed forward onto the slowly rotating drum's surface, spreading the adhesive glue on it for a certain distance that is a little longer than sheet, and is drawn back quickly by compressed air cylinder. There would be some curing time of adhesive scheduled once the adhesive is spread.

5. Next, the drum's homing sensor would notify the computer to pressed down the transfer roller and attach the sheet just over the drum surface area where adhesive is applied. A drying time of sheet is scheduled for a pre-determined period.

6. The creping procedure starts once the drum is accelerated promptly to a very high speed above 250 m/min (i.e., about 800 feet/min) (Ramasubramanian and Shmagin, 2000) in circumferential direction of the drum surface. When the speed reaches the desired value, the creping blade automatically moves toward the drum and presses on the fast rotating drum for about one second to scrape off the bonded sheet.

The preloading of the load cell is one more point needs to mention.

Since Z axis is the axial direction of drum, which is also the direction of the tightening bolt of creping blade, it is related to the tightness of the mounting bolt of creping blade. So there should be a preload of 25kN in Z axis to make sure the creping blade position and its angle are stable and accurate under impact during the creping process.

Another preload in X axis, the blade contact preload, needs to be established. When the blade moves forward, it needs to press firmly on the drum’s surface so that the bonded sheet could be scraped off. This compressive force is the blade contact preload, which is typically set at 85N. Definitely, it is a base force during the contact of blade tip and the drum surface in the conditions with or without adhesive coating and sheet application.

For convenience, those preloads above as the preset conditions would be directly excluded from the experimental results.

5.3 Adhesive Formulation and Paper Properties in Experiments

The adhesive formulation and paper properties directly effect on the delamination and buckling behaviors in creping analysis. It is necessary to get the knowledge from the industry about how those features may be possibly changed by different concentrations, constituents and processing method. Referring the relevant part in the work of Ramasubramanian *et al.* (2011), the industrial adhesive formulation and paper properties are listed in the followings.

5.3.1 Adhesive Formulation

It is common industrial practice to formulate combination of polymers for best performance on the creping process. In this section, the reasons for such practices are explored from the modeling context. In a study of synthesizing semi-IPN (interpolymer network) using PolyVinyl Alcohol (PVA), AcrylaMide (AM), and cross-linker Methylene Bis Acrylamide (MBA), it was reported that both the AM and MBA contributed substantially to the strength of the polymer blend without appreciably changing the elastic modulus (Mishra, 2008). If the cross-linking was excessive, the polymer blend became more brittle and weaker. Increasing the AM content from 33% to 50% in a PVA blend with 0.13% MBA, increased the strength by a factor of 4, without affecting the modulus appreciably. Increasing the cross linking agent MBA, decreased the strength of a 50-50% blend of PVA and AM by a factor of 2. In other words, there was an optimal cross-linking that produces the maximum strength improvement. Use of epichlorohydrin as a crosslinking agent for PVA is common in creping adhesive formulation. In a study of the manufacture of cross linked hydrogel of PVA

with epichlorohydrin, an increase in elastic modulus, tensile strength, and the strain to failure was observed (Bo, 1992).

In creping, the use of PVA and polyacrylamide blends is common (Soerens, 1985; Rose, 2004). Increasing the strength without increasing the modulus of the coating is beneficial as demonstrated by the stress model in Chapter 3. For stiff paper substrates, it is preferred to decrease the adhesive modulus while increasing the ultimate strength, which can be accomplished by polymer blends. For our laboratory creping studies, we simply used PolyVinyl Alcohol (PVA) for most experiments.

5.3.2 Properties of Paper Substrate

In conventional wet pressed paper systems, the wet sheet is transferred to the dryer drum and pressed against the Yankee dryer surface with the pressure roll device. The transverse pressure applied promotes bonding of the sheet to the drum. However, it also compresses the sheet and increases the elastic modulus as while decreasing the thickness. It has been shown that a densified thin sheet is less desirable from a creping point of view.

In through air dried (TAD) systems, the sheet is pre-dried without pressing to high solids content so that application of the pressure roll does not collapse the sheet and increase its density and decrease the thickness (Ramasubramanian *et al.*, 2011). Thus, the primary purpose of the pressure roll in such a system is to create improved bonding to the Yankee dryer drum without increasing sheet stiffness. It is well known that the TAD sheets produce a softer tissue which is directly a function of effective creping. Patent literature is replete with various ingenious ways of accomplishing good contact and adhesion without permanently

compacting sheet. The stress model results in Chapter 3 are consistent with industrial practice and have already provided a quantitative assessment of the relative importance of process options.

5.4 Discussion on Some Results from Creping Simulator

As mentioned earlier, the creping simulator's functions could be summarized in aspects of input and output. The inputs include the parameters of adhesive properties (i.e., application layer number, adhesive thickness), paper properties (i.e., elastic modulus, sheet thickness), creping blade angle, curing time, drying time, and drum speed, etc., while the outputs are mainly the creping forces and creping length.

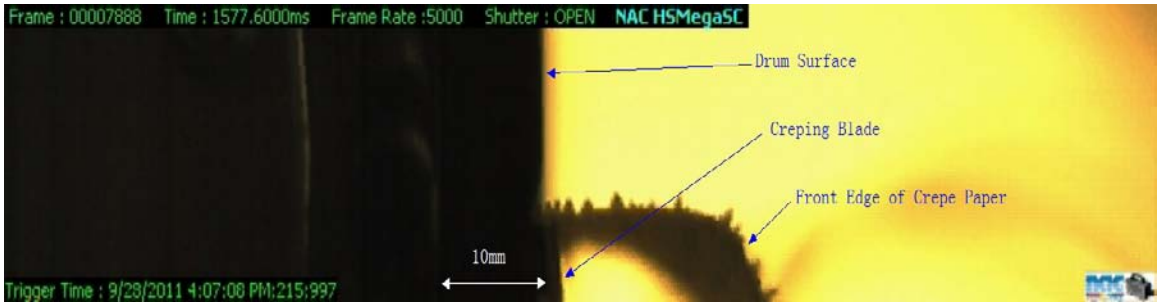

Figure 5.4 Creping process on micro Yankee dryer captured by high speed camera

Before the experimental results are discussed, the creping process would be exhibited to give a visual concept about how the morphology of corrugated crepe paper is generated. Figure 5.4 shows a snapshot for the creping process video captured by a high speed camera of Hotshot^{TM} NAC HSMegaSC. The light source is a fluorescent lamp located behind the creping blade. The video time interval is 1571.80 ms with a frame rate of 5000/s. The camera is installed in front of the creping blade about 40 cm away in distance and keeps its lens axis overlapped with the edge of the creping blade. In this test, the creping sample is in dimension of 15.24 cm$\times$5.08 cm (6 inches$\times$2 inches) (Ramasubramanian and Shmagin, 2000). The applied adhesive layer number is one, the sample thickness is about 95 μm~110 μm, the

curing time for adhesive is 20 seconds, drying time is also 20 seconds, and the drum speed is 304.8 m/min (1000ft/min). The front edge of crepe paper closer to the high speed camera significantly demonstrates many small uneven wavy buckled shapes along the creping direction. Near the creping blade tip on the down left corner of this figure, new wavy buckled shapes are being formed on the sample. Actually, each repeating cycle of those wavy shapes corresponds to a creping length respectively.

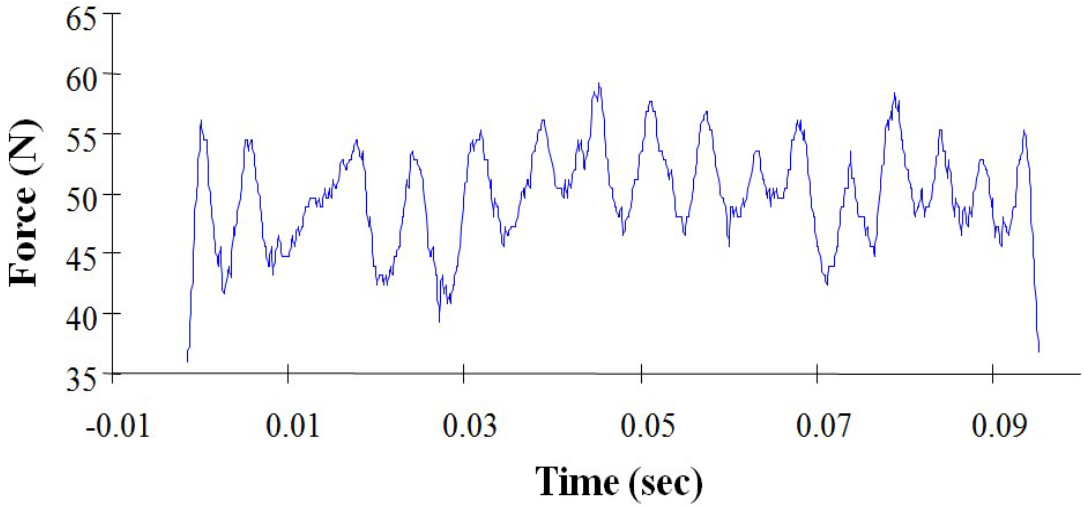

Figure 5.5 Y-axis Force versus time in a series of creping cycles (Beacham, 1998)

A Y-axis force curve versus time during the creping process is presented in Figure 5.5 by Beacham (1998) using the same adhesive formulation, properties of light weight paper with the fracture model in this dissertation. About 16 creping cycles are estimated from this figure from 0 to about 0.10 second. The sharp ascending and descending trends of Y-axis force are observed obviously for each cycle. The creping speed according to measure

condition in this figure is 15.8m/min (52 ft/min), so the averaged creping length should be calculated as 1.646 mm which is comparable to the results in Chapter 4.

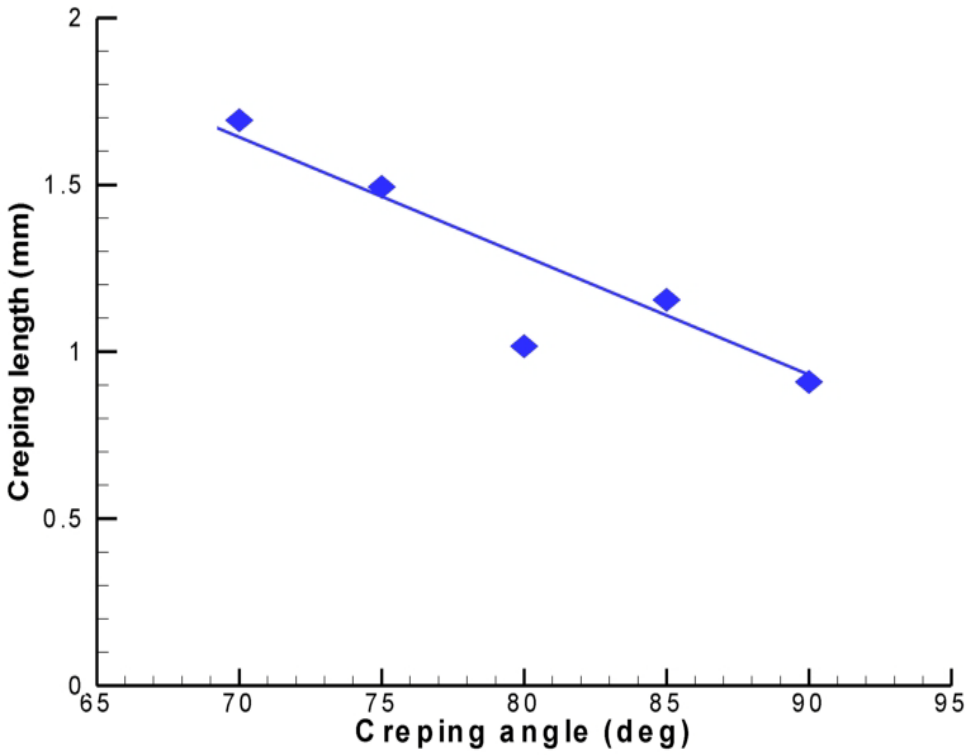

Figure 5.6 Creping length versus creping angle in creping experiment (Beacham, 1998)

The creping angle's effect on the morphological pattern of crepe paper was also obtained in experiment (Beacham, 1998). The crepe frequency instead of creping length was used by the author originally. To keep accordance with this dissertation, it is converted to creping length by taking the inverse value of crepe frequency.

Figure 5.6 shows the converted plot of creping angle versus creping angle. It is in the same trend with the result from fracture analysis that the creping length decreases as the creping angle increases. Again, this validated relationship between creping angle and creping length points out the conclusion of angle's effect on crepe paper's quality and the guidance of commercial production.

5.5 Conclusions

The micro scale Yankee dryer, also called the creping simulator has been introduced in this chapter. This experimental device is continuously developed in the past two decades up to now. The electro-mechanical system and working principle are demonstrated briefly to explain how this simulator reproduces the commercial creping product in similar micro scale process. This dissertation also shows a snapshot from the video of creping process recorded by a high speed camera. Some results referring to prior experiments on the same machine are selected to reflect the consistence with the observed phenomena and analytical results in this dissertation.

CHAPTER 6

CONCLUSIONS AND PROSPECTS

In this dissertation, the creping process used in the production of towel and tissue grades of low density absorbent paper production has been studied to elucidate the fundamental mechanisms, identification of important parameters, and their effects on the product outcome or characteristics. The creping process is a phenomenon in which a thin sheet is adhesively bonded to a large rotational rigid cylinder called Yankee dryer in wet state, completely dried by the heater dryer surface, and is debonded by a creping blade which essentially scrapes off the paper from the surface. This problem has similarities to the scraping of paint from surfaces, failure of surface layers under compression in a composite material, and the material removal processes such as machining and drilling. Such problem can be treated as the delamination buckling of thin surface layer over rigid and thick substrate under lateral compression. The related research topics in the past few decades have been extensively reviewed in delamination and buckling of thin films, composites and adhesive joints, delamination in dissimilar materials, and dynamic and post-buckling issues. Therefore creping is a special problem with an intricate dynamic process controlled by multi-parameters like material properties of sheet and adhesive, drum speed, temperature, moisture content, etc. and warranted this modeling effort for understanding.

This dissertation has considered the delamination and buckling as the basic failure and fracture mechanisms in creping process in order to simplify such a complex problem into

manageable fundamental problems. The dissertation proposes the stress criteria based creping analysis as one approach to modeling and also form the foundation for a fracture energy based method for modeling. Some parametric studies either in single or in combination with other parameters have been conducted and their results are discussed. The fracture energy method results have also been compared with numerical simulation using the Finite Element Methods and the results are discussed. A brief introduction to the experiment on a micro scale Yankee dryer called the creping simulator is presented. Some experimental results by prior studies are compared with the results of fracture energy method developed in this dissertation, only in a directional and qualitative sense. The conclusions are drawn and summarized in the following sections.

6.1 Model and Method Description

The main purpose of the dissertation is to study the physical phenomena of creping process and then build up a computational model that is realistic and capable of predicting the creping process outcome, namely, the creping length, which is a critical factor in determining the quality and morphology of the crepe paper. In order to develop such a method, the dissertation needs to create a model with reasonable assumptions to represent the creping process and incorporate the basic physical behavior of delamination and buckling. This progress is summarized in three stages as follows.

Firstly the dissertation studies the models by Chai *et al.* (1981), and Evans and Hutchinson (1984). Both these models have described conditions close to the condition of the delamination and buckling in creping process, although with different materials and bonding conditions. The model in the work of Evans and Hutchinson (1984) provides ideas for the dissertation to develop a fracture energy method as the main approach in creping calculation. Under this approach, the dissertation then used a validation model to reproduce the energy decrease in buckled of thin film suitable for the creping model where an adhesive layer is present. Buckling features were also investigated and the buckling type was decided for the creping model.

Second, the dissertation develops a stress analysis model to set up the boundary conditions, and to calculate the stress terms in adhesive layer for creping analysis that is needed to calculate the energy terms for the fracture approach. The stress criteria using the

stress strength of materials are also presented as one way of modeling the process. However, the shear strength of the adhesive layer is difficult to measure and the stress criteria fail to include the post-buckling features for creping analysis or bucking induced delamination.

Third, the dissertation describes an elastic 1-D fracture energy model for the creping process. The real problem can be reduced to a 1-D problem due to the following assumptions: (1). sheet thickness is infinitely small compared to the drum diameter; (2). Paper width is infinite compared to its thickness; (3). paper is infinitely long compared to crepe dimensions; (4). compressive loading is uniform along the sheet edge; and (5). materials are homogeneous and isotropic.

The 1-D fracture model adopts the three buckling stages of thin layer delamination buckling proposed by Chai *et al.* (1981). Further, it calculates the strain energies in the sheet-adhesive structure, while the strain energy in bonded part of sheet neglected. The energy release rates are then calculated by strain energies for different stages, and are applied to the fracture criteria in mixed-mode of mode I and mode II. The buckling effect is treated as opening effect whereas the lateral compression for sheet-adhesive structure as a whole is treated as shearing effect. In the determination of buckling state, a critical buckling strain is applied to the fracture model. The boundary conditions are also built up using the fixed-pinned ends boundary conditions. Post-buckling is addressed by the large deflection solution of 1-D column.

In addition, it is pointed out by the dissertation that the buckled sheet should not return back to its former unbuckled state, because the creping model is an isolated system so that all

structure in it follows the minimum total potential energy principle. The conclusion of fracture model's results for creping analysis would be discussed in the next section.

6.2 Results and Discussion

The conclusions of the results in this section mainly include three parts. The first one is the results by stress analysis using stress strength criteria. Second, the results by fracture energy analysis with fracture criteria are discussed. Third, the experimental results are referred to support the analytical results calculated by this dissertation.

The results of stress criteria based analysis concentrate on the parametric study and the stress study. In the parametric study, the creping length decreases as the creping angle increases. The creping length would be increased if sheet stiffness increases in general. However as the sheet thickness increases, the sensitivity of creping length to elastic modulus decreases. In the stress study, the adhesive stress strengths are investigated. The adhesive shear strength has a strong influence in decreasing the creping length, while the adhesive normal strength does not effect on creping length significantly. Further, the stress distribution functions in stress analysis reveal that the adhesive shear stress is maximum value at the crack tip and asymptotically reaches zero along adhesive layer. And they also reveals that the normal stress starts near zero at the crack tip, within a very short distance reaches a positive maximum and reverses to a negative minimum within one sheet thickness and asymptotically reaching zero.

For the fracture analysis results, a numerical calculation program is developed in MATLAB^{TM} using iteration method. Each time the sheet end displacement increases with a step length, buckling state is determined by buckling criterion. Meanwhile, the new crack

length is calculated and updated to satisfy the fracture criteria. This process continues until the crack length reaches to the creping length. The crack propagation history is demonstrated in one creping length period together with sheet buckling status controlled by strain and critical strain. Critical fracture energies in mixed-mode further show their influences on creping length. Three conclusions are reported. 1. Creping length decreases as the critical energy release rates increases; 2. Creping length decreases asymptotically with increase in critical energy release rates. The non-linear relation between the fracture criteria values and creping length indicates that creping length not only reduces its value to smaller one but also reduces its sensitivity to critical fracture energies, as the critical fracture energies increase; 3. The creping length would become very large if critical fracture energy in any mode decreases to a very small value, and the manufacturing processes should avoid this region to preserve product quality.

The more important part comes with the parametric study and the comparisons with other research methods.

In the parametric study part, effective parameters of creping angle in geometry, sheet elastic modulus, adhesive elastic modulus and sheet thickness of material properties are evaluated in the manner of changing one that is under focus while holding other parameters constant. Generally, the creping angle and adhesive elastic modulus show the effects on decreasing creping length, but the sheet elastic modulus and sheet thickness show increasing trends. The reasons are explained by the abilities of different parameters to store strain energy in the creping structure.

In the comparison part, the creping lengths of fracture analysis are compared with those of FEA. Because there are many control parameters affecting the creping length, the dissertation currently conducted the comparisons only in the areas of critical fracture energy and the ratio of sheet elastic modulus over sheet thickness. The critical fracture energies in mode I and mode II use a common value and change simultaneously for convenience. In the beginning of comparison, the value of critical fracture energy is found to match the creping length result best. Then under that fracture value, the creping length is compared between these two methods by constant ratios of sheet elastic modulus over sheet thickness. Better agreements are achieved with greater ratio of sheet elastic modulus to sheet thickness. The dissertation therefore points out two main limitations of the 1-D fracture model. On one hand, the lower ratio of sheet elastic modulus to sheet thickness weakens the long-column assumptions in 1-D model; on the other hand, the lower ratio brings in the error due to strong shear effects in 2-D, since the shear deformation along thickness would be large, and the bending moment along the thickness would not be uniform. These are not included in this 1-D model.

The experiment on a micro scale creping machine is another significant aspect for creping analysis. The reason and rationality of simulating creping process over micro creping machine are described. Unlike the computational method, the experiment is the most direct way of understanding the creping problem by physical observations. A snapshot from the creping process video is captured by high speed camera of Hotshot^{TM} NAC HSMegaSC. The snapshot clearly demonstrates the wrinkles in the formed crepe paper. Prior results are

referred to show the obvious fluctuation of creping force during many repeated creping cycle periods. One more referred result is the effect of creping angle on creping length. It shows the consistent trend in decreasing creping length with that by fracture analytical analysis.

6.3 The Prospects

The creping model and its computational method described in this dissertation is a reasonable attempt to apply fracture energy concepts and explain practically observed behavior and to provide a tool for identifying and optimizing the process parameters and design new adhesives.

The extension and prospective research of this dissertation would be roughly divided in two directions. One is the continuation study of the current model, and the other is the new derivative topics in this area.

The continuation study suggests some prospective research to move the current creping analysis further with either computational method or the experimental method. In computational method, for instance, the creping process actually contains many repeating delamination and buckling cycles, so it is worth and possible to extend the model from calculating the first creping length to calculating successive creping length in the presence of the first one thereby generating a series of creping length as in a real process. The boundary conditions for this will be challenging to come up with. By averaging these creping lengths, a more realistic estimate of the effect on crepe length can be obtained, because the first few creping length cycles usually are not the desirable creping length during the creping process according to industrial data and the video captured in this dissertation. The continuous computational analysis also needs to output the creping force in order to make the comparisons with the force data recorded in experiments.

In the experimental method, besides the creping force comparisons mentioned above, the development of testing methods for the critical fracture energy in mode I or mode II during creping would be another prospective issue for the fracture model, because only by using real physical values can the comparisons between computational and experimental results be really meaningful. In the current model, the critical fracture energy values are assumed values in analytical method, since they are not obtained through the creping experiment. Because the creping process is a special case that is different from any other conditions with basic peeling or shearing types, the classical bending and peeling tests in other references (Chai, 1986a, 1986b, 1988) are not be quite applicable to creping model. The design for such experiments for measuring critical fracture work in sheet-adhesive structure is important. For example, the measurement of critical fracture energy in mode I can be realized by bonding one end of the sheet on the blade tip and the rest of it on the drum surface by adhesive. Then a program could be developed to control the blade to move away from the drum meanwhile rotates the drum in the same linear speed in order to let the bonded sheet be peeled off perpendicularly to the drum surface. The peeling force is then recorded still by the load cell and charge amplifiers. Then the critical fracture energy should be obtained by dividing the work done from peeling force with the area of newly peeled off sheet.

The derivative topics from the creping analysis, however, study on the specific failure and fracture problems which are neglected or simplified by the assumptions of creping problem. For example, the 1-D model in this dissertation assumes the material property in

sheet cross section (i.e., perpendicular to creping direction) is uniform, but actually in micro structure it is not uniform. Its structure is like a composite material with many sheet fibers distributed in the sheet base or matrix that is much different from fibers and the sheet is orthotropic. This is probably why the buckling shapes in the wrinkle pattern of crepe paper appear like many discontinuous blisters in practical creping results rather than continuous straight ridges across the sheet width. The delamination buckling in non-uniform media is a challenging topic derived from creping analysis.

Finally, there is impact on the sheet-adhesive structure during creping process. Similarly, the impact on the thin layer bonded to other surface is another considerable topic. The impact would bring in oscillation for a structure. Prior impact studies mainly focus on the oscillation of dynamic buckling in single column and thin plate/shell members. If these members are partially free and partially bonded to other objects or surfaces including different geometries, the buckling and delamination behaviors will be influenced by impact and should be of interest in the creping process.

BIBLIOGRAPHY

Adan, N., Sheinman, I. and Altus, E., 1994. Post-buckling behavior of beams under contact constraints, *J. Appl. Mech.*, Trans. of the ASME, Vol. 61, No. 4, pp. 764-772.

Alfredsson, K. S. and Högberg, J. L., 2007. Energy release rate and mode-mixity of adhesive joint specimens. *Int. J. Fract.*, Vol. 144, No. 4, pp. 267-283.

Anderson, A. B., Mehandru, S. P. and Smialek, J. L., 1985. Dopant effect of yttrium and the growth and adherence of alumina on nickel-aluminum alloys. *J. electrochem. Soc.*, Vol. 132, No. 7, pp. 1695-1701.

Ari-Gur, J., Weller, T. and Singer, J., 1982. Experimental and theoretical studies of columns under axial impact. *Int. J. Solids Struct.*, Vol. 18, No. 7, pp. 619-641.

Audoly, B., 1999. Stability of straight delamination blisters. *Phys. Rev. Lett.*, Vol. 83, No. 20, pp. 4124-4127.

Beacham, J. A., Jr., 1998. Mechatronic simulation of a tissue manufacturing process. A Master's thesis submitted to North Carolina State University.

Beer, F. P., Johnston, E. R., Jr. and DeWolf, J. T., 2002. **Mechanics of Materials**. 3rd edition, McGraw-Hill, New York.

Bo, J., 1992. Study on PVA hydrogel crosslinked by epichlorohydrin. *J. Appl. Polym. Sci.*, Vol. 46, pp. 783-786.

Bottega, W. J. and Maewal, A., 1983. Delamination buckling and growth in laminates. *J. Appl. Mech.*, Trans. of the ASME, Vol. 50, No. 1, pp. 184-189.

Chai, H., 1986a. On the correlation between the mode I failure of adhesive joints and laminated composites. *Eng. Fract. Mech.*, Vol. 24, No. 3, pp. 413-431.

Chai, H., 1986b. Bond thickness effect in adhesive joints and its significance for mode I interlaminar fracture of composites. *7th ASTM Symp. On Composite Materials, Testing and Design, ASTM STP*, 893, 209-231.

Chai, H., 1988. Shear fracture. *Int. J. Fract.*, Vol. 37, No. 2, pp. 137-159.

Chai, H., 1998. The post-buckling response of a bi-Laterally constrained column. *J. Mech. Phys. Solids*, Vol. 46, No. 7, pp. 1155-1159, 1161-1181.

Chai, H., Babcock, C.D. and Knauss, W.G., 1981. One-dimensional modeling of failure in laminated plates by delamination buckling. *Int. J. Solids Struct.*, Vol. 17, No. 11, pp. 1069-1083.

Chan, K. S., 1997. A mechanics-based approach to cyclic oxidation. *Metall. Mater. Trans.*, Vol. 28A, No. 2, pp. 411-422.

Chen, H. and Virgin, L. N., 2006. Finite element analysis of post-buckling dynamics in plates—Part I: An asymptotic approach. *Int. J. Solids Struct.*, Vol. 43, pp. 3983-4007.

Cherepanov, G. P., 1962. The stress state in a heterogeneous plate with slits. *Izvestia ANSSSR, OTN, Mekhan. i Mashin*, Vol. 1, pp. 131-137.

Cherepanov, G. P., 1979. **Mechanics of Brittle Fracture**. McGraw Hill, New York.

Crosby, K. M. and Bradley, R. M., 1999. Pattern formation during delamination and buckling of thin films. *Am. Phys. Soc.*, Vol. 59, No. 3, pp. 2542-2545.

Duong, C. N., 2006. A unified approach to geometrically nonlinear analysis of tapered bonded joints and doublers. *Int. J. Solids Struct.*, Vol. 43, pp. 3498-3526.

England, A. H., 1965. A crack between dissimilar media. *J. Appl. Mech.*, Vol. 32, No. 2, pp. 400-402.

Erdogan, F., 1963. Stress distribution in a nonhomogeneous elastic plane with cracks. *J. Appl. Mech.*, Vol. 30, Trans. ASME, Vol. 85, Series E, pp. 232-236.

Erdogan, F., 1965. Stress distribution in bonded dissimilar materials with cracks. *J. Appl. Mech.*, Vol. 32, No. 2, pp. 403-510.

Erdogan, F. and Sih, G. E., 1963. On the crack extension in plates under plate loading and transverse shear. *J. Basic Eng.*, Vol. 85, pp. 519-527.

Evans, A. G. and Hutchinson, J. W., 1984. On the mechanics of delamination and spalling in compressed films. *Int. J. Solids Struct.*, Vol. 20, No. 5, pp. 455-466.

Evans, A. G. and Hutchinson, J. W., 1995. The thermomechanical integrity of thin films and multilayers. *Acta metall. mater.*, Vol. 43, No. 7, pp. 2507-2530.

Geubelle, P. H. and Knauss, W. G., 1994. Crack propagation at and near bimaterial interfaces: linear analysis. *J. Appl. Mech.*, Trans. of the ASME, Vol. 61, No. 3, pp. 560-566.

Gioia G. and Ortiz, M. 1997. Delamination of compressed thin films. *Adv. Appl. Mech.*, Vol. 33, pp. 119-192.

Gioia G. and Ortiz, M. 1998. Determination of thin-film debonding parameters from telephone-cord measurements. *Acta Mater.*, Vol. 46, No. 1, pp. 169-175.

Goland, M. and Reissner, E., 1944. The stress in cemented joints. *J. Appl. Mech.*, Vol. 66, pp. 17-27.

Gruttmann F. and Pham V. D., 2008. A finite element model for the analysis of buckling driven delaminations of thin films on rigid substrates. *Comput. Mech.*, Vol. 41, No. 3, pp. 361-370.

Gupta, S., 2011. Examination of stress intensity factors and comparison of crack propagation and cohesive surface model. (in progress).

He, M.-Y. and Hutchinson, J. W., 1989. Kinking of a crack out of an interface. *J. Appl. Mech.*, Vol. 57, pp. 270-278.

Hoff, N. J., 1951. The dynamics of the buckling of elastic columns. *J. Appl. Mech.*, Trans. ASME, Vol. 18, pp. 68-74.

Hu, Y.-T., *et al.*, 1999. The effects of bridging in a 3D composite on buckling, postbuckling and growth of delamination. *Arch. Appl. Mech.*, 69 (1999) 419-428.

Huang, Y., *et al.*, 1998. Intersonic crack growth in bimaterial interfaces : an investigation of crack face contact. *J. Mech. Phys. Solids*, Vol. 46, No. 11, pp. 2233-2259.

Hutchinson, J. W., 2001. Delamination of compressed films on curved substrates. *J. Mech. Phys. Solids*, Vol. 49, No. 9, pp. 1847-1864.

Hutchinson, J. W. and Suo, Z., 1992. Mixed mode cracking in layered materials. *Adv. Appl. Mech.*, Vol. 29, pp. 147-163.

Hutchinson, J. W., Thouless, M. D. and Liniger, E. G., 1992. Growth and configurational stability of circular, buckling-driven film delaminations. *Acta metall. mater.*, Vol. 40, No. 2, pp. 295-308.

Jagla, E. A., 2007. Modeling the buckling and delamination of thin films. *Am. Phys. Soc.*, Vol. 75, 085405(8).

Jensen, H. M. and Sheinman, I., 2001. Straight-sided, buckling-driven delamination of thin films at high stress levels. *Int. J. Fract.*, Vol. 110, No. 4, pp. 371-385.

Jensen, H. M. and Sheinman, I., 2002. Numerical analysis of buckling-driven delamination. *Int. J. Solids Struct.*, Vol. 39, pp. 3373-3386.

Johnson, W. S. and Mangalgiri, P. D., 1985. Influence of the resin on interlaminar mixed-mode fracture, NASA TM 87571.

Kachanov, L. M., 1988. **Delamination Buckling of Composite Materials**. Kluwer Academic Publishers, AA Dordrecht, The Netherlands.

Kim, H.-J. and Hong, C.-S., 1997. Buckling and postbuckling behavior of composite laminates with a delamination. *Compos. Sci. Technol.*, Vol. 57, pp. 557-564.

Kounadis, A. N., Mallis, J. and Sbarounis, A., 2006. Postbuckling analysis of columns resting on an elastic foundation. *Arch. Appl. Mech.*, Vol. 75, pp. 395-404.

Kwon, Y. W. and Serttunc, M., 1993. Static and dynamic buckling of a fiber embedded in a matrix with interface debonding. *J. Pressure Vessel Technol.*, Trans. ASME, Vol. 115, No. 3, pp. 297-301.

Lambros, J. and Rosakis, A. J., 1994. Dynamic decohesion of bimaterials: experimental observations and failure criteria. SM-Report 94-2, California Institute of Technology, Pasadena, California.

Lambros, J. and Rosakis, A. J., 1995. Shear dominated transonic crack growth in a bimaterial-I. Experimental observations. *J. Mech. Phys. Solids*, Vol. 43, No. 2, pp. 169- 188.

Lawn, B. R. and Wilshaw, T. R., 1974. **Fracture of Brittle Solids**. Cambridge University Press.

Lindberg, H. E., 1965. Impact buckling of a thin bar. *J. Appl. Mech.*, Trans. ASME, Vol. 32, pp. 315-322.

Lindberg, H. E., 1988. Random imperfections for dynamic pulse buckling. *J. Eng. Mech.*, Vol. 114, No. 7, pp. 1144 -1165.

Lindberg, H. E., 1991. Dynamic pulse buckling of imperfection-sensitive shells. *J. Appl. Mech.*, Vol. 58, No. 3, pp. 743-748.

Lindberg, H. E., 1992a. An evaluation of convex modeling for multimode dynamic buckling. *J. Appl. Mech.*, Trans. ASME, Vol. 59, pp. 929-936.

Lindberg, H. E., 1992b. Convex model for uncertain imperfection control in multimode dynamic buckling. *J. Appl. Mech.*, Trans. ASME, Vol. 59, pp. 937-945.

Lindberg, H. E. and Florence, A. L., 1987. **Dynamic pulse buckling**. Martinus Nijhoff Publishers, AD Dordrecht , The Netherlands., pp. 384.

Liu, C., Lambros, J. and Rosakis, A. J., 1993. Highly transient elastodynamic crack growth in a biomaterial interface: high order asymptotic analysis and optical experiments. *J. Mech. Phys. Solids*, Vol. 41, pp. 1887- 1954.

Lu, H. and Chiang, F. P., 1993. Photoelastic determination of stress intensity factor of an interfacial crack in a bi-material. *J. Appl. Mech.*, Vol. 60, No. 1, pp. 93-100.

Matos, P. P. L. *et al.*, 1989. A method for calculating stress intensities in biomaterial fracture. *Int. J. Fract.*, Vol. 40, pp. 235-254.

Mishra, S., *et al.*, 2008. On the mechanical strength of biocompatible semi-IPNs of polyvinyl alcohol and polyacrylamide. *Microsyst. Technol.*, Vol. 14, pp. 193-198.

Moon, M. W., *et al.*, 2002. The characterization of telephone cord buckling of compressed thin films on substrates. *J. Mech. Phys. Solids*, Vol. 50, No. 11, pp. 2355- 2377.

Mukai, D. J., Ballarini, R. and Miller, G. R., 1990. Analysis of branched interface cracks. *J. Appl. Mech.*, Vol. 57, pp. 887-893.

Muskhelishvili, N. I., 1953. **Some Basic Problems of the Mathematical Theory of Elasticity**. English translation, P. Noordoff and Company, New York.

Oliver, J. F., 1980. Dry-creping of tissue paper - a review of basic factors. *Tappi J.*, Vol. 63, No, 12, pp. 91-95.

Palaniswamy, K. and Knauss, W. G., 1978. **On the Problem of Crack Extension in Brittle Solids under General Loading**. *Mech. Today*, Vol. 4, S. Nemat-Nasser, ed., Pergamon Press, pp. 87-148.

Priest, J. R., *et al.*, 1962. **Transactions of the Ninth National Symposium of the American Vacuum Society**. G. H. Bancroft, ed., Macmillan, New York, pp. 121-124.

Ramasubramanian, M. K. and Crews, W. R., 1998. Shear strength of an adhesively bonded paper-metal interface, *J. Pulp Pap. Sci.*, Vol. 24, No. 1, pp. 31-36.

Ramasubramanian, M. K. and Shmagin, D. L., 2000. An experimental investigation of the creping process in low-density paper manufacturing. *J. Manuf. Sci. Eng.*, Vol. 122, pp. 576-581.

Ramasubramanian, M. K. and Sun, Z., 1999. Debonding and buckling of a thin film bonded to a rigid surface. *ASME summer conference*, Blacksburg, VA, April 27-30.

Ramasubramanian, M. K. and Sun, Z., 2000. On the thin film debonding and buckling from a rigid surface – a phenomenon in creping process, *Progress in Paper Physics*, Grenoble, France, September 11-15.

Ramasubramanian, M. K., Sun, Z. and Chen, G., 2011. A mechanics of materials model for the creping process. *J. Manuf. Sci. Eng.*, Vol. 133, No. 5, 051011(8).

Rice, J. R., 1968. **Mathematical Analysis in the Mechanics of Fracture**. *Fracture: An Advanced Treatise*. Vol. II, H. Liebowitz, ed., Academic Press, New York, pp. 191-311.

Rice, J. R., 1988. Elastic fracture mechanics concepts for interfacial cracks. *J. Appl. Mech.*, Vol. 55, No. 1, pp. 98-103.

Rice, J. R. and Sih, G. C., 1965. Plane problems of cracks in dissimilar media. *J. Appl. Mech.*, Vol. 32, No. 2, pp. 418-423.

Rosakis, A. J. *et al.*, 1998. Intersonic crack propagation in bimaterial systems. *J. Mech. Phys. Solids*, Vol. 46, No. 10, pp. 1789-1813.

Rose, G., 2004. Crepe adhesive modifiers improve tissue runnability, product quality. *Paper Age*, Vol. 120, No. 4, pp. 22-26.

Salomonsson, K., 2008. Mixed mode modeling of a thin adhesive layer using a meso-mechanical model. *Mech. Mater.*, Vol. 40, No. 8, pp. 665-672.

Sevin, E., 1960. On the elastic bending of columns due to dynamic axial forces including effects of axial inertia, *J. Appl. Mech.*, Trans. ASME, Vol. 27, No. 1, pp. 125-131.

Siede, P., 1958. Compressive buckling of a long simply supported plate on an elastic foundation. *J. Aeronaut. Sci.*, pp. 382-394.

Soerens, D. A.. Creping adhesives containing Polyvinyl Alcohol and Cationic Polyamide Resins. U. S. Patent 4,501,640, February 26, 1985.

Sørensen, K. D., Jensen, H. M. and Clausen, J., 2008. Delamination of compressed thin layers at corners. *Int. J. Solids Struct.*, Vol. 45, pp. 5867-5878.

Sun, Z., 2000. Debonding and buckling of a thin short-fiber nonwoven bonded to a rigid surface and its application to the creping process. A dissertation of Ph.D. submitted to North Carolina State University.

Thouless, M. D., Hutchinson, J. W. and Liniger, E. G., 1992. Plane-strain, buckling-driven delamination of thin films: model experiments and mode-II fracture. *Acta Metall. Mater.*, Vol. 40, No. 10, pp. 2639-2649.

Timoshenko, S. P. and Gere, J. M., 1961. **Theory of Elastic Stability**. 2nd edition, McGraw-Hill, New York.

Tvergaard, V. and Hutchinson, J.W., 1996. On the toughness of ductile adhesive joints. *J. Mech. Phys. Solids*, Vol. 44, No. 5, pp. 789-800.

Tvergaard, V. and Hutchinson, J.W., 2008. Mode III effects on interface delamination. *J. Mech. Phys. Solids*, Vol. 56, No. 1, pp. 215–229.

Wang, C. Y., 1984. Buckling and post-buckling of the lying sheet. *Int. J. Solids Struct.*, Vol. 20, No. 4, pp. 351-358.

Wang, J.-S. and Evans, A. G., 1998. Measurement and analysis of bucking and buckle propagation in compressed oxide layers on superalloy substrates. *Acta Mater.*, Vol. 46, No. 14, pp. 4993-5005.

Waters, P. and Volinsky, A. A., 2007. Stress and moisture effects on thin film buckling delamination. *Exp. Mech.*, Vol. 47, No. 1, pp. 163-170.

Wei, Y. and Hutchinson, J. W., 1997. Nonlinear delamination mechanics for thin films. *J. Mech. Phys. Solids*, Vol. 45, No. 7, pp. 1137-1159.

Whitcomb, J. D. and Shivakumar, K. N., 1989. Strain-energy release rate analysis of plates with postbuckled delaminations. *J. Compos. Mater.*, Vol. 23, No. 7, pp. 714-734.

Williams, M. L., 1959. The stresses around a fault or crack in dissimilar media. *Bull. Seismol. Soc. Am.*, Vol. 49, No. 2, pp. 199-204.

Wu, C. H., 1978. Maximum energy release rate criterion applied to a tension-compression specimen with crack. *J. Elast.*, Vol. 8, pp. 235-257.

Yu, H.-H. and Hutchinson, J. W., 2002. Influence of substrate compliance on buckling delamination of thin films. *Int. J. Fract.*, Vol. 113, No. 1, pp. 39-55.

Yu, H.-H. and Yang, W., 1995. Mechanics of transonic debonding of a bimaterial interface: the in-place case. *J. Mech. Phys. Solids*, Vol. 43, No. 2, pp. 207- 232.

Yu, H. Y., Kim, C. and Sanday, S. C., 1991. Buckle formation in vacuum-deposited thin films. *Thin Solid Films*, Vol. 196, No. 2, pp. 229-233.

Yuse, A. and Sano, M., 1994. Instability of a crack in a heated strip. *Phys. Rev. E.*, Vol. 49, No. 1, pp. 51-54.

Zhu, J.-F. *et al.*, 2003. Reference surface element modeling of composite plate/shell delamination buckling and postbuckling. *Compos. Struct.*, Vol. 61, pp. 255-264.

APPENDICES

Appendix A

MATLAB MAIN PROGRAM OF CREPING LENGTH CALCULATION BY FRACTURE ENERGY METHOD

MAIN PROGRAM:

```
%
%>>>>>>>>>>>>>>>>>>>>>>>>PROGRAM  START<<<<<<<<<<<<<<<<<<<<<<<<
%


clear all;
clc;
profile on
tic;
syms x cl;                  %declare symbols for matlab functions
global crepl itnum;       %declare global variables: creping length and iteration number
plotx=zeros(2,2);
ploty=zeros(2,2);
%
%====================| INPUT PARAMETERS |====================
%
theta=82/180*pi;        % Creping blade angle, degree (<90)
```

```
Es=100e6;                % Sheet elastic modulus, Pa (<150e6)
Ea=25e6;                 % Adhesive elastic modulus, Pa (<50e6)
ts=60/1e6;               % Sheet thickness, m (<200/1e6)
ta=2/1e6;                % Adhesive thickness, m (<6/1e6)
nu=0.3;                  % Poisson's ratio
Gic=32;                  % Mode I critical energy release rate, N/m
Giic=32;                 % Mode II critical energy release rate, N/m
creplmt=6/1e3;           % Upper limit for creping length output, m
%
%==================| CALL SUBROUTINE |=====================
%
disp('program starts');
disp('running in section 1....');
%
% call subroutine
[crepl,itnum,udata,ldata,strval,strcval,CrepF]=crepsub(theta,Es,Ea,ts,ta,Gic,Giic,creplmt);
%
disp('Iterations=');
disp(itnum);
disp('Creping length(mm)=');
disp(crepl*1e3);
```

```
%
%==================| OUTPUTS IN MATLAB |====================
%
plotx(1,1)=udata(itnum,1)*1e3;
plotx(2,1)=udata(itnum,1)*1e3;
ploty(1,1)=0;
ploty(2,1)=ldata(itnum,1)*1e3;
plotx(1,2)=0;
plotx(2,2)=udata(itnum,1)*1e3;
ploty(1,2)=ldata(itnum,1)*1e3;
ploty(2,2)=ldata(itnum,1)*1e3;

%  delamination history in figure 1.
figure(1)
plot(plotx(1,1),ploty(1,1),'xr',...
   plotx(1,2),ploty(1,2),'xr',...
   plotx(:,1),ploty(:,1),':m',...
   plotx(:,2),ploty(:,2),':m',...
   udata(itnum,1)*1e3,ldata(itnum,1)*1e3,'xr',...
   udata(1:itnum,1)*1e3,ldata(1:itnum,1)*1e3,'.-b','LineWidth',2,'MarkerSize',14);
box on;
```

```
grid on;
title('Delamination history','FontSize',18);
xlabel('End displacement, u(mm)','FontSize',14);
ylabel('Crack length, l(mm)','FontSize',14);
text(udata(itnum,1)*1e3,ldata(itnum,1)*1e3,'  Convergence','FontSize',14);
text(plotx(1,2),ploty(1,2)-0.05,'  Creping length','FontSize',14);
text(plotx(1,1),ploty(1,1)+0.08,'  Approached u','FontSize',14);

%  strain and critical strain history in figure 2.
figure(2)
plot(udata(1:itnum,1)*1e3,strval(1:itnum,1),'x:b',...
   udata(1:itnum,1)*1e3,strcval(1:itnum,1),'o:r',...
   plotx(1,1),ploty(1,1),'xr','LineWidth',2,'MarkerSize',8);
legend('Strain','Critical strain',-1);
%
box on;
grid on;
title('Buckling determination','FontSize',18);
xlabel('End displacement, u(mm)','FontSize',14);
ylabel('Strain&Critical strain in flat sheet','FontSize',14);
text(plotx(1,1),ploty(1,1)+0.02,'  Approached u','FontSize',14);
```

```
%
%==================| OUTPUTS IN DATA FILE |====================
%
SheetName = 'creping history';
crepingdata =
[num2cell(udata(1:itnum,1)),num2cell(ldata(1:itnum,1)),num2cell(strval(1:itnum,1)),num2ce
ll(strcval(1:itnum,1)),num2cell(CrepF(1:itnum,1))];
xlswrite('creping history.xls',crepingdata,'A1');
%
%============================================================
%
disp('all sections completed');
toc;
profile report;
%
%>>>>>>>>>>>>>>>>>>>>>>>> PROGRAM END <<<<<<<<<<<<<<<<<<<<<<<<
%
```